UNIVERSITY OF CALIFORNIA

Los Angeles

Fluorescence and Rotational Dynamics of Amphidynamic Crystals

A dissertation submitted in partial satisfaction of the

requirements for the degree Doctor of Philosophy

in Chemistry

by

Morgan Elizabeth Howe

2019

ABSTRACT OF THE DISSERTATION

Fluorescence and Rotational Dynamics of Amphidynamic Crystals

by

Morgan Elizabeth Howe

Doctor of Philosophy in Chemistry

University of California, Los Angeles, 2019

Professor Miguel A. Garcia-Garibay, Chair

Crystalline solids are a promising platform for the development of molecular machines due to their ability to take advantage of the preorganization and proximity of molecular elements and their potential for displaying emergent properties. Chapter 1 introduces a framework that can be used to design amphidynamic crystals and explain their dynamic behavior. A brief discussion of the history of molecular machinery is followed by the motivation for studying them in the solid state. Previous strategies for designing amphidynamic crystalline molecular rotors are discussed in light of an overarching comparison between packing coefficients and rotational rate constants of existing systems, and then a new framework is proposed. In this framework, extended porous solids with large cavities that can accommodate rotational motion and molecular crystals formed by close packing interactions are considered separately and their dynamics are explained by different factors. The rotational rates of extended porous solids are attributed to the intrinsic barriers of rotation around the bonds that form the axle of rotors, and these systems are considered

to be activation-controlled. The rotational rates of close-packed molecular crystals are attributed to the ability of atoms surrounding rotators to undergo small-amplitude displacements and create transient cavities that accommodate rotational motion, an ability termed "crystal fluidity." These systems that rely on crystal fluidity are considered to have inertial rotation and be diffusion-controlled. The chapter finishes with a discussion of the implications of these classifications.

While solid-state molecular machines have the potential to display unique properties, the observation of their motion can be challenging. Chapters 2 and 3 address methods to sense molecular motion using two different approaches based on fluorescence spectroscopy. In Chapter 2, the synthesis and characterization of a crystalline molecular rotor featuring an aggregation-induced emission (AIE) fluorophore is reported. Due to the reliance of both rotational motion and fluorescence intensity on crystal fluidity, we envisioned that the system would display an inverse relationship between rotational dynamics and fluorescence intensity, allowing for the measurement of rotational rate with fluorescence spectroscopy. The fluorescence lifetime of a powdered sample was on the order of 4–5 ns but showed no discernable trend between 77 K and 298 K, which was interpreted to indicate that the AIE fluorophore and its surroundings were essentially static over the fluorescence lifetime at all temperatures. This was supported by solid-state NMR studies that showed rotational dynamics between 198 K and 298 K in the kHz (μs) regime, which is three orders of magnitude too slow to affect fluorescence emission.

While Chapter 2 focuses on an indirect method for measuring a potential relationship between rotational dynamics and crystal fluidity using fluorescence spectroscopy, the work in Chapter 3 explores the use of a more direct method: fluorescence anisotropy decay. Six different acenes with axially linked trialkylsilylethynes of different sizes were synthesized and characterized in high-viscosity mineral oil solutions. The steady-state and time-resolved anisotropy of the

systems were observed in the mineral oil solutions in order to calculate the rotational correlation times of each molecule.

Chapter 4 describes an experiment designed for the high school level to help promote interest in nanoscience and expose younger students to the fundamentals of absorption spectroscopy, color, enzymes, and sensing in a qualitative, low-cost manner. The experiment features a glucose sensing assay encapsulated in a hydrogel bead. The students swell the beads in the assay and then expose them to a variety of conditions in a well plate in order to explore the sensing pathway of the assay, elucidate the advantages of encapsulating it in a nanostructured environment, create a calibration curve for sensing sugar, and determine the amount of sugar in sweetened drinks.

The dissertation of Morgan Elizabeth Howe is approved.

Kendall N. Houk

Yves F. Rubin

Harold G. Monbouquette

Miguel A. Garcia-Garibay, Committee Chair

University of California, Los Angeles,

2019

Table of Contents

List of Figures

List of Schemes

List of Tables

List of Equations

List of Abbreviations

A	pre-exponential factor
Å	angstrom
AAP	4-aminoantipyrine
ACQ	aggregation-caused quenching
AIE	aggregation-induced emission
ATR	attenuated total reflectance (infrared spectroscopy)
AMU	atomic mass units
BCO	[2.2.2]bicyclooctane
BODCA	bicyclo[2.2.2]octane dicarboxylate
br	broad (NMR)
°C	degrees celsius
^{13}C NMR	carbon-13 nuclear magnetic resonance spectroscopy
ca.	circa (approximately)
calcd.	calculated
$CDCl_3$	deuterated chloroform
$CHCl_3$	chloroform
C_k	packing coefficient
cm	centimeter
cP	centipoise
cryst	crystal
d	doublet (NMR)
DABCO	1,4-diazabicyclo[2.2.2]octane

DART	direct analysis in real time (mass spectrometery)
DCM	dichloromethane
dd	doublet of doublets (NMR)
ddd	doublet of doublet of doublets (NMR)
DEB	diethynylbenzene
DFT	density functional theory
DI	deionized
DLS	dynamic light scattering
DMF	dimethylformamide
DNA	deoxyribonucleic acid
ε	molar absoptivity
E	energy
E_a	activation energy
eq.	equivalent
ESI	electrospray ionization
Et	ethyl
et al.	et alia (and others)
EtOH	ethanol
g	gram
GOx	glucose oxidase
GS	ground state
h	hour
^{1}H NMR	proton nuclear magnetic resonance spectroscopy

^{2}H NMR	deuterium nuclear magnetic resonance spectroscopy
H_2O_2	hydrogen peroxide
HBS	3,5-dichloro-2-hydroxybenzenesulfonate
HE	high energy
HRMS	high resolution mass spectrometry
HRP	horseradish peroxidase
HSQC	heteronuclear single quantum coherence spectroscopy
Hz	hertz
i.e.	id est (namely)
iPrOH	isopropanol
IR	infrared (spectroscopy)
IRMOF	isoreticular metal-organic framework
J	coupling constant (NMR)
K	kelvin
kcal	kilocalorie
k_r	rotational rate constant
LE	low energy
λ_{em}	emission wavelength
λ_{ex}	excitation wavelength
λ_{max}	wavelength of maximum emission, excitation, or absorption
m	meta (benzene substitution)
m	multiplet (NMR)
M	molar

Me	methyl
mg	milligram
MHz	megahertz
min	minute
mL	milliliter
μL	microliter
μm	micrometer
μM	micromolar
mM	millimolar
mmol	millimole
MOF	metal-organic framework
mol	mole
m.p.	melting point
m/z	mass to charge ratio
nm	nanometer
ns	nanosecond
PBS	phosphate buffered saline
Ph	phenyl
pH	measure of acidity
ppm	parts per million
ps	picoseconds
R	general alkyl group substituent
RNA	ribonucleic acid

rt	room temperature
s	singlet (NMR)
s	second
S_0	singlet ground state
S_1	first excited singlet state
soln	solution
t	triplet (NMR)
τ	lifetime
THF	tetrahydrofuran
TIPS	triisopropylsilyl
TMS	trimethylsilyl
TOF	time of flight (mass spectrometery)
TPE	tetraphenylethylene
TPS	triphenylsilyl
trityl	triphenylmethyl
TS	transition state
tsp	teaspoon
UV-vis	ultraviolet-visible spectroscopy
V_{cell}	unit cell volume
V_{mol}	molecular volume
vs.	versus
VT	variable temperature
W	watts

Acknowledgements

I'd like to thank some of the people who have helped me along the way to reaching this milestone. First, thank you to my advisor Prof. Miguel Garcia-Garibay: your kind, patient support and expert scientific guidance have allowed me to grow into the researcher I am today. Your perpetual positive attitude in the face of stubborn experiments and entertaining metaphors for all things research-related will shape the way I see research for years to come.

Second, I'd like to thank two people who first inspired me to learn chemistry and eventually want to teach it myself: Suzanne Pakkala and Prof. Chris Smart. The care, excitement, and energy that both of you brought to your respective classrooms is what got me interested in chemistry in the first place, and you will always be inspirations to me as a teacher.

Many thanks also to the instrument specialists who helped me with the data collection for some of my more complex experiments: Bob Taylor and T.C. Ong for help with various NMR experiments and Ian Stanton for help with fluorescence. I am very grateful for your assistance.

Lastly, I would like to thank the people who helped support me during my time at UCLA. Dr. Vanessa Breslin, Dr. Geeta Vadehra, Dr. Xing Jiang, and Dr. Salvador Perez-Estrada: you helped me find my way when I first arrived in the Garcia-Garibay lab, and I appreciate both your friendship and all you did to help me succeed in my day-to-day life as a graduate student and scientist. To Jay McDaniel and Dr. Jennifer Casey: thank you for your patience and support over the past year. You have both helped me grow as an educator, an education researcher, and a person. It is my hope that you *understand* how important you have been in helping me succeed, and I can't wait to see what wonderful things you both contribute to the chemistry education community.

Associated Publications and Author Contributions

Chapter 1 is adapted with permission from Howe, M. E.; Garcia-Garibay, M. A. The Roles of Intrinsic Barriers and Crystal Fluidity in Determining the Dynamics of Crystalline Molecular Rotors and Molecular Machines *J. Org. Chem.* **2019**, *84*, 9835-9849 (doi 10.1021/acs.joc.9b00993). Prof. Garcia-Garibay was the PI of the project: both he and I contributed to analyzing existing literature and writing the manuscript.

Chapter 2 is adapted with permission from Howe, M. E.; Garcia-Garibay, M. A. Fluorescence and Rotational Dynamics of a Crystalline Molecular Rotor Featuring an Aggregation-Induced Emission Fluorophore. *J. Org. Chem.*, **2019**, *84*, 9570–9576 (doi 10.1021/acs.joc.9b01201). I synthesized and characterized all compounds, as well as performing fluorescence spectroscopy and NMR experiments. Prof. Garcia-Garibay was the PI of the project, and we both wrote the manuscript. This work was supported by National Science Foundation grants DMR-1700471, MRI-1532232 (solid-state NMR), and CHE-1048804 (solution NMR).

Chapter 3 is adapted from Howe, M. E.; Barbour, N. A.; Garcia, R. V.; Garcia-Garibay, M. A. The Use of Fluorescence Anisotropy Decay to Measure Rotation of Acenes in Viscous Solution, in preparation for publication. N. A. Barbour and R. V. Garcia both contributed to the synthesis of the compounds studied, and N. A. Barbour also performed preliminary fluorescence spectroscopy experiments. I synthesized the remaining compounds and performed all final fluorescence spectroscopy experiments. Prof. Garcia-Garibay and I wrote the manuscript, and he was also the PI of the project. This work was supported by grant DMR-1700471.

Chapter 4 is adapted with permission from Howe, M. E.; Blaik, R. A.; Tolbert, S. H. Encapsulating a Glucose Sensing Assay in a Hydrogel to Investigate Sensing Pathways in a High School Laboratory, in preparation for publication. I designed the experimental procedure, wrote

the laboratory manuals for both teachers and students, and designed the handouts accompanying the manuscript. R. A. Blaik helped organize the workshops at which the experiment was disseminated, and all authors contributed to editing the manuscript. Prof. Tolbert was the faculty advisor for the program that funded the development of the experiment. This work was supported by the California NanoSystems Institute Education Outreach Program.

Vita

Vassar College – Poughkeepsie, NY .....2010 – 2014

Bachelor of Arts: Chemistry, with general and departmental honors

Graduate Student Researcher – UCLA .....2015 – 2019

Advisor: Miguel A. Garcia-Garibay

Undergraduate Researcher – Vassar College .....2013 – 2014

Advisor: Christopher Smart

RISE Intern – UC Santa Barbara 2012

Advisor: Craig Hawker

Publications and Presentations

Publications

1. Aldeborgh, H.; George, K.; Howe, M. E.; Lowman, H.; Moustakas, H.; Strunsky, N.; Tanski, J. M. Analysis of Amall Molecule X-Ray Crystal Structures: Chemical Crystallography with Undergraduate Students in a Teaching Laboratory. *J. Chem. Crystallogr.* **2014**, *44*, 70-81.
2. Howe, M. E.; Garcia-Garibay, M. A. The Roles of Intrinsic Barriers and Crystal Fluidity in Determining the Dynamics of Crystalline Molecular Rotors and Molecular Machines. *J. Org. Chem.* **2019**, *84*, 9835-9849.
3. Howe, M. E.; Garcia-Garibay, M. A. Fluorescence and Rotational Dynamics of a Crystalline Molecular Rotor Featuring an Aggregation-Induced Emission Fluorophore. *J. Org. Chem.* **2019**, *84*, 9570-9576.

4. Howe, M. E.; Barbour, N. A.; Garcia, R. V.; Garcia-Garibay, M. A. The Use of Fluorescence Anisotropy Decay to Measure the Rotation of Acenes in Viscous Solutions. **2019**, *manuscript in preparation.*
5. Howe, M. E.; Blake, R.; Tolbert, S. H. Encapsulating a Glucose Sensing Assay in a Hydrogel to Investigate Sensing Pathways in a High School Laboratory. **2019**, *manuscript in preparation.*

Presentations

1. Howe, M. E.; Needleman, A.; Smart, C. Synthesis, Purification, and Functionalization of a Fullerene Derivative Containing a Reactive Handle. Poster session presented at: *ACS Mid-Hudson Section 15th Annual Undergraduate Research Symposium*; 2014 April 25; New Paltz, NY.
2. Howe, M. E.; Commins, P.; Garcia-Garibay, M. A. Synthesis of cross-linked molecular rotors in pursuit of fast rotational dynamics in the solid state. Poster session presented at: *250th ACS National Meeting & Exposition*; 2015 Aug 16-20; Boston, MA.
3. Howe, M.E.; Garcia-Garibay, M.A. Fluorescent Sensing of Molecular Motion in the Solid State. Oral presentation delivered at: *PhotoIUPAC 2018*; 2018 Jul 11; Dublin, Ireland.
4. Howe, M. E.; McDaniel, J. W.; Ramachandran, R.; Casey, J. R. The Implementation of Application-Based Science Education Videos in an Undergraduate General Chemistry Laboratory for Life Science Majors. Poster session presented at: *Gordon Research Conference on Chemistry Education Research and Practice*; 2019 Jun 17; Lewiston, ME.

CHAPTER 1

The Roles of Intrinsic Barriers and Crystal Fluidity in Determining the Dynamics of Crystalline Molecular Rotors and Molecular Machines

1.1. Molecular Machinery

Early concepts in the field of artificial molecular machines were based on appealing structural or functional analogies between macroscopic machines and molecules in solution, including gears, propellers, shuttles, and brakes.[1] This work relied on and promoted advances in the field of dynamic stereochemistry and helped the development of analytical tools to document the trajectories, equilibria, and kinetics of complex conformational motions.[2] Subsequent developments recognized that artificial molecular machinery would require structures that not only display the desired machine-like motion but that can be controlled under the influence of selected inputs, leading to the development of bistable molecular switches that operate on the basis of binding interactions, pH, redox processes, light absorption, and other suitable stimuli.[3] The design of structures based on the synchronized behavior of integrated components to perform sophisticated tasks led to the development of unidirectional motors,[4] molecular pumps,[5] and artificial muscles[6] by the groups of Feringa, Stoddart, and Sauvage, respectively, which was recognized with the 2016 Nobel Prize in Chemistry. Having developed the use of molecular dynamics and function to accomplish specific tasks in solution,[7] workers in the field have embraced the challenge of taking molecular-level functions into larger-scale systems, including surfaces,[8] silica nanoparticles,[9] gels,[10] and crystalline solids,[11,12] among others.[13]

1.2. Crystalline Molecular Machines

Our group has been interested in the development of artificial molecular machinery under the conditions of reduced entropy by taking advantage of crystalline solids.[11] We recognize not only that structural elements on a molecular scale determine supramolecular interactions that lead to crystallization but also that the presence of functional groups and molecular-scale structural

features can be used to engineer reactivity and internal molecular dynamics in the crystalline state.[11] Crystalline molecular machines have the potential of combining the molecular-level control of physical properties caused by isomerizations, conformational motions, or chemical reactions with the emergent properties that arise from changes in long-range order, including macroscopic changes such as salient phenomena in the form of shape changes, crystal moving, or jumping.[14] Depending on the characteristics of their constituents, crystalline molecular machines will be well suited for the long-range directional propagation and transduction of mechanical, thermal, electrical, magnetic and optical stimuli.[15] These characteristics make it possible to consider the use of controlled molecular motions in crystals to modulate physical properties, such as color, emission of light, polarization, conductivity, magnetism, and optics, to chemical properties, such as catalysis, molecular storage, and sieving. Furthermore, crystalline molecular machines will be an ideal platform to translate advanced molecular-level design and function to properties that are harvested at larger scales, covering dimensions from tens of nanometers and microns to the macroscopic dimensions of a human operator.

As a starting point to explore this promising new area of science and technology, we have selected a target platform that consists of an ordered array of interacting dipoles[16] mounted on molecular rotors.[17] These dipoles are capable of undergoing rapid reorientation in response to internal and external electric and electromagnetic fields in a manner that resembles a collection of macroscopic compasses.[11] As shown in Figure 1.2.1a, crystalline arrays of freely rotating molecular dipoles are expected to develop spontaneous ordering that depends on their symmetry.[18] Strong homogeneous fields can be used to alter the orientation of the dipoles to develop macroscopic polarization or to change its direction. This is illustrated in Figure 1.2.1b by a hypothetical crystal spontaneously adopting a nonpolar antiferroelectric state that can be forced

into alignment and macroscopic polarization by an external field. Alternatively, local perturbations are expected to result in the propagation of rotary waves across the crystal, which may provide new mechanisms for signal transport and transduction. Changes in physical properties resulting from different dipole configurations and dipolar motion can be interfaced with other stimuli (sound waves, heat transfer, color, light, polarization, charge, etc.) to provide a variety of emergent functions.[15]

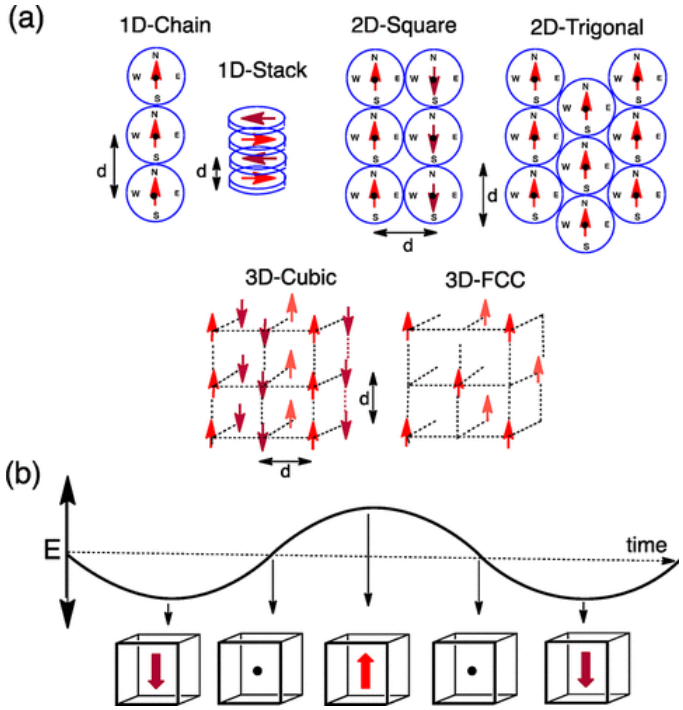

Figure 1.2.1. (a) Spontaneous order ideally expected from simple 1D, 2D, and 3D dipolar arrays with different symmetries. Some symmetries are expected to have an infinite number of degenerate ground-state orientations, which would result in collectively coupled rotational states. (b) Expected macroscopic polarization of a hypothetic antiferroelectric 3D cubic crystal that has no spontaneous polarization (at $E = 0$) but becomes macroscopically polarized in the presence of an external electric field ($E \neq 0$), whether the field is oscillating (as shown) or static.

1.3. Amphidynamic Crystals[11,19]

The realization of crystalline rotary dipolar arrays requires molecular structures that can form an ordered lattice and support the rotation of the central dipole. To attain a strong alignment, dipole–dipole interactions should be large, their distances should be short, and the dielectric constant of the medium should be low to diminish the attenuation of their interaction. However, the most important requirement is to have their rotary motion unhindered. In fact, the design of crystalline molecular machines based on functions that rely on mechanical motions requires the construction of crystals with moving parts, which are also known as "amphidynamic crystals".[19] For the original entry into the construction of amphidynamic crystals and dipolar arrays, we envisioned structures analogous to those of macroscopic compasses and gyroscopes. As shown in Figure 1.3.1, these are formed by lattice-building, encasing structures (shown in blue) covalently

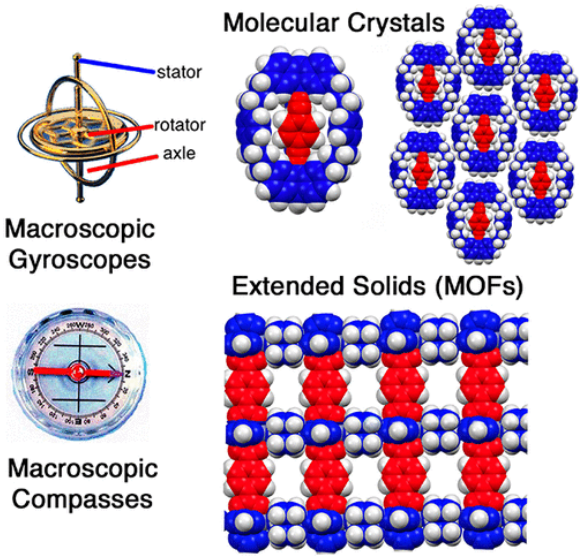

Figure 1.3.1. Structure of a macroscopic gyroscope illustrating its stator, rotator, and axle, compared with the topologies and space-filling model of potential crystal-forming molecular rotors with closed and open topologies. The blue color is used to represent the stator, and the red color is used to highlight the axle and the rotator.

connected by an axle to the rotating element (shown in red). Promising solutions for the construction of amphidynamic crystals can be based on extended solids with porous architectures, such as metal–organic frameworks (MOFs), where the functional rotators act as pillars linked by coordination bonds to static metal clusters.[20] Also illustrated in Figure 1.3.1, more challenging solutions may be based on the use of close-packing interactions between discrete molecular units. These two types of materials will be the primary focus of this account.

1.4. Amphidynamic Crystalline Molecular Rotors Based on Free Volume, the Use of Axially Symmetric Rotators, and/or Correlated (Gearing) Motion Strategies

While exploring structural solutions for the construction of amphidynamic crystals based on molecular units, we envision molecules with structures that are similar to those of macroscopic gyroscopes. They may have closed topologies formed by bridging units that link the upper and lower portions of the stator, as shown in Figure 1.3.1, or open topologies where the bridges are absent and the enclosure is formed by the surrounding molecules in the lattice. When considering the structural elements that may allow for internal molecular rotation in a crystal, we proposed three solutions:[11] (1) the creation of empty space, (2) an increase in the axial symmetry order of the rotator, and (3) the development of correlated motions. Empty space allows for unhindered motion, examples of which can be found in the extended networks of porous solids. Ultrafast hindered rotation,[21] shuttling,[22] and motion-gated diffusion[23] have been documented using MOFs. High-symmetry strategies assume the presence of short-range van der Waals interactions where adjacent molecules tend to conform to the shape of the rotator, such that the shape of its own cross section determines the height of the barriers it must overcome.[24] Assuming smooth polygonal (rather than ratcheted) structures, one can recognize that a rotator with a C_n rotational symmetry

axis will have "n" degenerate energy minima connected by $360/n^{o}$ angular displacements.[24] Furthermore, as $n \rightarrow \infty$ the shape of the rotator approaches the shape of a sphere or a cylinder, such that any steric hindrance begins to disappear. The third and most challenging approach is the design of correlated motions with high axial symmetry but interdigitated structures where the rotation of one unit is geared with the rotations of one or more of its close neighbors.

To visualize these limits in the context of closed packed molecular crystals, we need to consider the size and shape of the rotator, which may be represented by its van der Waals surface (Figure 1.4.1, thick dotted line) and the volume of revolution (thin dashed circle) that it creates as it rotates.[25]

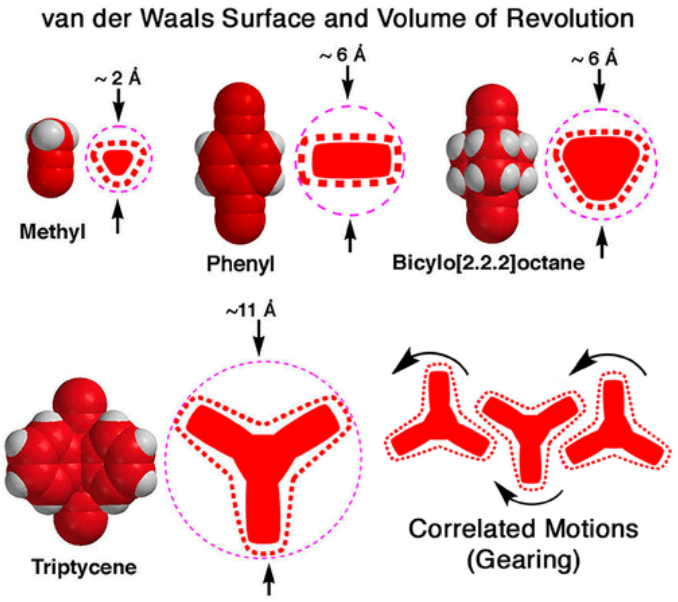

Figure 1.4.1. Space-filling models of methyl, phenylene, and BCO rotators with a schematic cross section of their van der Waals surface (thick red lines) and their volume of revolution (thin magenta circles). Knowing that near neighbors tend to maximize surface contacts, one may expect that in the absence of free volume the rotation of more spherical methyl and BCO rotators will be much less hindered than rotation of phenylene or triptycene rotators. In the absence of free volume, triptycene can only rotate by a correlated motion mechanism.

As illustrated in Figure 1.4.1 with hypothetical methyl, 1,4-phenylene, 1,4-bicyclo[2.2.2]octane (BCO), and 9,10-triptycene rotators, the van der Waals surface represents the closest approach that the rotator is likely to have with any static element in the lattice.

A 3-fold symmetric methyl group is close to spherical, and its van der Waals volume is very close to its volume of revolution, with a small ca. 2 Å diameter. Similarly, BCO rotators have a fairly regular, 3-fold symmetric van der Waals surface and have a volume of revolution that approaches a cylinder with a diameter of ca. 6 Å. It should therefore not be surprising that methyl groups have nearly unhindered rotation in the solid state[26] and that BCO rotators have been shown to have relatively low solid-state barriers, generally in the range of ca. 1–4 kcal/mol.[27] By contrast, the cross section of a phenylene rotator reveals that its van der Waals surface approaches a rectangular shape, such that most close-packed crystals will fill a rectangular shaped space (thick dotted line) in order to have optimal packing interactions. Therefore, even though the volume of revolution of phenylene and BCO rotators have similar diameters (ca. 6 Å), one may expect that phenylene rotation will generally be hindered, such that its use will require architectures with free volume or able to undergo correlated motions for rotation to take place. Finally, triptycene illustrates an example of a high-symmetry (3-fold) "star"-shaped rotator that requires either the design of structures with free volume extending beyond its van der Waals surface in order to accommodate its volume of revolution (ca. 11 Å) or a structure where close neighboring triptycenes rotate in a geared fashion, as illustrated in the bottom right portion of Figure 1.4.1.

The creation of free volume in close-packed molecular crystals is a significant challenge. Using the potential energy diagram in Figure 1.4.2, we consider the energetic adversities that arise when one attempts to maintain two benzene molecules at a given distance.[28] We will refer to the same figure to explore some of the solutions.

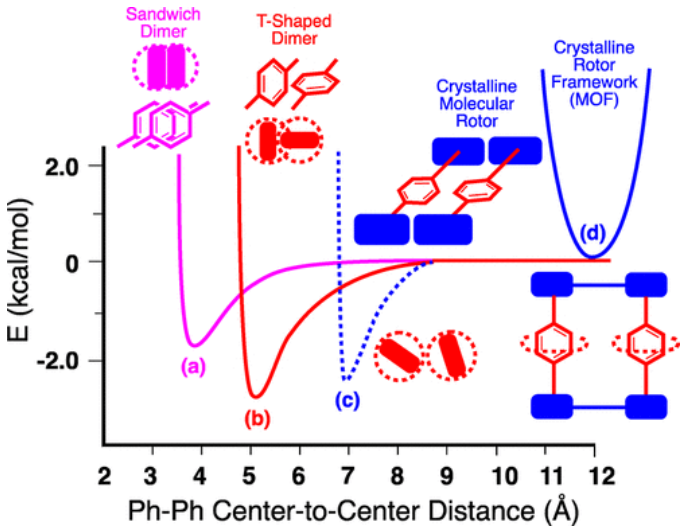

Figure 1.4.2. Potential energy profile for two benzene molecules leading to (a) "sandwich" and (b) "T-shaped" dimer structures and as part of crystal structures based on (c) molecular crystals and (d) metal organic frameworks.

The magenta line (a) in Figure 1.4.2 represents the potential energy for two benzene molecules coming to their closest approach to form a sandwich dimer with a center-to-center distance of ca. 3.7–3.8 Å.(28) One can see how the two molecules fill in a significant fraction of each other's volume of revolution, making it impossible for them to rotate (a parallel-displaced dimer is actually more stable, but is less relevant to our analysis and is not included in Figure 1.4.2). The red line (b) illustrates the energy changes as two benzene molecules approach each other in a T-shaped configuration with a center-to-center distance of ca. 4.9–5.0 Å.(28) Their overlapping volumes of revolution suggest that while they should be able to rotate, it would have to be in a correlated manner. One can hypothesize that for two parallel benzene molecules to rotate independently, they would have to be at a center-to-center distance of ca. $\geqslant$7.0 Å. In molecular crystals, this separation would require a stable framework created by a suitable stator, as suggested by the blue blocks. Close-packing interactions in this case would have to be satisfied by sufficient

contact between adjacent stators, with their energy represented by the dotted blue line. However, the free volume generated in this case may have a tendency to trap solvent molecules or lead to the collapse of the crystal lattice. The final scenario is illustrated by benzene molecules at distances greater than ca. 9 Å, which make it possible for the molecules to rotate independently. Notably, large free volumes can remain stable in solid-state systems that are well beyond the attractive region of the intermolecular potential and also take advantage of coordination and covalent bonds to create robust structures. These structures give rise to the solid blue potential, examples of which can be found in a number of MOFs.[29]

1.5. Rotational Dynamics and Packing Coefficients

A measure of the average free volume that exists in a crystalline solid can be obtained by determination of the packing coefficient (C_k),[30] which is given by the volume of the unit cell contents (V_{Mol}) in relation to the volume of the unit cell (V_{Cell}), $C_k = V_{Mol}/V_{Cell}$. It can be expected that packing forces will tend to make the maximum number of surface contacts, which will depend on the shape of the molecule. For example, it has been shown that the densest 3D packing for spheres of equal size uses approximately 74% of the volume ($C_k = 0.74$), while the densest packing for cubes of equal size can use 100% of the space. It has been shown that organic crystals with irregular molecular shapes tend to have packing coefficients that vary from ca. 0.64 to 0.77, with structures characterized by voids and protuberances producing the lower-end values.[29] By contrast, extended crystal structures based on coordination bonds between relatively rigid spacers (such as MOFs) can sustain large amounts of empty space with C_k values as low 0.10 (i.e., void volumes of 90%).[31] While C_k values do not give an indication of how the free volume is distributed in the unit cell, at a first approximation it seems reasonable to expect that packing coefficients should be

inversely correlated with internal dynamics. If this were the case, then one would expect a rough inverse correlation between packing coefficient and rotational rate and the data points should cluster along a diagonal that goes from the top left to the bottom right in Figure 1.5.1. However, ambient temperature k_r values on the vertical axis as a function of the calculated C_k for 31 amphidynamic crystals with 36 crystallographically distinct rotational sites fail to follow the expected trend, indicating that there are other factors to consider.

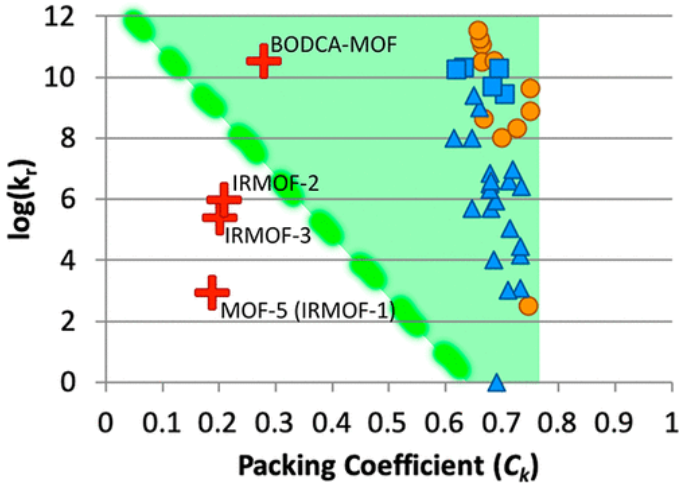

Figure 1.5.1. (a) Scatter plot of the room-temperature Brownian rotational velocities (k_r, s^{-1}) of amphidynamic crystals as a function of their packing coefficients (C_k). The different symbols correspond to four different sets of amphidynamic crystals: (I) the "plus" signs correspond to MOFs; (II) circles are the high symmetry rotators; (III) triangles are molecular rotors with phenylene rotators and stators derived from a trityl or triptycyl motif, and (IV) squares correspond to supramolecular rotors.

Figure 1.5.1 includes packing coefficients from four different types of amphidynamic crystals that have well (or reasonably well) characterized ambient temperature (300 K) rotational dynamics. These include (I) MOF rotors (crosses), (II) molecular rotors with rotators that have a

rotational symmetry order higher than C_2 (circles), (III) molecular rotors with phenylene or heterocyclic rotators and stators derived from a trityl or triptycyl motif (triangles), and (IV) molecular rotors with supramolecular axles (squares).

We obtained each of the packing coefficients with molecular volumes determined with modeling software[32,33] and the unit cell volumes from their single-crystal X-ray diffraction structures. Rotational Brownian motion in crystals, k_r, was measured using three variable-temperature (VT) solid-state NMR methods depending on the rates (or frequencies, in units of s^{-1}, or hertz) at which the moving groups exchange between different sites along their rotational potential.[19] Motions occurring with slow exchange rates (ca. 100 to 10000 Hz) can be obtained by VT ^{13}C CPMAS NMR when the different sites have sufficiently different chemical shifts. Rotational exchange rates in the regime of 10 kHz to 10 MHz can be obtained by taking advantage of line-shape analysis of the spectra obtained by quadrupolar echo ^2H NMR using ^2H-labeled samples. This is a powerful method, as it provides information not only on the site-exchange frequencies but also the trajectories of motion. Finally, the most convenient method to measure rotational dynamics in the high frequency regime of ca. 10 MHz to >600 MHz is the VT measurements of spin–lattice relaxation of magnetic nuclei (^1H, ^2H, ^{13}C, ^{19}F, etc.) in the rotator. After gathering exchange rate (k_r) data from these techniques as a function of temperature, one can use the Arrhenius equation, $k_r = A \exp(-E_a/RT)$, to determine activation energies (E_a) and pre-exponential factors (A), which make it possible to estimate the rate of rotation at 300 K. While the activation energy represents the height of the barrier along the rotational potential, the pre-exponential factors represent an attempt frequency, which is related to the frequency of the torsional mode that causes oscillations at the bottom of the potential energy well. For small rotators, the pre-exponential factor has values on the order of 10^{11}–10^{12} s^{-1}.

It is clear from Figure 1.5.1 that there are significant deviations from the expected behavior with data points roughly segregated on the high- and low-packing density regions. Molecular and supramolecular crystals cluster on the right side of the plot, covering packing coefficients that vary from ca. 0.6 to 0.8 and rotational frequencies that range from static to those that are close to the upper theoretical limit, given by the pre-exponential factor, ca. $k_r \approx A = 10^{11}$–10^{12} s^{-1}. By contrast, the molecular rotors incorporated as MOF pillars studied by our group so far cluster on the left side of the figure. One can see that despite MOFs having the lowest packing coefficients (C_k < 0.3), the data points reveal examples of MOF kinetics that range from slow ($k_r \approx 10^3$ s^{-1}) to moderate ($k_r \approx 10^6$ s^{-1}) to ultrafast ($k_r \approx 5 \times 10^{11}$ s^{-1}) rotation. To explain these differences, one must consider that in addition to intermolecular forces, which determine the energetics of rotation in terms of free volume, axial symmetry, or gearing motions, one of the key parameters in determining rotational dynamics is the intrinsic rotational potential of an isolated rotator. When intramolecular and intermolecular factors are analyzed together, one can recognize two general regimes of dynamic behavior. These correspond to the limits of (A) activation control, when rotational motion is limited by the intrinsic barrier of the rotator, and (B) diffusion control, when rotational motion is limited by intermolecular hindrance arising from near neighbors in the lattice, which can be seen as a measure of crystal fluidity (see section 1.9).

1.6. Activation-Controlled Rotation in Amphidynamic Metal–Organic Frameworks

While it should be possible to prepare metal–organic frameworks that cover the range of rotor–rotor distances and interactions shown in Figure 1.4.2, the MOFs in Figure 1.5.1 were selected with the expectation that they would have sufficiently large free volumes for their rotators to have no steric hindrance. Their structures are based on zinc oxide clusters linked by aromatic

dicarboxylate rotators [Zn_4(rotatorC_2O_4)$_3$] related to the iconic MOF-5, which is also known as IRMOF-1 (Figure 1.6.1).

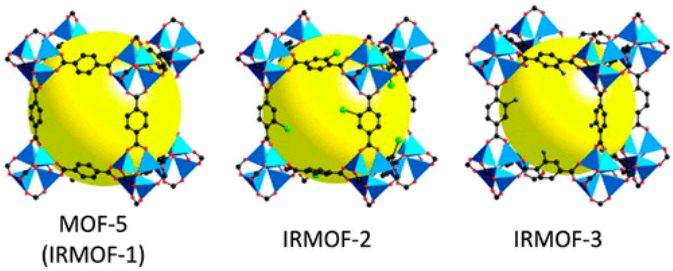

Figure 1.6.1. Structure of cubic isoreticular metal organic frameworks (IRMOF) with substituted benzene dicarboxylate linkers and zinc oxide clusters.[34]

Importantly, all of these structures have empty volumes that are greater than the volumes of revolution of the rotator, and the four IRMOFs included in Figure 1.5.1 are a good example of the conditions shown in Figure 1.4.2d, with $C_k < 0.3$. Lacking steric hindrance, their rates of rotation vary significantly because those rates are determined by intrinsic electronic barriers. It was first shown that the loss of π-conjugation between the two coplanar carboxylates and the central phenylene at the rotational transition state of IRMOF-1 gives rise to a relatively high energy barrier of 11.3 kcal/mol.[20] This high barrier and a pre-exponential factor of ca. 1.6×10^{12} s^{-1} lead to rates of rotation of ca. 10^4 s^{-1} near ambient temperature. It was subsequently shown that changes in the intrinsic rotational potential of the aromatic rotators are altered by substituents. In that vein, a bromine substituent on the phenylene rotator in the case of IRMOF-2 studied by Winston et al.[35] showed a 300 K rotational frequency that was increased by 2 orders of magnitude to ca. 2.6×10^6 s^{-1}. This increased rotational frequency is the result of having a similar pre-exponential factor ($A = 5 \times 10^{11}$ s^{-1}) and a lower barrier of $E_a = 7.3$ kcal/mol. However, as suggested in Figure 1.6.2a,

the smaller barrier is the result of the ground state destabilization that occurs from the steric congestion around the metal centers, which prevents full conjugation between the 2-bromophenylene and the carboxylate groups in the ground state. The effect of a 2-aminophenylene in the case of IRMOF-3 was shown to be more complex.[36] A very slow rotational frequency of *ca.*

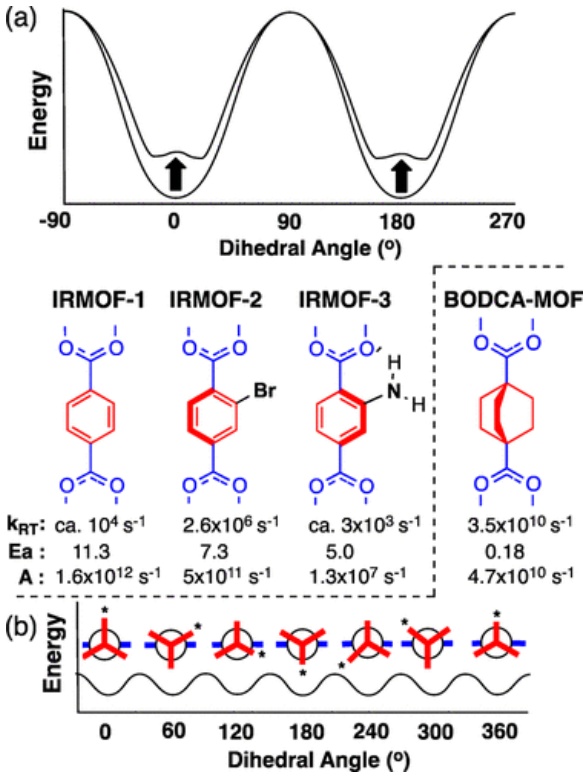

Figure 1.6.2. (a) Differences in rotational frequencies of IRMOF-1, IRMOF-2 (2-Br), and IRMOF-3 (2-NH_2) can be assigned to changes in the barrier height that result from the ground-state steric destabilization by the *ortho*-substituents, which prevent planarization and full π-conjugation, and changes in the low pre-exponential factor in the case of IRMOF-3 (see text). (b) Removal of π-conjugation and a 6-fold rotational symmetry potential in the aliphatic bicyclo[2.2.2.]octane dicarboxylate rotator in the case of BODCA-MOF reduces the activation energy (0.12 kcal/mol) to values that are much lower than thermal energies near 300 K (ca. 0.6 kcal/mol).

3×10^3 s^{-1} at 300 K was estimated despite a lower activation barrier of only E_a = 5.0 kcal/mol as a result of a lower pre-exponential factor, $A = 1.3 \times 10^7$ s^{-1}, which is about 3 orders of magnitude smaller than those of IRMOF-1 and IRMOF-2. While the lower barrier seems to be the result of a substantial ground-state destabilization, the low pre-exponential factor reflects an attempt frequency for rotation that is not uniquely determined by the frequency of the thermal oscillations of the rotator but is instead modulated by the need to cleave the N–H···O═C hydrogen bond, which becomes a rotational rate-limiting step.

That the electronics of the intrinsic energetic potential are responsible for the rotational frequency of the benzenedicarboxylates in the IRMOF series could be shown by the design and synthesis of a new structure with a saturated bicyclo[2.2.2]octanedicarboxylate (BODCA) rotator (Figure 1.6.2b).[21] In addition to the removal of a significant electronic barrier, the BODCA linker has a 3-fold axis of symmetry, which combines with the 2-fold rotational symmetry of the carboxylate to generate a 6-fold rotational potential, as shown in the bottom of Figure 1.6.2b, where Newman projections of the rotamers are shown along with the corresponding small changes in energy. The rotational dynamics of samples of BODCA-MOF measured between 298 and 6 K revealed a barrier of only 0.18 kcal/mol and a pre-exponential factor of 4.7×10^{10} s^{-1}, which makes it the first example of a crystalline solid with structural components that undergo barrierless rotation over a broad temperature range. While a low intrinsic barrier and the lack of intermolecular hindrance may suggest high temperature gas phase-like rotation, molecular dynamics simulations confirm that BODCA-MOF behaves as a diffusion-controlled molecular rotor. With rotational barriers that are smaller than thermal energies, Brownian rotation is determined by the coupling of angular motion with normal modes and lattice vibrations, which can have the same or different

phase, such that motion occurs in a random fashion with no sustained directionality and angular momentum.

1.7. Diffusion-Controlled Rotation in Close-Packed Molecular Crystals

Disubstituted acetylenes are among the most versatile design elements for the construction of molecular rotors. Taking advantage of robust synthetic methods based on transition-metal-catalyzed coupling reactions and nucleophilic additions with acetylide anions, alkynes can be used to link a wide variety of stators and rotators while also providing them with an axle for rotation. Importantly, acetylenes have orthogonal π-orbitals with an effective cylindrical symmetry, such that rotation about triple bonds causes no changes in ground-state energetics[37] (Figure 1.7.1, red line) even when the rotator and the stator at the two ends are linked through sp^2-hybridized carbon atoms. On the basis of these characteristics, many molecular rotors with alkyne axles are based on a simple design where there is a central rotator coaxially linked to bulky groups that play the role of the stator (Figure 1.7.1). Molecular motion in such close-packed molecular crystals is hindered by contacts between the otherwise freely moving rotator and neighboring molecules in the lattice,

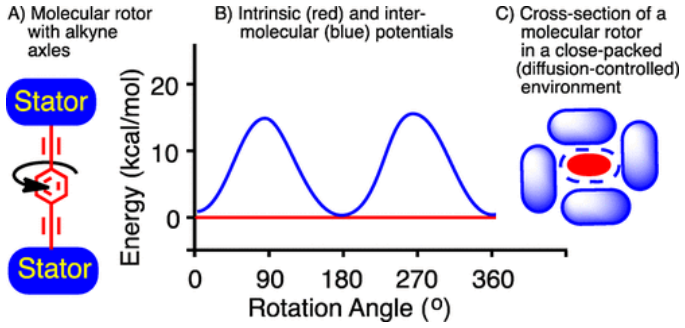

Figure 1.7.1. Molecular rotors with alkyne axles have a (nearly) barrierless intrinsic potential, which makes their solid-state rotational dynamics fall in the diffusion-controlled regime. Barriers depend on the rigidity of the environment.

which form a relatively hard boundary that conforms to the van der Waals surface of the rotator. As indicated in Figure 1.7.1, rotational motion under these conditions falls in a diffusion-controlled regime where local volume fluctuations are needed for rotation to take place.[38]

1.8. Variations in the Structure of the Rotator: Axial Symmetry Order[24]

Based on simple geometric arguments, we suggested a few years ago that the extent of overlap between the shape of the rotator and its volume of revolution should be a key factor in determining rotational dynamics. Since the crystal environment is expected to conform to the shape of the rotator, the corresponding overlap will depend on the size, shape, and the axial symmetry order of the rotator.(24) As illustrated in Figure 1.8.1, a set of polygonal rotators with a given rotational symmetry order C_n will have periodic rotary potentials with energy profiles that have "n" minima and "n" maxima, angular displacements of 360/n°, and barriers that become smaller as the shape of the rotator approaches the shape of a cylinder, when $n \rightarrow \infty$. Ideal potential energy surfaces will have a periodic dependence on rotational angle (θ) given by $E(\theta) = {}^1/_2E_0\ (1 - \cos n\theta)$. One of the most interesting applications of rotational symmetry can be found in the design of the bacterial flagellum[39] where the symmetry order of the flagellar rotator (n_{Rot} = 24–26) does not match the symmetry of the stator (n_{Stat} = 34–36), giving rise to a potential energy profile where the effective symmetry is the product of the two, $n_{Effective} = n_{Rot} \times n_{Stat}$, such that combined they approach a smooth cylinder-like surface. Furthermore, an increase in the number of "n" results in greater directional resolution that may be addressed with external stimuli when a suitable dipole is included in the rotator structure.[40,41] Similarly, rotators with $n > 2$ and vertices extending in a radial manner may be envisioned as structural elements for the design of n-toothed molecular gears, as shown for the three-toothed triptycene gear in Figure 1.4.1.

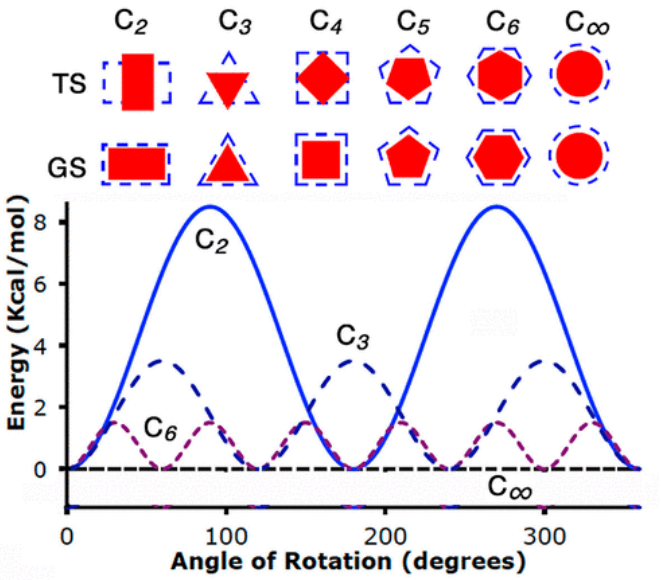

Figure 1.8.1. (Top) Overlap between the cross sections (solid red) and van der Waals surface boundary (dotted blue) of a set of hypothetical polyhedral molecular rotators with axial symmetry order varying from C_2 to C_∞ in their rotational ground state (GS) and transition state (TS). (Bottom) Changes in the potential energy profile for rotators with C_2, C_3, C_6, and C_∞ rotational axis (adapted from ref 24).

Figure 1.8.2 shows a series of halogen (**1**–**5**, **7**, and **14**) and hydrogen (**8**, **9**) bonded supramolecular rotors, as well as molecular rotors with steroidal (**11**) or triaryl-substituted stators (**6**, **10**, **12**, **13**, and **15**) that are linked to high axial symmetry rotators. Among them, a homologous set of with triphenylsilyl stators and alkyne axles have rotators with an increasing rotational symmetry order (C_n). These include phenylene rotor **6** (C_2), cubyl rotor **15**, and BCO rotor **12** (C_3) and a *para*-closo-dodecacarborane rotor **10** (C_5). It was shown that crystals of the 2-fold symmetric phenylene rotor **6** have a barrier of 8.5 ± 2.5 kcal/mol and a rotational frequency of 9 MHz at 300 K. Increasing the symmetry to BCO **12** decreases the barrier to 3.5 ± 0.2 kcal/mol while increasing the room temperature rotational frequency by an order of magnitude, to 105 MHz. The trend

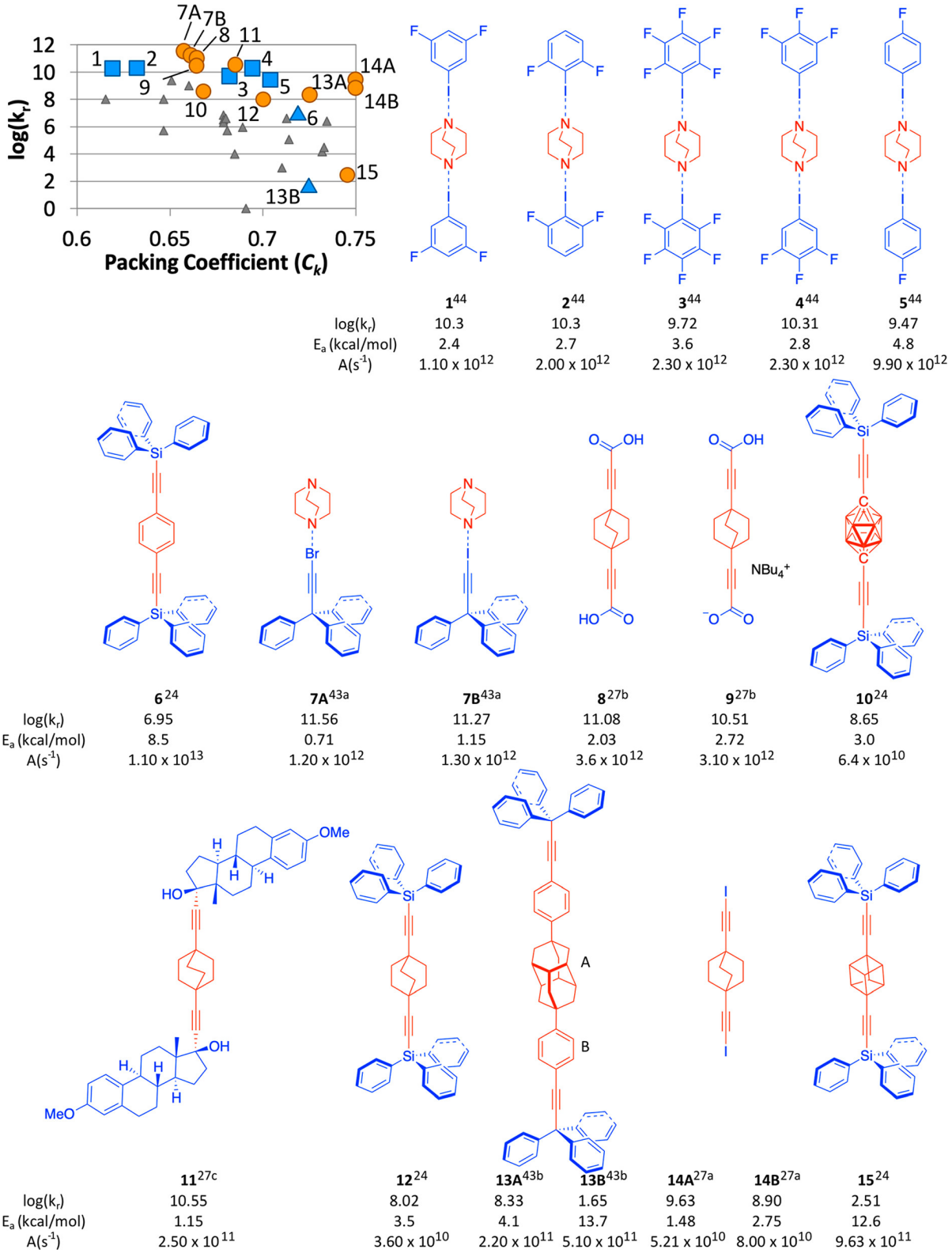

Figure 1.8.2. Scatter plot of the ambient-temperature Brownian rotational velocities (k_r, s^{-1}) of amphidynamic crystals of molecular and supramolecular rotors with high axial symmetry order as

a function of their packing coefficients (C_k). Squares correspond to supramolecular rotors, circles to other high-symmetry rotators, and triangles to molecular rotors with phenylene rotators and trityl or triptycyl stators. Numbered rotor structures are shown with their literature reference as a superscript as well as their 300 K rotational velocities [log(k_r)], activation barriers (E_a), and pre-exponential factors (A). Both the diamantane and the phenylene in compound **13** rotate; they are labeled **13A** and **13B**, respectively. Molecular rotor **14** crystallizes in two distinct sites that are labeled **14A** and **14B**.

continues with the 5-fold symmetric carborane rotor **10**, which was shown to have an even lower barrier of 3.0 ± 0.1 kcal/mol and an increase in its room temperature rotation to 446 MHz. An exception was encountered with the smaller 3-fold symmetric cubyl rotor **15**. This relatively small rotator displays an unexpectedly slow rotational frequency of only 320 Hz at 300 K due to specific packing interactions wherein a phenyl group from an adjacent triphenylsilyl stator is packed exceptionally close to the rotator in a way that obstructs rotation and results in an unusually high activation energy of 12.6 kcal/mol.[24]

It should be pointed out that high-symmetry rotators may adopt rotationally disordered structures that increase the average symmetry of their crystal space group. For example, crystal structures with BCO rotators are often solved with an inversion center that is not present in the BCO structure but that can be satisfied on average by a local disorder where the BCO group adopts two positions related by a 60° rotation with equal probability.[42] Usually observed at higher temperatures, this disorder transforms the point group of the BCO from a local D_{3h} into an average D_{6h} and the rotational axis from C_3 to C_6. An example is shown in Figure 1.8.2 with the halogen-bonded supramolecular rotor **3** formed with 1 equiv of 1,4-diazabicyclo[2.2.2]octane (DABCO)

and two of pentafluoroiodo benzene. The structure solution of the X-ray diffraction data displays increasing rotational disorder in going from 103 to 200 K, with a phase transition occurring between 220 and 250 K (Figure 1.8.3).

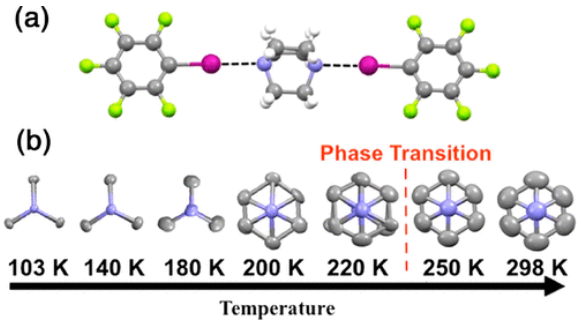

Figure 1.8.3. (a) Crystal structure data of a representative supramolecular rotor based on halogen bonding between 2,4-diazabicylo[2.2.2]octane (DABCO) and pentafluoroiodobenzene. (b) Crystal structures obtained at increasing temperature display increasing rotational disorder of the DABCO group.

The 3-fold symmetry and the relatively spherical shape of the BCO rotator make it an ideal rotator for creating systems with low rotational barriers in close packed crystals when linked to the stator by a barrierless alkyne linkage or a supramolecular bond. In fact, all of the supramolecular high symmetry rotors highlighted in Figure 1.8.2 feature a BCO rotator, and they all have ambient temperature rotational frequencies greater than 200 MHz with activation energies that are less than 5 kcal/mol.[27,43,44] Additionally, most of these crystals have packing coefficients of 0.65 or greater, so that their fast dynamics are not the result of a lower density environment but rather the result of a volume-conserving rotational motion.[24]

1.9. Variations in the Structure of the Stator: The Emergence of "Crystal Fluidity"

In order to explore the effects of structural variations in the stator, we took advantage of a synthetically accessible 1,4-phenylene rotator and two sets of stator structures that are relatively easy to obtain and modify. One set consists of triptycyl molecular rotors prepared by the installation of two coaxial 9-triptycyl acetylenes, prepared by the Diels–Alder addition of benzynes to ethynylanthracenes, onto 1,4-dihalogenated benzenes by a Pd(0)-mediated Sonogashira reaction (Figure 1.9.1a).[45] The other is based on triarylmethyl molecular rotors obtained in a similar manner by taking advantage of readily available triarylacetylenes (Figure 1.9.1b).[46] The relatively rigid 3-fold symmetric triptycyl and triarylmethyl stators were expected to help guide the packing structure and the integrity of the crystal lattice while providing the conditions needed for the mobility of the rotator, which might include the steric shielding hypothesized in Figure 1.4.2c. The starting point to explore this concept began with molecular rotors **16** and **17**, with unsubstituted triptycyl and triarylmethyl groups (Figure 1.9.1, R = H), which turned out to be robust crystalline solids with their rigid rod-like structures adopting a low symmetry order (space group $P\bar{1}$), which

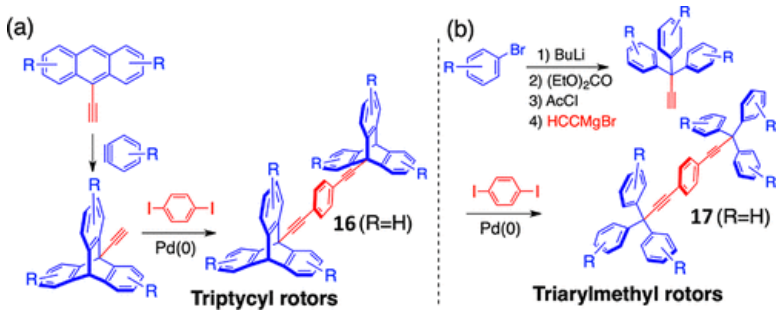

Figure 1.9.1. (a) General synthetic pathway for rotors containing triptycyl stators: ethynylanthracenes undergo a Diels–Alder cyclization with a benzyne to form the triptycyl stator before being coupled to the rotator. (b) General synthetic pathway for rotors containing trityl stators: diethylcarbonate and a bromobenzene are used to form the trityl stator before being coupled to the rotator.

would ensure that all phenylenes rotate on the same plane of the crystal, as would be desired for a dipolar array.[45,46] However, rather than leaving a low-packing density region in the area of the rotator, crystals of molecular rotor **16** grown from *m*-xylene incorporated the solvent into the structure. On the other hand, triarylmethyl molecular rotor **17** could be obtained either solvent-free from CH_2Cl_2, or with solvent incorporated when grown from benzene.[47] It was shown that crystals of molecular rotor **17** undergo a reconstructive phase transition upon solvent removal. A stark difference between the crystals of molecular rotors **16** and **17** is that, while the former is essentially static, VT solid-state ^{13}C CPMAS NMR showed that the latter undergoes ambient temperature rotational site exchange in the kilohertz regime with activation energies in the range of 12–15 kcal/mol and pre-exponential factors of ca. 10^{14} s^{-1}. A comparison of their packing coefficients revealed that crystals of **16** and **17** have similar packing densities (C_k = 0.7), demonstrating that the same average amount of empty space does not result in similar rotational freedom. A simple analysis of the cross section of the phenylene rotators in crystals of **16** and **17** in Figure 1.9.2a confirms that there are no significant differences in the volume available. In fact, the primary reason for their different dynamic behavior was suggested by subsequent computational modeling of the two crystal forms of triarylmethyl structure **17**, which revealed that rotation in the crystal lattice relies on conformational degrees of freedom available to the triphenylmethyl groups. It was discovered that all of the phenyl groups in the crystal lattice oscillate about their equilibrium positions, creating transient cavities that enable the central phenylene to rotate.[38] The magnitude of the conformational motions and the corresponding cavity fluctuations can be qualitatively appreciated by tracking the displacement of every atom in the surrounding phenyl groups as a function of the rotational angle during a 180° ring flip of the central phenylene. This is shown in Figure 1.9.2b with data corresponding to rotational angles of 30°, 60°, 90°, 150°, and 180°, where

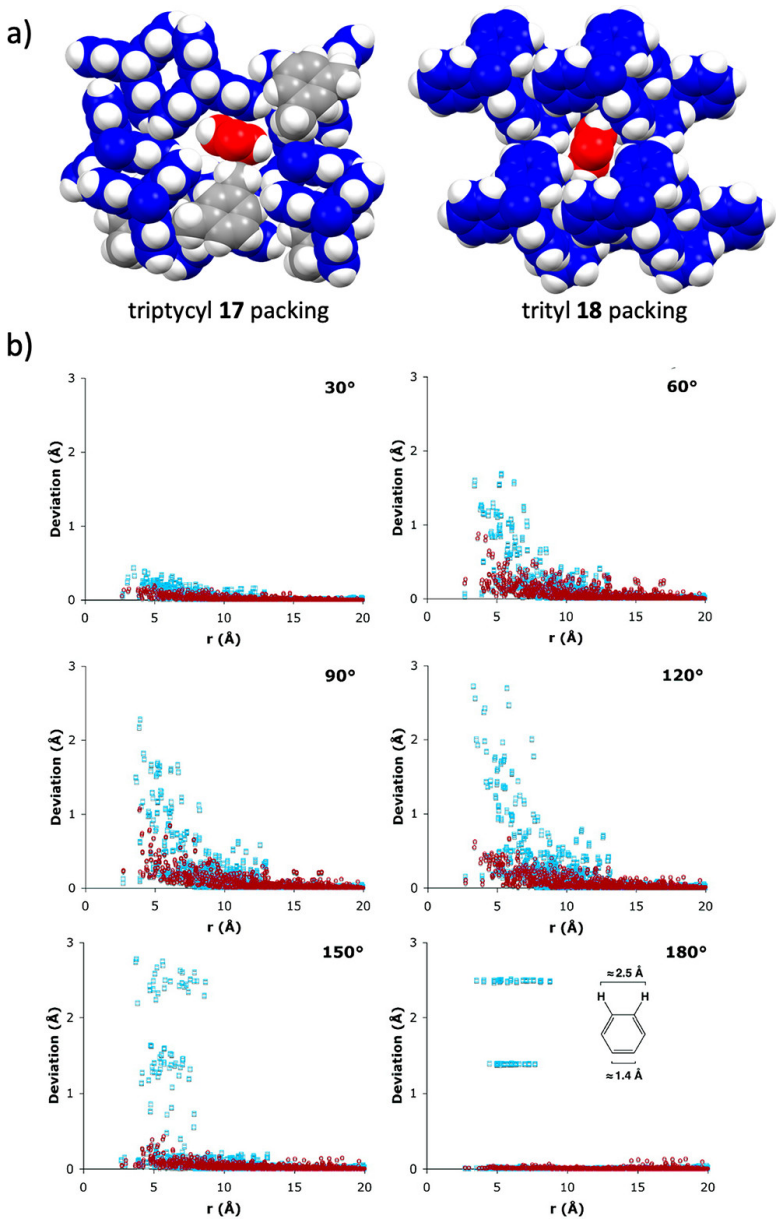

Figure 1.9.2. (a) Cross sections of the crystal structures around the phenylene rotators of triptycyl and trityl rotors **16** and **17** showing the lack of free volume surrounding each phenylene rotator. (b) Calculated displacement of neighboring atoms surrounding a reference rotator as it undergoes a 180° flip. The phenyl groups corresponding to near neighbor trityl stators are shown in red, and those corresponding to the solvated crystal, including benzene molecules, are shown in blue. Blue

atoms undergoing displacements of 1.4 and 2.5 Å correspond to benzene molecules undergoing a correlated rotation with the central phenylene (adapted from ref 38).

each point corresponds to a single atom in the neighboring trityl groups and also benzene molecules in the case of solvated structure (data points shown in blue). One can see that rotation of the central phenylene is accompanied by a significant rearrangement of the neighboring lattice with the maximum observed at the rotational transition state of 90° and a return to the equilibrium positions after 180°, with the exception of the benzene molecules that undergo a correlated 60° rotation. While the simulations of analogous molecular rotors would be needed to confirm it, we propose that the type of lattice fluctuation displayed by the nearby atoms, or *crystal fluidity*, is likely to play an important role in the rotational dynamics of close-packed crystalline molecular rotors.

It is worth highlighting that the ambient temperature dynamics of analogues of **17**[46] with a bridging azobenzene (**18**[48e]), a gold(I) phosphane extended axle (**19**[48d]), mixed trityl and tryptycene stator (**20**[48f]), imine-extended rotator (**21**[48g]), polar fluorinated phenylenes (**22**[48b] and **24**[48a]), N-heterocyclic rotators (**23**[48c]), and a dual rotor with a pentypticene core (**25**[48h]) display dynamics that range over 3 orders of magnitude, from the $10^3 s^{-1}$ to the 10^6 s^{-1} regime, even though their packing coefficients are narrowly clustered between 0.65 and 0.74 (Figure 1.9.3).[48]

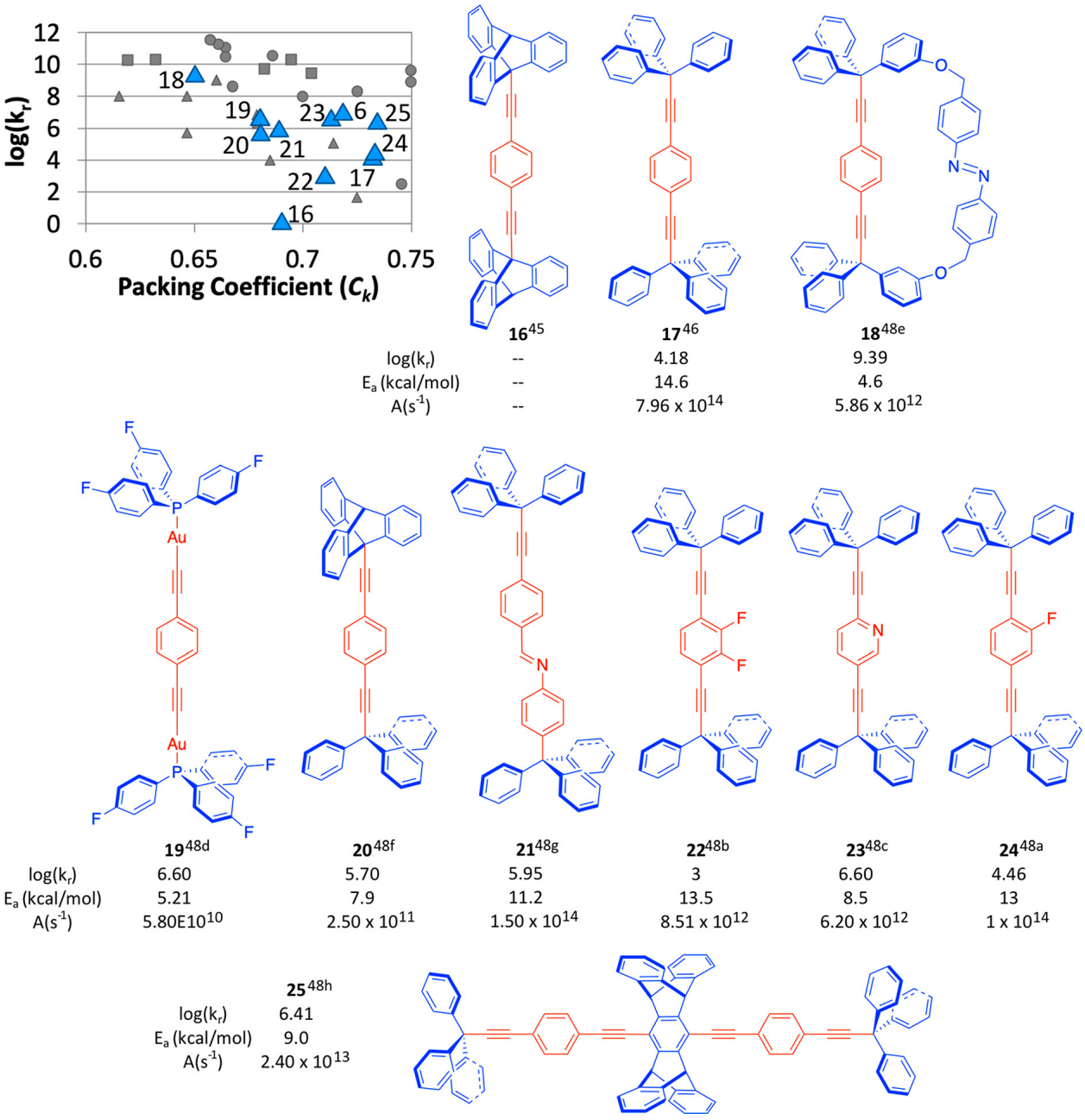

Figure 1.9.3. Scatter plot of the ambient-temperature Brownian rotational velocities (k_r, s^{-1}) and packing coefficients of amphidynamic crystals with unsubstituted triptycyl and/or trityl stators shown as blue triangles. Numbered rotor structures are shown with their literature reference as a superscript as well as their 300 K rotational velocities [log(k_r)], activation barriers (E_a), and pre-exponential factors (A). Compound **6** is shown in Figure 1.8.2.

We hypothesize that crystal fluidity accounts for the lack of a simple correlation between C_k and k_r displayed in Figure 1.5.1, with points that occur above the diagonal signaling the presence of internal degrees of freedom that cause volume fluctuations where rotation can take place.

1.10. Engineering Crystal Fluidity with Expanded Stators

The significance of crystal fluidity is also supported by results with molecular rotor **26** with peripheral *tert*-butyl groups that increase the rotational frequency of the central phenylene up to 10^8 s^{-1} by increasing the number of degrees of freedom in the structure.[50a] Similarly, triptycyl rotor **27** (Figure 1.10.1), where the size of the stator was extended by the addition of peripheral methyl groups,[49] which intended to prevent the interdigitation of adjacent molecules in the lattice while promoting a layered packing motif. While the desired solid-state architecture was achieved, the space formed by adjacent rotors was relatively large and stable crystals could only be obtained with the inclusion of bromobenzene, which was used as the solvent of crystallization (Figure 1.10.1). Despite relatively tight packing, phenylene rotation in crystals of **27** occurred with a relatively low activation energy of 4.4 kcal/mol, which leads to ambient temperature rotational rates of ca. 1.1×10^9 s^{-1}. Considering the disposition of the solvent and rotator revealed by the cross section in Figure 1.10.1, it seems very likely that rotation in the case of **27** may involve the correlated motion of the solvent molecules, implying that the solvent contributes a certain level of fluidity to the amphidynamic crystal. Furthermore, a number of expanded stators based on trityl motifs have also been investigated.[50] Trityl rotors with *meta*-methoxy, 3,5-di-*tert*-butyl, 2,5-diphenyl, and *m*-trialkylsilyl substituents have all been explored and shown to have both faster dynamics and lower packing coefficients than the unsubstituted compound **17**. These compounds

lend additional credibility to the idea that added conformational degrees of freedom are likely to increase the fluidity of the lattice.

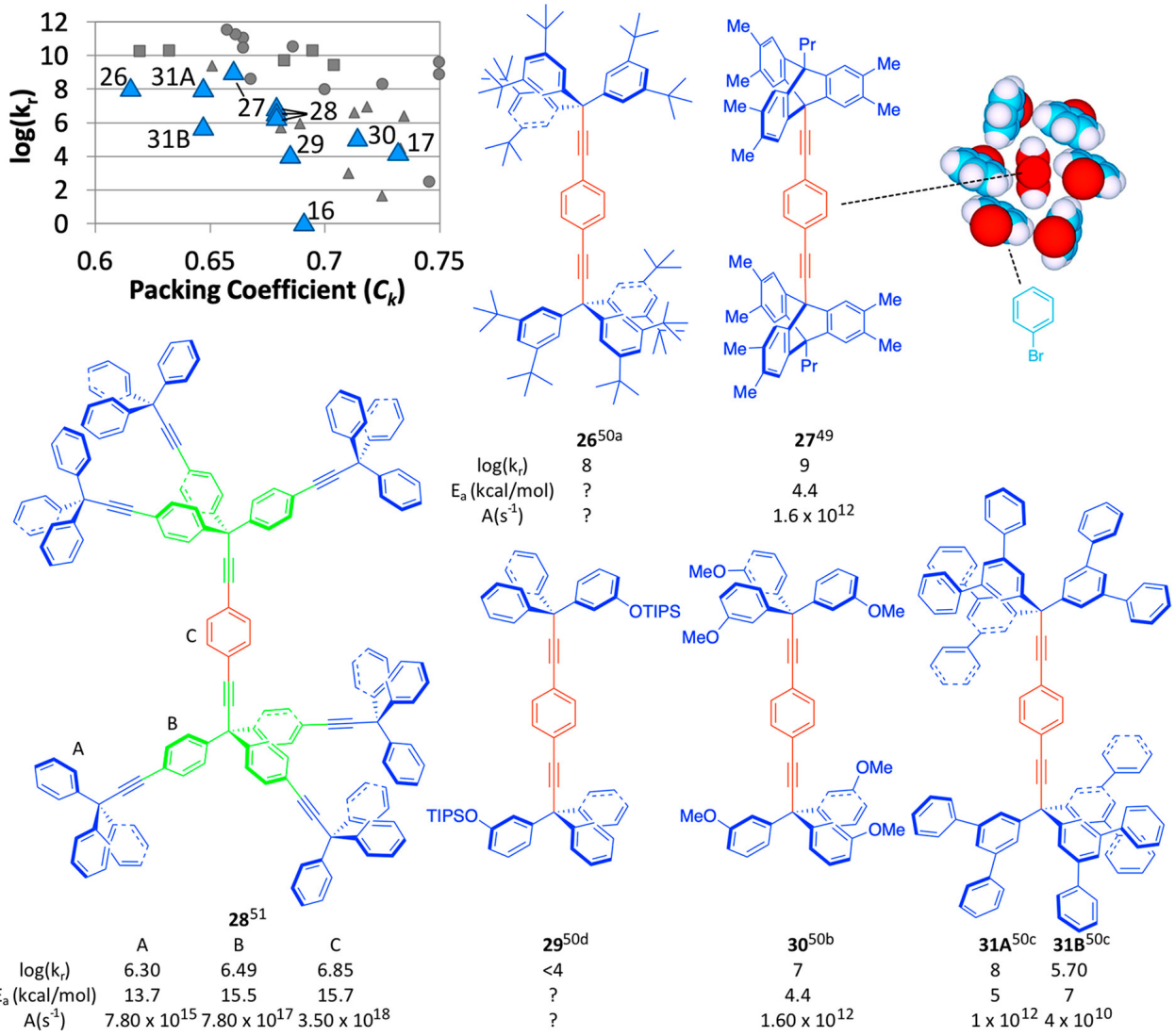

Figure 1.10.1. Scatter plot of the ambient-temperature Brownian rotational velocities (k_r, s^{-1}) and packing coefficients of amphidynamic crystals with expanded stators highlighted as triangles. A view down the rotational axis of the phenylene in **27** suggests that correlated motion of surrounding bromobenzene molecules may be responsible for the fast rotation observed. Fast rotation was measured at all three sites in dendritic rotor **28**. Compound **31** crystallizes with distinct crystallographic sites **31A** and **31B**. Numbered rotor structures are shown with their literature

reference as a superscript as well as their 300 K rotational velocities [log(k_r)], activation barriers (E_a), and pre-exponential factors (A). Unsubstituted triptycyl and trityl model systems **16** and **17** are shown along with their dynamics in Figure 1.9.3.

1.11. Dynamics of Fluid Crystalline Rotors

An additional powerful example of this concept emerged from the observation of dendritic rotor **28**, which was designed to test the effects of an expanded stator on the dynamics of the central rotator (Figure 1.10.1).[51] Recognizing that this rotor has three separate positions where rotation could be observed as a manifestation of crystal fluidity, selectively ^{2}H-labeled samples were prepared to determine the dynamics of the central phenylene shown in red, the branch phenylenes shown in green, and the peripheral phenyl groups shown in blue. Molecular rotor **28** is unique because the stator is defined by the σ bonding framework of the structure while all of the bulky aromatic groups are mobile. All three positions display apparent pre-exponential factors and activation energies with values that are over 10^{15} s^{-1} and 13 kcal/mol, respectively, which give rise to ambient temperature rotation in the MHz regime. It should be noted that these pre-exponential factors exceed the 10^{12} s^{-1} maximum that is expected for an elementary process.[52] This was observed in another case where the steep slope of the Arrhenius plot and a large pre-exponential factor were interpreted as the result of softening of a rigid glass on its way to become a rotational fluid.[53] Part of this increased fluidity is due to the mobility of the three elements, but it is also enabled by a large amount of disordered solvent that allows for a packing coefficient of ca. 0.68.

1.12. Conclusions

A simple approach for the design of molecular rotors based on the volume of revolution and center-to-center distance between neighboring rotators suggests that rotational dynamics should be governed by (1) the creation of free space, (2) the use of volume-conserving shapes, like spheres or cylinders, or (3) gearing motions when adjacent rotators are interdigitated. However, for general structures lacking the latter two properties, a comparison of average free volume measured in terms of packing coefficient (C_k) and ambient temperature Brownian rotational velocities revealed that this simple approach ignores several key aspects of the behavior of amphidynamic solids. The survey presented herein reveals two sets of governing principles: one applies to MOFs and extended solids with rotations enclosed in large empty cavities and the other determines the rotational dynamics of close-packed molecular crystals. It can be shown that rotational motion in the solid state occurs in an activation-controlled regime when there is sufficient free volume for rotational dynamics to depend on the intrinsic (gas phase) electronic barrier about the bond (axle) that links the rotator and the stator. For π-conjugated systems, the energy cost of breaking conjugation can lead to very high barriers, which can be reduced by taking advantage of structural factors that can destabilize the ground state. The use of nonconjugated rotators with high orders of rotational symmetry can lead to ultralow intrinsic barriers and ultrafast rotation. By contrast, molecular crystals do not benefit from large amounts of free volume and their dynamics become diffusion-controlled, such that rotational barriers are determined by how well crystal packing can accommodate the motion of the rotator. For spherically shaped, volume-conserving rotators such as bicyclo[2.2.2]octane,[21] 1,12-dicarbaclosocarborane,[24] and C_{60},[54] there is a good overlap between the volume of revolution and the volume of the packing cavity that contains it, such that fast dynamics and low barriers can be observed despite a relatively high

packing coefficient. For molecular rotators with nonspherical shapes, such as 1,4-phenylenes, Brownian dynamics are determined by whether or not the crystal environment around the rotator can reaccommodate to create transient cavities for rotation to occur, a property that we have termed "crystal fluidity". The importance of crystal fluidity is strongly supported by the comparison of molecular rotors with vastly different degrees of torsional freedom.[37] For example, molecular rotors based on conformationally flexible triphenylmethyl stators are significantly more dynamic than analogous molecular rotors based on rigid triptycene stators. The effect of crystal fluidity is highlighted by the fast rotational motion of all phenylene branches in dendritic rotors with local conformational flexibility.[51] The survey presented in this perspective revealed a new set of governing design principles for crystalline molecular rotors, which had previously been centered around the creation of free space. The concept of crystal fluidity will inform the future design of crystalline molecular rotors and amphidynamic crystals by considering the use of flexible frameworks in addition to the creation of empty space. It is reasonable to expect that improvements in the design and preparation of molecular rotors will make it possible to improve their performance in a number of promising applications.[15,55]

Author's Note: Chapter 1 is modified from the publication Howe, M. E.; Garcia-Garibay, M. A. The Roles of Intrinsic Barriers and Crystal Fluidity in Determining the Dynamics of Crystalline Molecular Rotors and Molecular Machines *J. Org. Chem.* **2019**, *84*, 9835-9849.

1.13. References

[1] (a) Iwamura, H.; Mislow, K. Stereochemical Consequences of Dynamic Gearing. *Acc. Chem. Res.* **1988**, *21*, 175−182. (b) Oki, M. Unusually high barriers to rotation involving the tetrahedral carbon atom. *Angew. Chem., Int. Ed. Engl.* **1976**, *15*, 87−93. (c) Mislow, K. Stereochemical consequences of correlated rotation in molecular propellers. *Acc. Chem. Res.* **1976**, *9*, 26−33. (d) Anelli, P. L.; Spencer, N.; Stoddart, J. F. A molecular shuttle. *J. Am. Chem. Soc.* **1991**, *113*, 5131−5133. (e) Kelly, T. R.; Bowyer, M. C.; Bhaskar, K. V.; Bebbington, D.; Garcia, A.; Lang, F.; Kim, M. H.; Jette, M. P. A molecular brake. *J. Am. Chem. Soc.* **1994**, *116*, 3657−3658. (f) Bedard, T. C.; Moore, J. S. Design and synthesis of molecular turnstiles. *J. Am. Chem. Soc.* **1995**, *117*, 10662−10671. (g) Gakh, A. A. Molecular devices: an introduction to technomimetics and its biological applications; Wiley: Hoboken, **2018**. (h) Jimenez-Bueno, G.; Rapenne, G. Technomimetic molecules: synthesis of a molecular wheelbarrow. *Tetrahedron Lett.* **2003**, *44*, 6261−6263.

[2] (a) Mislow, K. Stereochemical consequences of correlated rotation in molecular propellers. *Acc. Chem. Res.* **1976**, *9*, 26−33. (b) Sedo, S.; Ventosa, N.; Molins, M. A.; Pons, M.; Rovira, C.; Veciana, J. Stereoisomerism of molecular multipropellers. 1. Static stereochemistry of bis- and tris-triaryl systems. *J. Org. Chem.* **2001**, *66*, 1567−1578. (c) Wolf, C. Dynamic stereochemistry of chiral compounds: Principles and applications; The Royal Society of Chemistry: Cambridge, **2008**.

[3] (a) Kay, E. R.; Leigh, D. A.; Zerbetto, F. Synthetic molecular motors and mechanical machines. *Angew. Chem., Int. Ed.* **2007**, *46*, 72−191. (b) Hanozin, E.; Mignolet, B.; Morsa, D.; Sluysmans, D.; Duwez, A.-S.; Stoddart, J. F.; Remacle, F.; De Pauw, E. Where ion mobility and molecular dynamics meet to unravel the (un)folding mechanisms of an oligorotaxane molecular switch. *ACS Nano* **2017**, *11*, 10253−10263. (c) Chen, Q.; Sun, J.; Li, P.; Hod, I.; Moghadam, P. Z.; Kean, Z. S.; Snurr, R. Q.; Hupp, J. T.; Farha, O. K.; Stoddart, J. F. A redox-active bistable molecular switch mounted inside a metal- organic framework. *J. Am. Chem. Soc.* **2016**, *138*, 14242−14245. (d) Sun, J.; Wu, Y.; Wang, Y.; Liu, Z.; Cheng, C.; Hartlieb, K. J.; Wasielewski, M. R.; Stoddart, J. F. An electrochromic tristable molecular switch. *J. Am. Chem. Soc.* **2015**, *137*, 13484−13487. (e) Sun, J.; Wu, Y.; Liu, Z.; Cao, D.; Wang, Y.; Cheng, C.; Chen, D.; Wasielewski, M. R.; Stoddart, J. F. Visible light-driven artificial molecular switch actuated by radical-radical and donor-acceptor interactions. *J. Phys. Chem. A* **2015**, *119*, 6317−6325. (f) Grunder, S.; McGrier, P. L.; Whalley, A. C.; Boyle, M. M.; Stern, C.; Stoddart, J. F. A Water-soluble pH-triggered molecular switch. *J. Am. Chem. Soc.* **2013**, *135*, 17691−17694. (g) Durola, F.; Heitz, V.; Reviriego, F.; Roche, C.; Sauvage, J.-P.; Sour, A.; Trolez, S. Cyclic [4]rotaxanes containing two parallel porphyrinic plates: Toward switchable molecular receptors and compressors. *Acc. Chem. Res.* **2014**, *47*, 633−645.

[4] (a) Koumura, N.; Zijlstra, R. W. J.; van Delden, R. R.; Harada, N.; Feringa, B. L. Light-driven monodirectional molecular rotor. *Nature* **1999**, *401*, 152−155. (b) Faulkner, A.; van Leeuwen, T.; Feringa, B. L.; Wezenberg, S. J. allosteric regulation of the rotational speed in a light-driven

molecular motor. *J. Am. Chem. Soc.* **2016**, *138*, 13597−13603. (c) Collins, B. S. L.; Kistemaker, J. C. M.; Otten, E.; Feringa, B. L. A chemically powered unidirectional rotary molecular motor based on a palladium redox cycle. *Nat. Chem.* **2016**, *8*, 860− 866. (d) Vachon, J.; Carroll, G. T.; Pollard, M. M.; Mes, E. M.; Brouwer, A. M.; Feringa, B. L. An ultrafast surface-bound photo-active molecular motor. *Photochem. Photobiol. Sci.* **2014**, *13*, 241−246. (e) Ruangsupapichat, N.; Pollard, M. M.; Harutyunyan, S. R.; Feringa, B. L. Reversing the direction in a light-driven rotary molecular motor. *Nat. Chem.* **2011**, *3*, 53−60.

[5] (a) Cheng, C.; McGonigal, P. R.; Schneebeli, S. T.; Li, H.; Vermeulen, N. A.; Ke, C.; Stoddart, J. F. An artificial molecular pump. *Nat. Nanotechnol.* **2015**, *10*, 547−553. (b) Pezzato, C.; Nguyen, M. T.; Cheng, C.; Kim, D. J.; Otley, M. T.; Stoddart, J. F. An efficient artificial molecular pump. *Tetrahedron* **2017**, *73*, 4849−4857.

[6] (a) Jimeńez, M. C.; Dietrich-Buchecker, C.; Sauvage, J.-P. Towards synthetic molecular muscles: Contraction and stretching of a linear rotaxane dimer. *Angew. Chem., Int. Ed.* **2000**, *39*, 3284. (b) Niess, F.; Duplan, V.; Sauvage, J.-P. Molecular Muscles: From Species in Solution to Materials and Devices. *Chem. Lett.* **2014**, *43*, 964−974.

[7] (a) Zhang, L.; Marcos, V.; Leigh, D. A. Molecular machines with bio-inspired mechanisms. *Proc. Natl. Acad. Sci. U. S. A.* **2018**, *115*, 9397−9404. (b) Erbas-Cakmak, S.; Leigh, D. A.; McTernan, C. T.; Nussbaumer, A. L. Artificial Molecular Machines. *Chem. Rev.* **2015**, *115*, 10081−10206. (c) Ashton, P. R.; Balzani, V.; Kocian, O.; Prodi, L.; Spencer, N.; Stoddart, J. F. A Light-Fueled "Piston Cylinder" Molecular-Level Machine. *J. Am. Chem. Soc.* **1998**, *120*, 11190− 11191. (d) Le Poul, N.; Colasson, B. Electrochemically and Chemically Induced Redox Processes in Molecular Machines. *ChemElectroChem* **2015**, *2*, 475−496. (e) Baroncini, M.; Canton, M.; Casimiro, L.; Corra, S.; Groppi, J.; La Rosa, M.; Silvi, S.; Credi, A. Photoactive Molecular-Based Devices, Machines, and Materials: Recent Advances. *Eur. J. Inorg. Chem.* **2018**, *2018*, 4589−4603. (f) Michl, J.; Sykes, C. H. Molecular Rotors and Motors: Recent Advances and Future Challenges. *ACS Nano* **2009**, *3*, 1042−1048.

[8] (a) Badjić, J. D.; Balzani, V.; Credi, A.; Silvi, S.; Stoddart, J. F. *Science* **2004**, *303*, 1845−1849. (b) Kudernac, T.; Ruangsupapichat, N.; Parschau, M.; Maciá, B.; Katsonis, N.; Harutyunyan, S. R.; Ernst, K.-H.; Feringa, B. L. Electrically driven directional motion of a four- wheeled molecule on a metal surface. *Nature* **2011**, *479*, 208−211.

[9] (a) Klichko, Y.; Liong, M.; Choi, E.; Angelos, S.; Nel, A. E.; Stoddart, J. F.; Tamanoi, F.; Zink, J. I. Mesostructured Silica for Optical Functionality, Nanomachines, and Drug Delivery. *J. Am. Ceram. Soc.* **2009**, *92*, S2−S10. (b) Ferris, D. P.; Zhao, Y.-L.; Khashab, N. M.; Khatib, H. A.; Stoddart, J. F.; Zink, J. I. Light-Operated Mechanized Nanoparticles. *J. Am. Chem. Soc.* **2009**, *131*, 1686. (c) Tarn, D.; Ashley, C. E.; Xue, M.; Carnes, E. C.; Zink, J. I.; Brinker, C. J. Mesoporous Silica Nanoparticle Nanocarriers: Biofunctionality and Biocompatibility. *Acc. Chem. Res.* **2013**, *46*, 792−801.

[10] (a) Mariani, G.; Goujon, A.; Moulin, E.; Rawiso, M.; Giuseppone, N.; Buhler, E. Integration of molecular machines into supramolecular materials: actuation between equilibrium polymers and crystal-like gels. *Nanoscale* **2017**, *9*, 18456−18466. (b) Asshoff, S. J.; Lancia, F.; Iamsaard,

S.; Matt, B.; Kudernac, T.; Fletcher, S. P.; Katsonis, N. High-power actuation from molecular photoswitches in enantiomerically paired soft springs. *Angew. Chem., Int. Ed.* **2017**, *56*, 3261−3265. (c) Kwon, H. J.; Shikinaka, K.; Kakugo, A.; Gong, J. P.; Osada, Y. Gel biomachine based on muscle proteins. *Polym. Bull.* **2007**, *58*, 43−52.

[11] (a) Vogelsberg, C. S.; Garcia-Garibay, M. A. Crystalline molecular machines: function, phase order, dimensionality, and composition. *Chem. Soc. Rev.* **2012**, *41*, 1892−1910. (b) Khuong, T. V.; Nuñez, J. E.; Godinez, C. E.; Garcia-Garibay, M. A. Crystalline Molecular Machines: A Quest Toward Solid-State Dynamics and Function. *Acc. Chem. Res.* **2006**, *39*, 413−422. (c) Garcia-Garibay, M. A. Crystalline molecular machines: Encoding supramolecular dynamics into molecular structure. *Proc. Natl. Acad. Sci. U. S. A.* **2005**, *102*, 10771−10776.

[12] Nagarkar, S. S.; Desai, A. V.; Ghosh, S. K. Stimulus-Responsive Metal-Organic Frameworks. *Chem. - Asian J.* **2014**, *9*, 2358−2376.

[13] (a) Ellis, E.; Moorthy, S.; Chio, W. K.; Lee, T.-C. Artificial molecular and nanostructures for advanced nanomachinery. *Chem. Commun.* **2018**, *54*, 4075−4090. (b) Abendroth, J. M.; Bushuyev, O. S.; Weiss, P. S.; Barrett, C. J. Controlling Motion at the Nanoscale: Rise of the Molecular Machines. *ACS Nano* **2015**, *9*, 7746−7768. (c) Endo, M.; Sugiyama, H. DNA Origami Nanomachines. *Molecules* **2018**, *23*, 1766. (d) Ariga, K.; Ito, H.; Hill, J. P.; Tsukube, H. Molecular recognition: from solution science to nano/materials technology. *Chem. Soc. Rev.* **2012**, *41*, 5800−5835.

[14] (a) Naumov, P.; Chizhik, S.; Panda, M. K.; Nath, N. K.; Boldyreva, E. Mechanically responsive molecular crystals. *Chem. Rev.* **2015**, *115*, 12440−12490. (b) Takanabe, A.; Tanaka, M.; Johmoto, K.;Uekusa,H.;Mori,T.;Koshima,H.;Asahi,T. Optical activity and optical anisotropy in photomechanical crystals of chiral salicylidene- phenylethylamines. *J. Am. Chem. Soc.* **2016**, *138*, 15066−15077. (c) Kim, T.; Al-Muhanna, M. K.; Al-Suwaidan, S. D.; Al-Kaysi, R. O.; Bardeen, C. J. Photoinduced Curling of Organic Molecular Crystal Nanowires. *Angew. Chem., Int. Ed.* **2013**, *52*, 6889−6893. (d) Kitagawa, D.; Tsujioka, H.; Tong, F.; Dong, X.; Bardeen, C. J.; Kobatake, S. Control of Photomechanical Crystal Twisting by Illumination Direction. *J. Am. Chem. Soc.* **2018**, *140*, 4208−4212.

[15] Viswanathan, B. *Structure and Properties of Solid State Materials*; Alpha Science Intl. Ltd.: Oxford, UK, **2006**.

[16] (a) Kushida, S.; Smarsly, E.; Bojanowski, N. M.; Wacker, I.; Schröder, R. R.; Oki, O.; Yamamoto, Y.; Melzer, C.; Bunz, U. H. F. Dipole-Switchable Poly(para-phenyleneethynylene)s: Ferroelectric Conjugated Polymers. *Angew. Chem., Int. Ed.* **2018**, *57*, 17019− 17022. (b) Kaleta, J.; Wen, J.; Magnera, T. F.; Dron, P. I.; Zhu, C.; Michl, J. Structure of a monolayer of molecular rotors on aqueous subphase from grazing-incidence X-ray diffraction. *Proc. Natl. Acad. Sci. U. S. A.* **2018**, *115*, 9373−9378. (c) Dron, P. I.; Zhao, K.; Kaleta, J.; Shen, Y.; Wen, J.; Shoemaker, R. K.; Rogers, C. T.; Michl, J. Bulk Inclusions of Pyridazine-Based Molecular Rotors in Tris(o-phenylenedioxy)cyclotriphosphazene (TPP). *Adv. Funct. Mater.* **2016**, *26*, 5718−5732. (d) Horinek, D.; Michl, J. Molecular dynamics of a grid-mounted molecular dipolar rotor in a rotating electric field. *Proc. Natl. Acad. Sci. U. S. A.* **2005**, *102*, 14175−14180. (e) Vacek, J.;

Michl, J. Artificial Surface-Mounted Molecular Rotors: Molecular Dynamics Simulations. *Adv. Funct. Mater.* **2007**, *17*, 730−739. (f) Thomas, J. C.; Schwartz, J. J.; Hohman, J. N.; Claridge, S. A.; Auluck, H. S.; Serino, A. C.; Spokoyny, A. M.; Tran, G.; Kelly, F.; Mirkin, C. A.; Gilles, J.; Osher, S. J.; Weiss, P. S. Defect tolerant aligned dipoles within two-dimensional lattices. *ACS Nano* **2015**, *9*, 4734−4742.

[17] Kottas, G. S.; Clarke, L. I.; Horinek, D.; Michl, J. Artificial Molecular Rotors. *Chem. Rev.* **2005**, *105*, 1281−1376.

[18] (a) Rozenbaum, V. M. Orientation states of dipoles on 2D Bravais lattices. *Sov. Phys. JETP* **1991**, *72*, 1028. (b) Rozenbaum, V. M. Ground state and vibrations of dipoles on a honeycomb lattice. *Phys. Rev. B: Condens. Matter Mater. Phys.* **1995**, *51*, 1290. (c) Rozenbaum, V. M. Coulomb interactions in two-dimensional lattice structures. *Phys. Rev. B: Condens. Matter Mater. Phys.* **1996**, *53*, 6240. (d) Rozenbaum, V. M. Long-range orientational order in a two-dimensional degenerate system of dipoles on a square lattice. *JETP Lett.* **1996**, *63*, 662−667.

[19] Karlen, S. D.; Garcia-Garibay, M. A. Amphidynamic crystals: Structural blueprints for molecular machines. *Top. Curr. Chem.* **2005**, *262*, 179−227.

[20] Gould, S. L.; Tranchemontagne, D.; Yaghi, O. M.; Garcia- Garibay, M. A. Amphidynamic Character of Crystalline MOF-5: Rotational Dynamics of Terephthalate Phenylenes in a Free-Volume, Sterically Unhindered Environment. *J. Am. Chem. Soc.* **2008**, *130*, 3246−3247.

[21] Vogelsberg, C. S.; Uribe-Romo, F. J.; Lipton, A. S.; Yang, S.; Houk, K. N.; Brown, S.; Garcia-Garibay, M. A. Ultrafast rotation in an amphidynamic crystalline metal organic framework. *Proc. Natl. Acad. Sci. U. S. A.* **2017**, *114*, 13613−13618.

[22] Zhu, K.; O'Keefe, C. A.; Vukotic, N.; Schurko, R. W.; Loeb, S. J. A molecular shuttle that operates inside a metal-organic framework. *Nat. Chem.* **2015**, *7*, 514−519.

[23] (a) Inukai, M.; Tamura, M.; Horike, S.; Higuchi, M.; Kitagawa, S.; Nakamura, K. Storage of CO_2 into Porous Coordination Polymer Controlled by Molecular Rotor Dynamics. *Angew. Chem., Int. Ed.* **2018**, *57*, 8687−8690. (b) Gu, C.; Hosono, N.; Zheng, J.-J.; Kusaka, S.; Sakaki, S.; Kitagawa, S. Design and control of gas diffusion process in a nanoporous soft crystal. *Science* **2019**, *363*, 387−391.

[24] Karlen, S. D.; Reyes, H.; Taylor, R. E.; Khan, S. I.; Hawthorne, F.; Garcia-Garibay, M. A. Symmetry and dynamics of molecular rotors in amphidynamic molecular crystals. *Proc. Natl. Acad. Sci. U. S. A.* **2010**, *107*, 14973−14977.

[25] Jiang, X.; Rodriguez-Molina, B.; Nazarian, N.; Garcia-Garibay, M. A. Rotation of a Bulky Triptycene in the Solid State: Towards Engineered Nanoscale Artificial Molecular Machines. *J. Am. Chem. Soc.* **2014**, *136*, 8871−8874.

[26] (a) Beckmann, P. A.; Schneider, E. Methyl group rotation, ^1H spin-lattice relaxation in an organic solid, and the analysis of nonexponential relaxation. *J. Chem. Phys.* **2012**, *136*, No.

054508. (b) Wang, X.; Beckmann, P. A.; Mallory, C. W.; Rheingold, A. L.; DiPasquale, A. G.; Carroll, P. J.; Mallory, F. B. Intramolecular and intermolecular contributions to the barriers for rotation of methyl groups in crystalline solids: Electronic structure calculations and solid- state NMR relaxation measurements. *J. Org. Chem.* **2011**, *76*, 5170. (c) Conn, K. G.; Beckmann, P. A.; Mallory, C. W.; Mallory, F. B. Methyl reorientation in methylphenanthrenes. I. Solid state proton spin-lattice relaxation in the 3-methyl, 9-methyl, and 3,9-dimethyl systems. *J. Chem. Phys.* **1987**, *87*, 20−27. (d) Wang, X.; Rotkina, L.; Su, H.; Beckmann, P. A. Single-crystal x-ray diffraction, isolated molecule and cluster electronic structure calculations, and scanning electron microscopy in an organic solid: models for intramolecular motion in 4,4′ dimethoxybiphenyl. *ChemPhysChem* **2012**, *13*, 2082− 2089.

[27] (a) Lemouchi, C.; Vogelsberg, C. S.; Zorina, L.; Simonov, S.; Batail, P.; Brown, S.; Garcia-Garibay, M. A. Ultra-fast rotors for molecular machines and functional materials via halogen bonding: crystals of 1,4-bis(iodoethynyl)bicyclo[2.2.2]octane with distinct gigahertz rotation at two sites. *J. Am. Chem. Soc.* **2011**, *133*, 6371− 6379. (b) Lemouchi, C.; Meźierè, C.; Zorina, L.; Simonov, S.; Rodríguez-Fortea, A.; Canadell, E.; Wzietek, P.; Auban-Senzier, P.; Pasquier, C.; Giamarchi, T.; Garcia-Garibay, M. A.; Batail, P. Design and evaluation of a crystalline hybrid of molecular conductors and molecular rotors. *J. Am. Chem. Soc.* **2012**, *134*, 7880−7891. (c) Rodríguez-Molina, B.; Peŕez-Estrada, S.; Garcia-Garibay, M.A. Amphidynamic crystals of a steroidal bicyclo[2.2.2]octane rotor: a high symmetry group that rotates faster than smaller methyl and methoxy groups. *J. Am. Chem. Soc.* **2013**, *135*, 10388−10395.

[28] Hill, J. G.; Platts, J. A.; Werner, H.-J. Calculation of intermolecular interactions in the benzene dimer using coupled- cluster and local electron correlation methods. *Phys. Chem. Chem. Phys.* **2006**, *8*, 4072−4078.

[29] Yaghi, O.; Li, H.; Davis, C.; Richardson, D.; Groy, T. L. Synthetic strategies, structure patterns, and emerging properties in the chemistry of modular porous solids. *Acc. Chem. Res.* **1998**, *31*, 474− 484.

[30] Kitaigorodsky, A. I. *Molecular crystals and molecules*; Academic Press, New York, **1973**.

[31] Furukawa, H.; Ko, N.; Go, Y. B.; Aratani, N.; Choi, S. B.; Choi, E.; Yazaydin, A. Ö.; Snurr, R. Q.; O'Keeffe, M.; Kim, J.; Yaghi, O. Ultrahigh porosity in metal-organic frameworks. *Science* **2010**, *329*, 424−428.

[32] Spartan'08; Wavefunction, Inc.: Irvine, CA.

[33] (a) Gavezzotti, A. The calculation of molecular volumes and the use of volume analysis in the investigation of structured media and of solid-state organic reactivity. *J. Am. Chem. Soc.* **1983**, *105*, 5220− 5225. (b) Bondi, A. van der Waals volumes and radii. *J. Phys. Chem.* **1964**, *68*, 441−451.

[34] Eddaoudi, M.; Kim, J.; Rosi, N.; Vodak, D.; Wachter, J.; O'Keeffe, M.; Yaghi, O. M. Systematic Design of Pore Size and Functionality in Isoreticular MOFs and Their Application in Methane Storage. *Science* **2002**, *295*, 469−472.

[35] Winston, E. B.; Lowell, P. J.; Vacek, J.; Chocholousŏva, J.; Michl, J.; Price, J. C. Dipolar molecular rotors in the metal-organic framework crystal IRMOF-2. *Phys. Chem. Chem. Phys.* **2008**, *10*, 5188−5191.

[36] Morris, W.; Taylor, R. E.; Dybowski, C.; Yaghi, O. M.; Garcia- Garibay, M. A. Framework mobility in the metal-organic framework crystal IRMOF-3: Evidence for aromatic ring and amine rotation. *J. Mol. Struct.* **2011**, *1004*, 94−101.

[37] Rotation about alkynyl single bonds is nearly frictionless: (a) Saebo, S.; Almlöf, J.; Boggs, J. E.; Stark, J. G. Two approaches to the computational determination of molecular structure: the torsional angle in tolane and the effect of fluorination on the structure of oxirane. *J. Mol. Struct.: THEOCHEM* **1989**, *200*, 361−373. (b) Sipachev, V. A.; Khaikin, L. S.; Grikina, O. E.; Nikitin, V. S.; Trættberg, M. Structure, spectra and internal rotation of bis- (trimethylsilyl) acetylene: spectral analysis by scaling quantum- chemical force fields and two methods for calculating vibrational effects. *J. Mol. Struct.* **2000**, *523*, 1−22.

[38] Jarowski, P. D.; Houk, K. N.; Garcia-Garibay, M. A. Importance of correlated motions on the low barrier rotational potentials of crystalline molecular gyroscopes. *J. Am. Chem. Soc.* **2007**, *129*, 3110− 3117.

[39] Minamino, T.; Imada, K.; Namba, K. Molecular motors of the bacterial flagella. *Curr. Opin. Struct. Biol.* **2008**, *18*, 693−701.

[40] Akutagawa, T.; Koshinaka, H.; Sato, D.; Takeda, S.; Noro, S. I.; Takahashi, H.; Kumai, R.; Tokura, Y.; Nakamura, T. Ferroelectricity and polarity control in solid state flip-flop supramolecular rotors. *Nat. Mater.* **2009**, *8*, 342−347.

[41] Vacek, J.; Michl, J. Molecular dynamics of a grid-mounted molecular dipolar rotor in a rotating electric field. *Proc. Natl. Acad. Sci. U. S. A.* **2001**, *98*, 5481−5486.

[42] As compared to BCO, p-carborane rotators belong in the point group S_{10} and have an inversion center (i) such that rotational disorder does not generate a higher symmetry space group.

[43] (a) Catalano, L.; Perez-Estrada, S.; Wang, H.-H.; Ayitou, A. J.- L.; Khan, S. I.; Terraneo, G.; Metrangolo, P.; Brown, S.; Garcia- Garibay, M. A. Rotational dynamics of diazabicyclo[2.2.2]octane in isomorphous halogen-bonded co-crystals: entropic and enthalpic effects. *J. Am. Chem. Soc.* **2017**, *139*, 843−848. (b) Karlen, S. D.; Ortiz, R.; Chapman, O. L.; Garcia-Garibay, M. A. Effects of rotational symmetry order on the solid state dynamics of phenylene and diamantane rotators. *J. Am. Chem. Soc.* **2005**, *127*, 6554−6555.

[44] Catalano, L.; Peŕez-Estrada, S.; Terraneo, G.; Pilati, T.; Resnati, G.; Metrangolo, P.; Garcia-Garibay, M. A. Dynamic characterization of crystalline supramolecular rotors assembled through halogen bonding. *J. Am. Chem. Soc.* **2015**, *137*, 15386−15389.

[45] Godinez, C. E.; Zepeda, G.; Garcia-Garibay, M. A. Molecular compasses and gyroscopes. ii. synthesis and characterization of molecular rotors and axially substituted bis[2-(9-triptycyl)ethynyl]- arenes. *J. Am. Chem. Soc.* **2002**, *124*, 4701−4707.

[46] Dominguez, Z.; Dang, H.; Strouse, M. J.; Garcia-Garibay, M. A. Molecular "compasses" and "gyroscopes." I. Expedient synthesis and solid state dynamics of an open rotor with a bis(triarylmethyl) frame. *J. Am. Chem. Soc.* **2002**, *124*, 2398−2399.

[47] Dominguez, Z.; Dang, H.; Strouse, M. J.; Garcia-Garibay, M. A. Molecular "compasses" and "gyroscopes." III. Dynamics of a phenylene rotor and clathrated benzene in a slipping-gear crystal lattice. *J. Am. Chem. Soc.* **2002**, *124*, 7719−7727.

[48] (a) Horansky, R. D.; Clarke, L. I.; Price, J. C.; Khuong, T.-A. V.; Jarowski, P. D.; Garcia-Garibay, M. A. Dielectric response of a dipolar molecular rotor crystal. *Phys. Rev. B: Condens. Matter Mater. Phys.* **2005**, *72*, No. 014302. (b) Horansky, R. D.; Clarke, L. I.; Winston, E. B.; Price, J. C.; Karlen, S. D.; Jarowski, P. D.; Santillan, R.; Garcia-Garibay, M. A. Dipolar rotor-rotor interactions in a difluorobenzene molecular rotor crystal. *Phys. Rev. B: Condens. Matter Mater. Phys.* **2006**, *74*, No. 054306. (c) Rodriguez-Molina, B.; Ochoa, M. E.; Farfań, N.; Santillan, R.; Garcia-Garibay, M. A. Synthesis, characterization, and rotational dynamics of crystalline molecular compasses with n-heterocyclic rotators. *J. Org. Chem.* **2009**, *74*, 8554−8565. (d) Jin, M.; Chung, T. S.; Seki, T.; Ito, H.; Garcia-Garibay, M. A. Phosphorescence control mediated by molecular rotation and aurophilic interactions in amphidynamic crystals of 1,4-bis[tri-(p- fluorophenyl)phosphane-gold(I)-ethynyl]benzene. *J. Am. Chem. Soc.* **2017**, *139*, 18115−18121. (e) Commins, P.; Garcia-Garibay, M. A. Photochromic Molecular Gyroscope with Solid State Rotational States Determined by an Azobenzene Bridge. *J. Org. Chem.* **2014**, *79*, 1611−1619. (f) Karlen, S. D.; Godinez, C. E.; Garcia-Garibay, M. A. Improved Physical Properties and Rotational Dynamics in a Molecular Gyroscope with an Asymmetric Stator Structure. *Org. Lett.* **2006**, *8*, 3417−3420. (g) Staehle, I. O.; Rodríguez-Molina, B.; Khan, S. I.; Garcia-Garibay, M. A. Engineered Photochromism in Crystalline Salicylidene Anilines by Facilitating Rotation to Reach the Colored trans-Keto Form. *Cryst. Growth Des.* **2014**, *14*, 3667−3673. (h) Hughs, M.; Jimenez, M.; Khan, S.; Garcia-Garibay, M. A. Synthesis, Rotational Dynamics, and Photophysical Characterization of a Crystalline Linearly Conjugated Phenyleneethynylene Molecular Dirotor. *J. Org. Chem.* **2013**, *78*, 5293−5302.

[49] Garcia-Garibay, M. A.; Godinez, C. E. Engineering crystal packing and internal dynamics in molecular gyroscopes by refining their components. fast exchange of a phenylene rotator by ^{2}H NMR. *Cryst. Growth Des.* **2009**, *9*, 3124−3128.

[50] (a) Khuong, T.-A. V.; Zepeda, G.; Ruiz, R.; Khan, S. I.; Garcia- Garibay, M. A. Molecular compasses and gyroscopes: engineering molecular crystals with fast internal rotation. *Cryst. Growth Des.* **2004**, *4*, 15−18. (b) Khuong, T.-A. V.; Dang, H.; Jarowski, P. D.; Maverick, E. F.; Garcia-Garibay, M. A. Rotational dynamics in a crystalline molecular gyroscope by variable-temperature ^{13}C NMR, ^{2}H NMR, X- ray diffraction, and force field calculations. *J. Am. Chem. Soc.* **2007**, *129*, 839−845. (c) O'Brien, Z. J.; Natarajan, A.; Khan, S.; Garcia- Garibay, M. A. Synthesis and solid-state rotational dynamics of molecular gyroscopes with a robust and low density structure built with a phenylene rotator and a tri(meta-terphenyl)methyl stator. *Cryst.*

Growth Des. **2011**, *11*, 2654−2659. (d) Arcos-Ramos, R.; Rodriguez-Molina, B.; Gonzalez-Rodriguez, E.; Ramirez-Montes, P. I.; Ochoa, M. E.; Santillan, R.; Farfań, N.; Garcia-Garibay, M. A. Crystalline arrays of molecular rotors with TIPS-trityl and phenolic- trityl stators using phenylene, 1,2-difluorophenylene and pyridine rotators. *RSC Adv.* **2015**, *5*, 55201−55208.

[51] Jiang, X.; O'Brien, Z. J.; Yang, S.; Lai, L. H.; Buenaflor, J.; Tan, C.; Khan, S.; Houk, K. N.; Garcia-Garibay, M. A. Crystal fluidity reflected by fast rotational motion at the core, branches, and peripheral aromatic groups of a dendrimeric molecular rotor. *J. Am. Chem. Soc.* **2016**, *138*, 4650−4656.

[52] Kawski, A. Fluorescence anisotropy: theory and applications of rotational depolarization. *Crit. Rev. Anal. Chem.* **1993**, *23*, 459−529.

[53] Vogelsberg, C. S.; Bracco, S.; Beretta, M.; Comotti, A.; Sozzani, P.; Garcia-Garibay, M. A. Dynamics of molecular rotors confined in two dimensions: transition from a 2d rotational glass to a 2D rotational fluid in a periodic mesoporous organosilica. *J. Phys. Chem.* B **2012**, *116*, 1623−1632.

[54] (a) Lorbach, A.; Maverick, E.; Carreras, A.; Alemany, P.; Wu, G.; Garcia-Garibay, M. A.; Bazan, G. C. A Fullerene−carbene adduct as a crystalline molecular rotor: remarkable behavior of a spherically- shaped rotator. *Phys. Chem. Chem. Phys.* **2014**, *16*, 12980−12986. (b) Pekker, S.; Kovats, E.; Oszlanyi, G.; Benyei, G.; Klupp, G.; Bortel, G.; Jalsovszky, I.; Borondics, E. J. F.; Kamaras, K.; Bokor, M.; Kriza, G.; Tompa, K.; Faigel, G. Rotor-stator molecular crystals of fullerenes and cubane. *Nat. Mater.* **2005**, *4*, 764−767.

[55] (a) Ye, H. Y.; Li, S. H.; Zhang, Y.; Zhou, L.; Deng, F.; Xiong, R.-G. Solid state molecular dynamic investigation of an inclusion ferroelectric: [(2.6-diisopropylanilinium)[18]crown-6)]BF_4. *J. Am. Chem. Soc.* **2014**, *136*, 10033−10044. (b) Harada, J.; Shimojo, T.; Oyamaguchi, H.; Hasegawa, H.; Takahashi, Y.; Satomi, K.; Suzuki, Y.; Kawamata, J.; Inabe, T. Directionally tunable and mechanically deformable ferroelectric crystals from rotating polar globular ionic molecules. *Nat. Chem.* **2016**, *8*, 946−952. (c) Akutagawa, T.; Koshinaka, H.; Sato, D.; Takeda, S.; Noro, S.-I.; Takahashi, H.; Kumai, R.; Tokura, Y.; Nakamura, T. Ferroelectric and polarity control in solid-state flip-flop supramolecular rotors. *Nat. Mater.* **2009**, *8*, 342−347. (d) Zhang, W.; Xiong, R.-G.; Yoshikawa, H.; Awaga, K. Exceptional dielectric phase transition in a pervoskite-type cage compound. *Angew. Chem., Int. Ed.* **2010**, *49*, 6608−6610. (e) Sun, Z.; Chen, T.; Luo, J.; Hong, M. Bis(imidazolium) L-tartrate: A hydrogen bonded displacive molecular ferroelectric material. *Angew. Chem., Int. Ed.* **2012**, *51*, 3871−3876.

CHAPTER 2

Fluorescence and Rotational Dynamics of a Crystalline Molecular Rotor Featuring an Aggregation-Induced Emission Fluorophore

2.1. Introduction

Continued interest in the field of molecular machinery has led to the development of molecular structures that are able to couple mechanical processes with the transduction of different forms of energy.[1] Among those platforms, amphidynamic crystals offer advantages related to their long-range structural order and intermolecular interactions, which have the potential for the development of emergent properties and controlled molecular dynamics.[2] Amphidynamic crystals are composed of rigid, lattice-forming elements linked to moving parts designed to introduce functionality. One of the most robust design strategies relies on creating molecular rotors akin to macroscopic compasses and gyroscopes.[3] Their structures possess a shielding stator linked by a barrierless axle to a suitable rotator.[4]

As illustrated with molecular rotor **1** in Figure 2.1.1a, several structures reported up to date contain two triphenylmethyl (trityl) groups acting as a stator that are linked by triple bonds to a central phenylene that acts as the rotator. In the case of **1**, it was shown using solid-state NMR that phenylene rotation occurs in the kilohertz regime at ambient temperature, and computational analysis revealed that suitable models require a flexible lattice.[5] This is also illustrated in Figure 2.1.1a with a scatterplot where the points indicate the displacement of atoms in close neighboring molecules between ca. 2.5 and 20 Å from the center of the rotating phenylene in **1** at the rotational transition state.[5] Light blue dots correspond to a crystalline benzene solvate and red dots correspond to a crystal that is solvent-free. These results showed that rotation in **1** relies heavily on the ability of phenyl groups in the stator and the included solvent molecules to experience a significant degree of torsional and rotational motions, which we subsequently have referred to as crystal fluidity.[6] Relatively high-amplitude segmental motions in the crystalline state create transient cavities or allow for correlated motions that enable the motion of the rotator. An

interesting example of crystal fluidity was recently highlighted in a molecular rotor dendrimer where phenylene groups at the core, branches, and surface groups were all shown to undergo fast 180° rotations.[6]

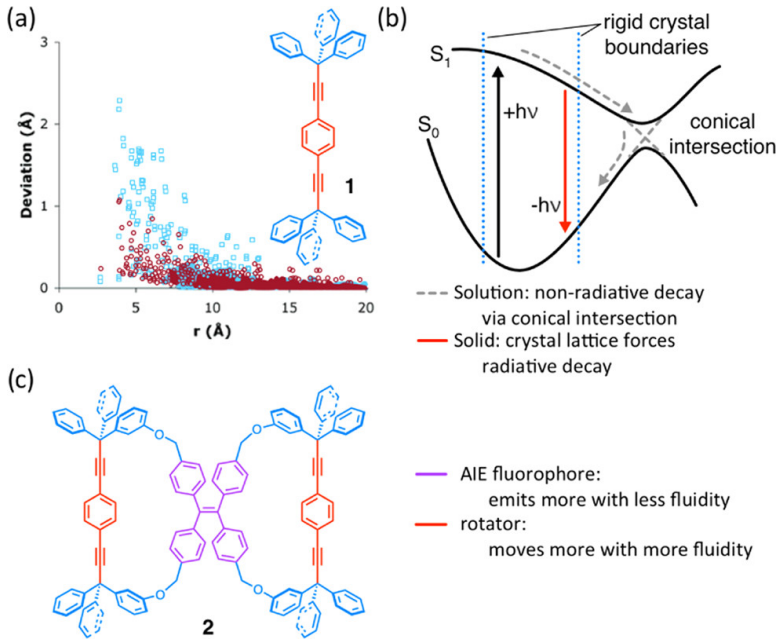

Figure 2.1.1. (a) Structure of molecular rotor **1** and the displacement of the atoms (deviation, in Å) in close proximity (*r*, in Å) to the central rotator at the rotational transition state, indicating local flexibility in the crystalline environment. Red circles indicate displacements of atoms in the desolvated crystal; blue squares indicate displacements of atoms in the benzene clathrate (adapted from ref 5). (b) Fluorescence behavior of an aggregation-induced emission (AIE) fluorophore: nonradiative decay in solution through a conical intersection (gray dashed lines) and radiative decay in the solid state (red solid line) due to the restrictions of the rigid crystal boundaries (blue dotted line). (c) Molecular dirotor **2** with an integrated AIE fluorophore.

To probe the nature of crystal fluidity and its relation to molecular rotation in the solid state, we designed structure **2**,[7] with two diethynylbenzene (DEB) molecular rotators having their triphenylmethyl stators covalently linked to tetraphenylethylene (TPE) core.[8] TPE is known as a

fluorescence probe for its aggregation-induced emission (AIE) characteristics. It remains dark when excited in fluid solution but becomes brightly emissive in rigid environments.[8] As suggested in Figure 2.1.1b, AIE fluorophores excited in solution are able to reach a conical intersection that allows them to decay nonradiatively back to the ground state, as indicated by the gray dashed arrows. However, restricted molecular motions caused by aggregation or complexation,[9] as indicated by the blue dotted lines, prevent the excited state from reaching the conical intersection, and the molecule has an opportunity to return to the ground state by emitting a fluorescence signal, as shown by the red arrow. This AIE pathway has been exploited in several recent advances in the field of aggregated-state molecular motion.[10]

In this article, we report the synthesis of molecular dirotor **2** and how we established that it is indeed an AIE fluorophore using standard water-induced aggregation procedures in organic solvents. We determined the rotational dynamics of **2** between 198 and 298 K using solid-state ^{2}H NMR and measured its solid-state fluorescence over the temperature range of 77–300 K. We find that the dynamic window where the rotation of the DEB occurs does not show a significant effect on fluorescence emission, suggesting that the fluidity of **2** is not fast enough for the TPE chromophore to reach its conical intersection within the lifetime of its excited state.

2.2. Results and Discussion

The synthesis of fluorescent molecular dirotor **2** shown in Scheme 2.2.1 builds on the previously reported[11] synthesis of a benzophenone-bridged rotor **4**, which was synthesized in five steps starting from 3-bromoanisole. Since an isotopologue of **2** with deuterium-labeled rotators was also required for solid-state NMR analysis, **4**-d_4 was synthesized using the same macrocyclization conditions as for **4** from known compound **3**-d_4.[12] Initial attempts to subject **4** directly to McMurry coupling conditions resulted in many side products and a low yield of the

intended dirotor **2**. To form the sterically demanding C–C bond between the two macrocycles, we resorted instead to a photoinduced coupling to form benzopinacol **5** as a white powder in 89% yield (Scheme 2.2.1). The reaction was run in very dilute conditions (0.8 mg/mL) in a 1:1 mixture of benzene and isopropanol. Curiously, the reaction appeared to proceed more smoothly and with fewer byproducts when the solvent was removed, and the solid was resuspended to facilitate the precipitation of the product as soon as it is formed. The resulting product was characterized by one-dimensional and two-dimensional NMR, as well as by attenuated total reflectance-Fourier transform infrared (ATR-FTIR) and high-resolution mass spectrometry. Having the C–C bond already formed, benzopinacol **5** was subjected to McMurry coupling conditions where the reaction gave a much more efficient 36% yield of isolated **2** as a white powder (Scheme 2.2.1). The desired structure was confirmed by spectroscopic analysis, including ^{1}H and ^{13}C NMR, as well as ATR-FTIR, UV–vis spectroscopy, and high-resolution mass spectrometry. Unfortunately, numerous attempts to obtain single crystals that are suitable for structural determination were not successful, but powder X-ray diffraction patterns revealed some sharp peaks and a broad baseline as expected for mixtures of amorphous and crystalline domains.

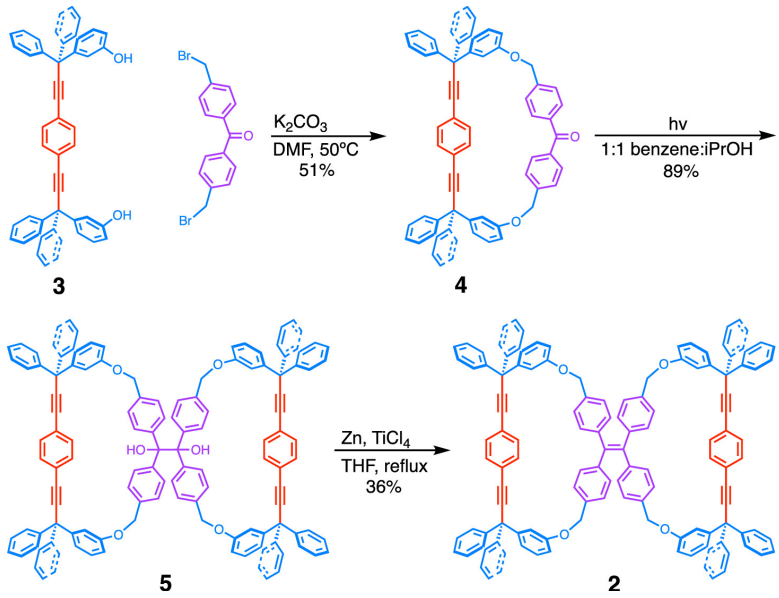

Scheme 2.2.1. Synthetic Pathway toward Molecular Dirotor **2**

Analysis of the UV–vis spectrum of molecular dirotor **2** alongside its isolated component chromophores, TPE **6** and bismethoxy rotor **7**, revealed that the spectrum of **2** (Figure 2.2.1, black solid line) could be approximated by a linear combination (black dotted line) of the absorption spectra of **6** (purple, long dashed line) and **7** (red, short dashed line), indicating that there is minimal electronic communication between the two chromophores. Fluorescence emission

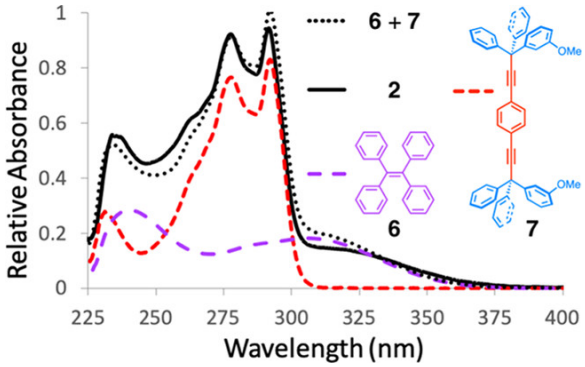

Figure 2.2.1. UV–vis spectra of dirotor **2** (solid purple line) and its isolated chromophores TPE **6** (long dashed red line) and bismethoxy rotor **7** (short dashed blue line). A linear combination of the spectra of **6** and **7** is shown as a dotted line.

measurements in solution carried out by excitation at 290 nm supported this conclusion with the unexpected observation of two emission bands. One at higher energies is relatively narrow with two close maxima at 306 nm and 314 nm. The other is significantly broader with a red-shifted maximum at 455 nm (Figure 2.2.2a, gray line). The first band well matches the emission of molecular rotor **7** in Figure 2.2.2b (light red, short dashed line) and can be assigned to the diethynylbenzene (DEB) chromophore. The 455 nm emission can be assigned to the TPE chromophore based on the fact that unsubstituted TPE has a similar broad band in aqueous THF with a maximum of 467 nm (Figure 2.2.2b, light purple, long dashed line). Similarly, the excitation spectrum of **2** measured by monitoring changes in emission at 467 nm contains spectral components corresponding to those of DEB and TPE. The quantum yield of **2** was found to be

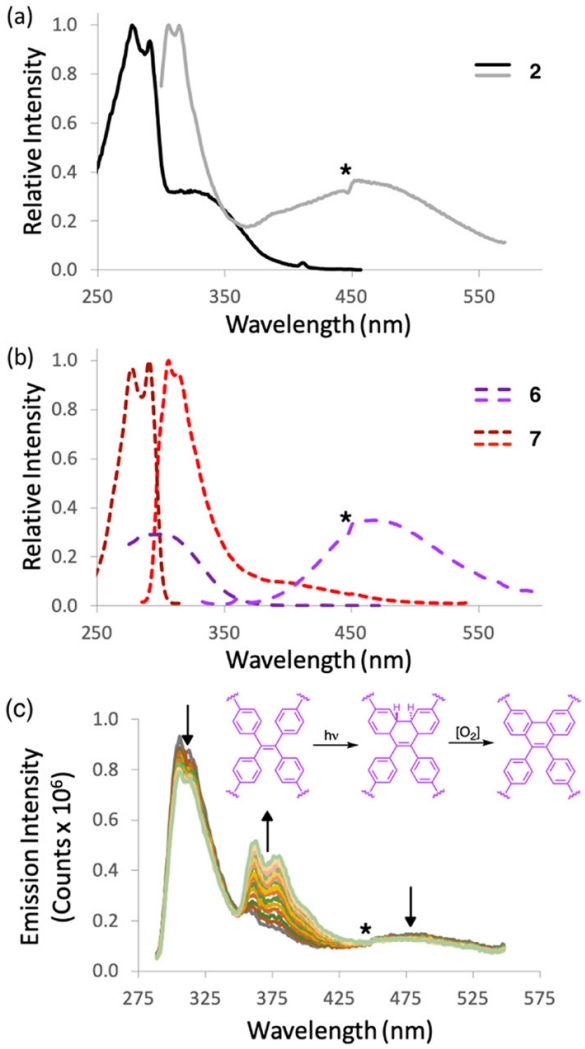

Figure 2.2.2. (a) Steady-state excitation (black line) and emission (gray line) spectra of 4.4 μM solution of **2** in THF. (b) Steady-state excitation and emission spectra of 7.1 μM solution of dimethoxy rotor **7** in THF (red, short dashes) and 1.9 μM TPE in THF/water (purple, long dashes). (c) Emission of **2** over 30 sequential scans showing the growth of a phenanthrene photoproduct formed upon excitation at 290 nm. *The notch at 450 nm is an artifact of the emission detector.

0.01 when excited at 292 nm and 0.03 when excited at 350 nm by comparison to a quinine sulfate standard. The lower quantum yield of TPE emission upon excitation of the DEB chromophore is consistent with the observation of a weak DEB emission. Considering the excellent spectral

overlap between the emission of DEB and the absorption of TPE and the close proximity between the two chromophores, it would be reasonable to expect the efficient transfer of energy by both dipole–dipole (Förster) and electron exchange (Dexter) mechanisms.[13]

The observation of the DEB emission in molecular dirotor **2** indicates that the alignment of the transition dipole moments and/or the extent of orbital overlap is not ideal since complete alignment or overlap would lead to complete energy transfer and the absence of an observable DEB emission signal.

We observed that the irradiation of the molecule at 290 nm resulted in the growth of new emission peaks at 363 and 380 nm (Figure 2.2.2c). Based on the analogy with reported spectra,[13] these are interpreted as corresponding to the photoinduced 6π-electron pericyclic reaction and oxidation of the TPE moiety to form the corresponding 9,10-diphenylphenanthrene. Previous work has shown that hindered TPEs undergo cyclization as a prominent method of relaxation from the first excited singlet state.[14]

Addition of water to a THF solution of **2** resulted in its aggregation, as demonstrated by the gradual change from a spectrum with a weak DEB emission and even weaker TPE emission, to one where the signal of DEB almost disappears and that of TPE becomes much stronger (Figure 2.2.3a). While the solutions used for fluorescence were too dilute for dynamic light scattering (DLS), evidence of aggregation was provided by measurements of a sample with the same water content and a concentration of **2** that was 10 times higher. DLS measurements of this sample showed a mean particle size of ca. 250 nm. A dramatic increase in TPE emission of the original dilute sample, shown by red circles in Figure 2.2.3b, was observed when solutions reached 50% water by volume, as is commonly observed for hydrophobic AIE chromophores. Conversely, the DEB emission illustrated by the blue diamonds in Figure 2.2.3b showed a decrease in emission

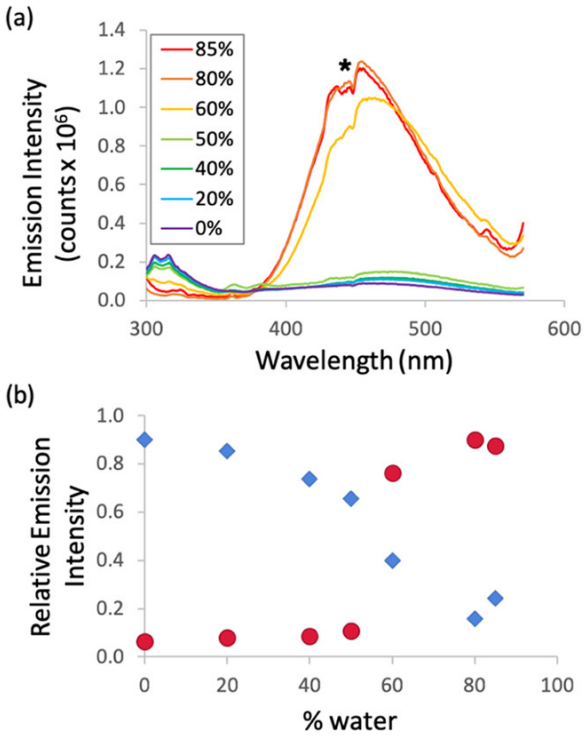

Figure 2.2.3. (a) Steady-state emission spectra of **2** when excited at 290 nm in solutions of THF and the indicated water by volume percentage. *The notch at 450 nm is an artifact of the emission detector. (b) Normalized relative emission intensities of **2** at 314 nm (DEB, blue diamonds) and 467 nm (TPE, red circles).

intensity with an increase in water content, suggesting that intermolecular pathways for energy transfer become available in the aggregated state. This is in contrast to the solution behavior, where the presence of TPE emission when the DEB is excited indicates that intramolecular energy transfer is present, but the observation of higher-energy DEB emission indicates that the energy transfer is only partial. These results indicate that even though the TPE is incorporated into two locked macrocycles, it is still flexible enough to undergo nonradiative decay in solution and display the characteristic AIE behavior. While it was not possible to document changes in the UV absorption in the isolated and aggregated states of **2**, there were no changes in the normalized excitation spectra, suggesting that there is strong intermolecular interaction in the aggregated state.

Attempts to document a potential correlation between fluorescence lifetimes and emission intensities led to scattered data with no definitive trend. We found that TPE emission lifetimes varied within a given sample as a function of time over periods shown to extend up to several days (Figure 2.5.3.1). We interpret this as an indication of exceedingly slow kinetics for the formation of stable supramolecular structures.

The solid-state emission spectrum of **2** obtained by excitation at 290 nm showed a broad band that extends from ca. 375 to 550 nm with a maximum at 458 nm. The excitation spectrum recorded by measuring changes in emission at 445 nm is also very broad with a maximum at 368 nm (Figure 2.2.4). Notably, the emission of solid samples showed no indication of the DEB chromophore, suggesting that intermolecular energy transfer is very efficient in the solid state. The formation of the phenanthrene photoproduct previously observed in solution (Figure 2.2.2c) was also determined to occur in the solid state by measuring the emission spectra of samples that had been exposed to UV light as powders after being dissolved in THF (Figure 2.5.4.1).

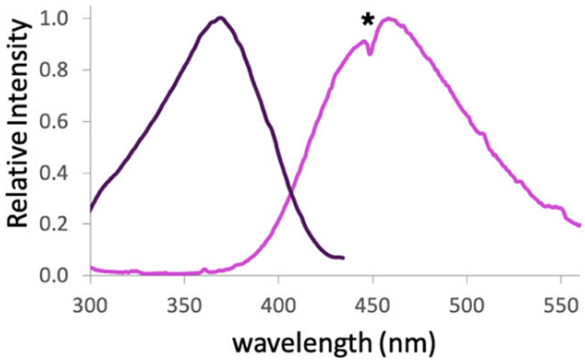

Figure 2.2.4. Steady-state emission and excitation spectra of **2** as a bulk powder. *The notch at 450 nm is an artifact of the emission detector.

In search of an inverse correlation between solid-state fluorescence and rotational dynamics potentially indicating their divergent dependence on local fluidity, we measured the emission spectrum of molecular dirotor **2** at 77, 195, and 298 K. Accurate intensity measurements

as a function of temperature in the solid state turned out to be challenging, and considering that no striking differences were observed, we decided to look for changes in fluorescence lifetimes as it may be expected that they may increase in a proportional manner. Lifetime measurements at varying temperatures carried out by excitation at 375 nm and emission detection at 470 nm using a time-correlated single-photon lifetime instrument showed very similar complex decays. To carry out a simple and qualitative analysis, we fitted the data to a triple exponential and used the pre-exponential values to calculate weighted average lifetimes of 4.8, 4.9, and 4.3 ns, at 77, 195, and 298 K, respectively. Based on the lack of discernible trend, we conclude that the TPE moiety of **2** reflects a solid-state environment that is essentially rigid in the nanosecond timescale.

However, while changes in the fluidity of the bulk powder were not reflected by changes in fluorescence, they are reflected in the rotational exchange dynamics of the phenylene rotator in **2**-d_8. Variable-temperature T_1 measurements of quadrupolar echo solid-state ^{2}H NMR of **2**-d_8 measured over a range of 173–298 K (Figure 2.2.5) were shown to contain two components, with one of them contributing more than 98% of the signal. Line-shape analysis of the T_1-edited ^{2}H NMR spectra of the major component (Figure 2.2.5a) revealed dynamics in the intermediate exchange regime that could be simulated (Figure 2.2.5b) with rotational exchange frequencies varying from 4 kHz at 198 K to 375 kHz at 298 K.[15] These values were used to construct an Arrhenius plot that resulted in a pre-exponential factor of 3.6×10^9 s^{-1} and an activation energy of 5.5 kcal/mol (Figure 2.2.5c). Notably, while the activation energy is relatively low, the pre-exponential factor is ca. 3 orders of magnitude smaller than the value expected for an elementary process in the solid state, which is also consistent with either an unfavorable activation entropy or rotational motion in an amorphous phase.[16] The amorphous nature of the material was further

corroborated by the fact that the simulated spectra used to fit the data included a log-Gaussian distribution of jump rates with a 12-decade full width at half maximum.

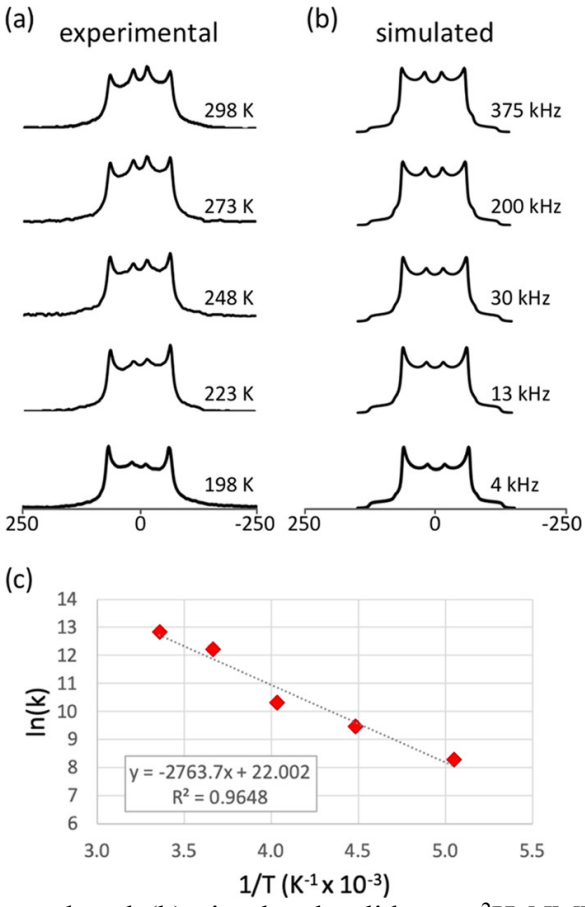

Figure 2.2.5. (a) Experimental and (b) simulated solid-state ^{2}H NMR spectra of **2** with their corresponding temperatures and rotational exchange frequencies indicated. (c) Arrhenius plot from the data shown in (a) and (b).

2.3. Conclusions

Structure **2** with two diethynylbenzene (DEB) molecular rotors attached to an aggregation-induced emission (AIE) tetraphenylethylene (TPE) chromophore was designed to explore a potential inverse correlation between rotational dynamics and fluorescence emission. Molecular dirotor **2**, later shown to be a semicrystalline solid, was synthesized by taking advantage of a

photoinduced coupling reaction of a molecular rotor with a bridging benzophenone (**4**) followed by reduction of the resulting benzopinacol (**5**) using McMurry coupling conditions. Absorption spectra measured in THF solution showed no significant electronic interaction between the two chromophores, which were shown to display independent emission despite conditions that are almost ideal for energy transfer from DEB to TPE. The AIE properties of the hydrophobic molecular dirotor **2** were confirmed by the addition of water, which resulted in a large increase in the TPE emission after values of ca. 50% v/v. A concomitant decrease in the emission of the DEB group was interpreted as the result of an intermolecular energy transfer in the aggregate state. The originally sought-after measurements revealed that rotational dynamics measured with ^{2}H-labeled samples of molecular dirotor **2**-d_8 in the solid state occur by a 2-fold phenylene flipping mechanism in the kHz (μs) regime over a 100 K temperature range. By contrast, fluorescence lifetimes from 77 to 298 K were shown to not vary significantly. One may conclude that rotational dynamics and fluorescence properties did not show the expected inverse correlation as a function of temperature due at least, in part, to the mismatch in the dynamic windows where they operate. This work suggests that TPE could be an appropriate indicator of solid-state fluidity when incorporated into systems with sufficiently fast rotation, such as is often observed with molecular rotors containing bicyclo[2.2.2]octane rotators.[17] Alternatively, since it has been recently shown that molecular rotors built with phosphorescent gold complexes may have emission that correlates with rotational motion,[18] one may expect that sufficiently long-lived luminophores may have photophysical properties that correlate better with solid-state molecular rotors featuring hindered molecular rotators such as the DEB reported in this work.

2.4. Experimental Section

2.4.1. General Experimental Details

IR spectra were acquired on a PerkinElmer spectrum two spectrometer equipped with a universal ATR sampling accessory. ^{1}H and ^{13}C NMR spectra were obtained using a Brüker NMR spectrometer at 500 MHz with $CDCl_3$ as the solvent unless otherwise noted. NMR coupling constants were calculated using Topspin. High resolution mass spectrometry (HRMS) was collected using Thermo LTQ FT ultra mass spectrometer at a 100 000 resolving power using direct analysis in real time (DART) source ionization and an Orbitrap mass analyzer. The benzene, isopropanol, zinc powder, and 1.0 M titanium tetrachloride in dichloromethane (DCM) were commercially available and used without further purification. THF for synthesis purposes was distilled from sodium and kept under argon. Bis[4-(bromomethyl)phenyl]methanone for the synthesis of 7 was prepared as described in the literature.[19] Compounds 6 and 7 were also prepared as previously described.[11,12]

Spectrophotometric-grade THF for fluorescence and UV–vis studies was commercially available and used without further purification. Solutions in THF/water mixtures were made by quickly adding a solution of THF containing the analyte to the appropriate amount of water while vortexing. UV–vis spectra were obtained using an ocean optics flame spectrometer with DT-MINI-2-GS light source and Oceanview software package. Fluorescence spectra were obtained using an Edinburgh Instrument FLS 920 spectrometer equipped with a 450 W ozone-free xenon arc lamp for steady-state measurements, as well as EPLED-300 and EPL-375 picosecond pulsed laser diodes for lifetime measurements. Fluorescence data were collected using the F900 software package. The notch at 450 nm in emission spectra is an artifact of the correction file that is applied to the emission detector. Weighted average lifetimes are calculated by eqs 2.4.1.1 and 2.4.1.2

$$\%\tau_n = \frac{I_n\tau_n}{I_1\tau_1 + I_2\tau_2 + I_3\tau_3} \quad (2.4.1.1)$$

$$\tau_{avg} = \tau_1(\%\tau_1) + \tau_2(\%\tau_2) + \tau_3(\%\tau_3) \quad (2.4.1.2)$$

2.4.2. Synthetic Procedures

Synthesis of Deuterated Benzophenone-Bridged Rotor **(4-d$_4$)**

Benzophenone-bridged molecular gyroscope **4** has been previously reported.[11] The deuterated analog **4**-d_4 was prepared in a similar fashion from bisphenol rotor **3**-d_4[12] and 4,4′-bis(bromomethyl)benzophenone,[19] both previously reported. The ^{1}H NMR matched with the previously reported spectrum, with the exclusion of the singlet at 7.22 ppm for the central rotator. Isolated 164 mg (51% yield) of a white solid. Decomposes above 243 °C. ^{1}H NMR (400 MHz, $CDCl_3$): δ 7.60 (d, J = 8.4 Hz, 4H), 7.40 (d, J = 8.4 Hz, 4H), 7.31–7.22 (m, 24H), 7.16 (t, J = 8.0 Hz, 2H), 6.96 (ddd, J = 0.9, 2.6, 8.2 Hz, 2H), 6.35 (ddd, J = 0.9, 1.6, 7.8 Hz, 2H), 5.23 (s, 4H). ^{13}C{^{1}H} NMR (125 MHz, $CDCl_3$): δ 195.8, 158.2, 146.4, 145.0, 142.2, 136.6, 131.0 (t, J_{CD} = 25 Hz, 1C), 130.4, 129.1, 128.8, 128.0, 126.9, 126.4, 122.9, 121.9, 115.2, 115.0, 96.9, 84.6, 68.9, 56.2. FTIR (powder, ATR, cm^{-1}), 3061, 3029, 2927, 1728, 1653, 1593, 1486, 749, 698 cm^{-1}. HRMS (DART) m/z: [M]$^-$ calcd for $C_{63}H_{40}D_4O_3$ 852.3536; found: 852.3542.

Synthesis of Benzopinacol-Bridged Rotor **(5)**

Benzophenone-bridged rotor **4** (151 mg (0.18 mmol)) was dissolved in 180 mL of 1:1 benzene:isopropanol in a 4.5 cm × 15 cm cylindrical borosilicate flask with a stir bar and degassed with argon for 90 min. The reaction mixture was irradiated in a Rayonet photochemical reactor with four 12 in. 8 W (BLE-8T365) 365 nm bulbs for 24 h while stirring vigorously, and then the solvent was removed by rotary evaporation, and the resulting solids were washed with diethyl ether. The reaction appears to work best when precipitation of the pinacol product is facilitated by

evaporation and resuspension of the mixture multiple times over the course of the reaction; so, the solids were then resuspended in 150 mL of 1:1 benzene:isopropanol and degassed for 60 min before irradiation using a medium-pressure Hg Hanovia lamp for 30, 90, 180, and 240 min. All irradiations were carried out under argon while stirring vigorously. Between each irradiation, the solvent was removed by rotary evaporation, the reaction mixture was resuspended in 150 mL of 1:1 benzene:isopropanol, and the resulting suspension was degassed for 60 min. After the final irradiation, the solvent was removed to recover 135 mg (89% yield) of a white solid. mp = 233–236 °C. ^{1}H NMR (500 MHz, $CDCl_3$): δ 7.59 (t, J = 2.1 Hz, 4H), 7.40 (s, 8H), 7.33–7.16 (m, 60H), 6.88 (ddd, J = 0.5, 2.5, 8.3 Hz, 4H) 6.43 (ddd, J = 0.6, 1.7, 7.9 Hz, 4H), 4.94 (dd, J = 10.9, 20.6 Hz, 8H), 2.98 (br s, 2H); ^{13}C{^{1}H} NMR (125 MHz, $CDCl_3$): δ 159.1, 146.8, 145.3,* 145.2,* 144.1, 135.5, 131.7, 129.3,* 129.2,* 128.9, 128.7, 128.2, 127.4, 127.0, 123.2, 121.9, 117.6, 111.4, 97.1, 85.4, 83.0, 69.8, 56.3. FTIR (powder, ATR, cm^{-1}), 3569, 3059, 3030, 2925, 2865, 1661, 1598, 1486, 1447, 1240, 1034, 698 cm^{-1}. HRMS (DART) *m*/*z*: $[M - H_2 + H]^+$ calcd for $C_{126}H_{89}O_6$ 1697.6654; found: 1697.6682. (*Split signals attributed to a single carbon due to axial chirality; see Section 2.5.1 for full details.)

Synthesis of Deuterated Benzopinacol-Bridged Rotor **(5-d$_8$)**

Prepared in the same fashion as pinacol **5**. Recovered 74 mg (74% yield) of a white solid from 100 mg **4**-d_4. mp = 213–215 °C. ^{1}H NMR (500 MHz, $CDCl_3$): δ 7.59 (t, J = 2.1 Hz, 4H) 7.33–7.16 (m, 60H), 6.88 (ddd, J = 0.6, 2.6, 8.2 Hz, 4H), 6.43 (ddd, J = 0.6, 1.7, 7.9 Hz, 4H), 4.94 (dd, J = 10.9, 20.5 Hz, 8H), 2.98 (br s, 2H). ^{13}C{^{1}H} NMR (125 MHz, $CDCl_3$): δ 159.1, 146.8, 145.3,* 145.2,* 144.1, 135.5, 131.3 (t, J_{CD} = 24 Hz, 1C), 129.3,* 129.2,* 128.9, 128.7, 128.2, 127.4, 127.0, 123.0, 121.9, 117.6, 111.4, 97.1, 85.4, 83.0, 69.8, 56.3. FTIR (powder, ATR, cm^{-1}), 3576, 3058, 3030, 2923, 2856, 1659, 1599, 1484, 1447, 1245, 1035, 698 cm^{-1}. HRMS (DART) *m*/*z*: [M – H_2

+ H]$^+$ calcd for $C_{126}H_{81}D_8O_6$1705.7156; found: 1705.7167 (*signals attributed to two carbons confirmed by heteronuclear single quantum coherence (HSQC) (Figure 2.5.2.13)).

Synthesis of Tetraphenylethylene-Bridged Rotor **(2)**

Zinc powder (58 mg (0.89 mmol)) and 3.5 mL dry THF were added to a round-bottomed flask containing a magnetic stir bar and condenser. The suspension was stirred until it reached 0 °C, and a 1.0 M titanium tetrachloride solution in DCM (0.44 mL, 0.44 mmol) was added dropwise at 0 °C. The resulting mixture was heated to reflux for 2 h. Pinacol-bridged rotor **5** (151 mg, 0.089 mmol) was added in 9.5 mL THF, and the reaction was refluxed overnight. The reaction was removed from heat and quenched slowly with a 25 mL saturated ammonium chloride solution and extracted with 3 × 40 mL DCM. The combined organic layers were washed with 2 × 50 mL water and 2 × 50 mL saturated brine. The solvent was removed under reduced pressure, and the crude solid was washed with minimal benzene. The pure product (54 mg (36% yield)) was recovered as a white solid. Decomposes above 262 °C. ^{1}H NMR (500 MHz, $CDCl_3$): δ 7.60 (t, J = 2.1 Hz, 4H), 7.40 (s, 8H), 7.33–7.21 (m, 40H), 7.17 (t, J = 8.1 Hz, 4H), 7.13 (d, J = 8.3 Hz, 8H), 6.99 (d, J = 8.3 Hz, 8H), 6.85 (dd, J = 2.2, 7.9 Hz, 4H), 6.43 (ddd, J = 0.7, 1.8, 7.9 Hz, 4H), 4.91 (s, 8H); ^{13}C{^{1}H} NMR (125 MHz, $CDCl_3$): δ 158.9, 146.6, 145.1, 143.3, 140.3, 134.9, 131.5,[1] 129.1, 128.6, 128.0, 127.5, 126.9, 123.1, 121.6, 117.8, 111.1, 96.9, 85.3, 69.7, 56.1 FTIR (powder, ATR, cm^{-1}), 3057, 2867, 1600, 1579, 1491, 1232, 1021, 701 cm^{-1}. HRMS (DART) *m*/*z*: [M]$^+$ calcd for $C_{126}H_{88}O_4$ 1664.6677; found: 1664.6707.

Synthesis of Deuterated Tetraphenylethylene-Bridged Rotor **(2-d$_8$)**

Prepared in the same fashion as **2**. Isolated 36 mg (29% yield) as a white solid from 127 mg **5**-d_8. Decomposes above 240 °C. ^{1}H NMR (500 MHz, $CDCl_3$): δ 7.60 (t, J = 2.2 Hz, 4H), 7.34–7.21 (m, 40H), 7.17 (t, J = 8.0 Hz, 4H), 7.13 (d, J = 8.3 Hz, 8H), 6.99 (d, J = 8.3 Hz, 8H), 6.85

(dd, J = 2.2, 8.0 Hz, 4H), 6.43 (ddd, J = 0.7, 1.8, 7.9 Hz, 4H), 4.91 (s, 8H); $^{13}C\{^{1}H\}$ NMR (125 MHz, $CDCl_3$): δ 159.1, 146.7, 145.2, 143.4, 140.4, 135.0, 131.7, 131.3 (t, J_{CD} = 24 Hz, 1C) 129.2, 128.7, 128.2, 127.6, 127.0, 123.1, 121.8, 117.9, 111.2, 97.0, 85.4, 69.9, 56.2. FTIR (powder, ATR, cm^{-1}), 3057, 3027, 2921, 1598, 1580, 1483, 1447, 1234, 1020, 698 cm^{-1}. HRMS (DART) m/z: $[M]^+$ calcd for $C_{126}H_{80}D_8O_4$ 1672.7179; found: 1672.7186.

Author's Note: Chapter 2 is modified from the publication Howe, M. E.; Garcia-Garibay, M. A. Fluorescence and Rotational Dynamics of a Crystalline Molecular Rotor Featuring an Aggregation-Induced Emission Fluorophore. *J. Org. Chem.*, **2019**, *84*, 9570–9576.

2.5. Appendix

Supplementary Information For Chapter 2

*2.5.1. Discussion of ^{13}C NMR data for compounds **2** and **5***

Characterization of pinacol-bridged rotor **5** by ^{13}C NMR revealed 23 signals, rather than the expected 21. Initially, this was interpreted as hindered rotation of one or more phenylene groups (most likely the benzopinacol phenylenes) in a sterically crowded molecule. However, taking another spectrum at 75 °C resulted in two pairs of the peaks moving closer together, but no broadening was observed that would indicate that they would coalesce into a single peak (Figure S9). Additionally, 2D NMR analysis allowed the peaks in question to be assigned to one of the unsubstituted phenyl groups on the triphenylmethyl stator. Ultimately, we attribute the extra peaks to a stereochemical consequence of the complex axial chirality available to the molecule. Each of the four triphenylmethyl stators, as well as the central pinacol bond can be arranged in an M or P fashion, and our evidence suggests that at least one of these stereoisomers gives a magnetically distinct environment to the stator phenyls.

The TPE-bridged rotor **2** also gave unexpected ^{13}C NMR results. Specifically, instead of the expected 21 signals, it showed only 20. Further investigation via HSQC revealed cross-peaks between the carbon signal at 131.5 ppm and both the rotator proton signal and the TPE proton closest to the alkene linker (Figure S13). Due to this, we assign the 131.5 ppm carbon signal to both the rotator carbon and the methine carbon closest to the alkene linker, and conclude that the signals are coincidentally degenerate.

2.5.2. Compound spectra (^{1}H NMR, ^{13}C NMR, IR)

Figure 2.5.2.1. ^{1}H NMR ($CDCl_3$, 400MHz) spectrum of deuterated benzophenone-bridged rotor **4-d$_4$**.

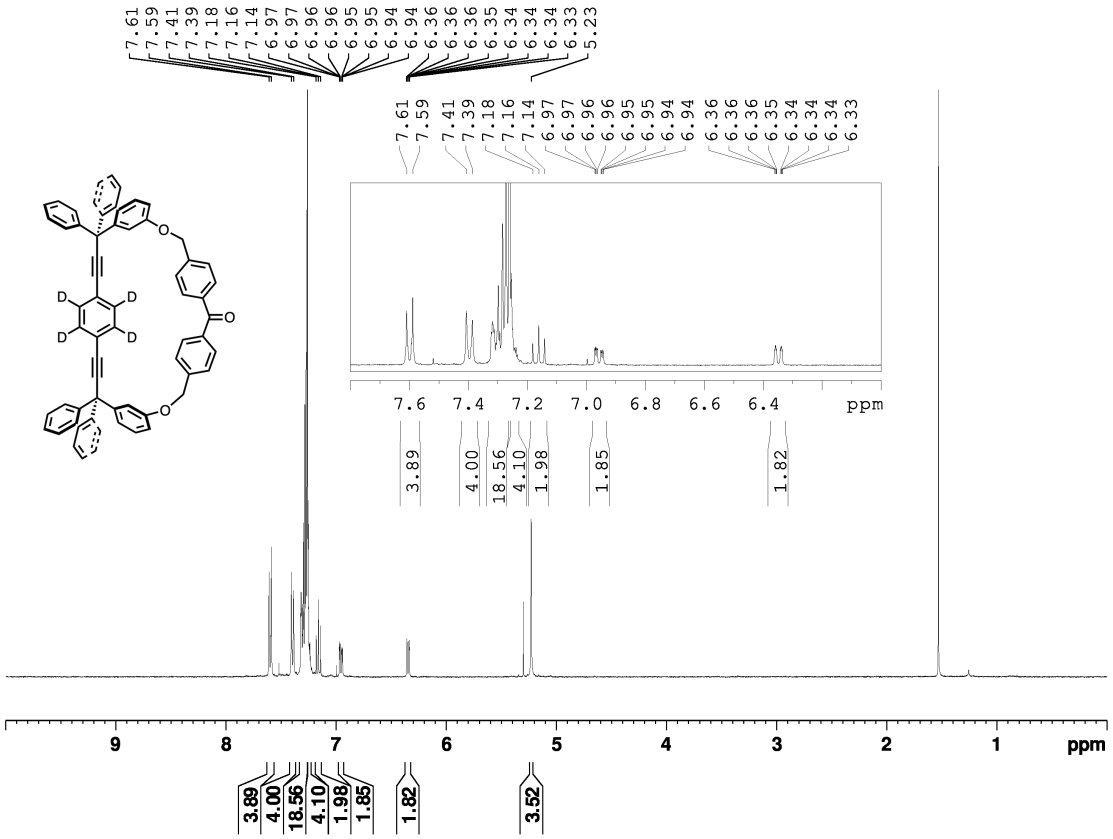

Figure 2.5.2.2. $^{13}C\{^{1}H\}$ NMR ($CDCl_3$, 500MHz) spectrum of deuterated benzophenone-bridged rotor **4-d$_4$**.

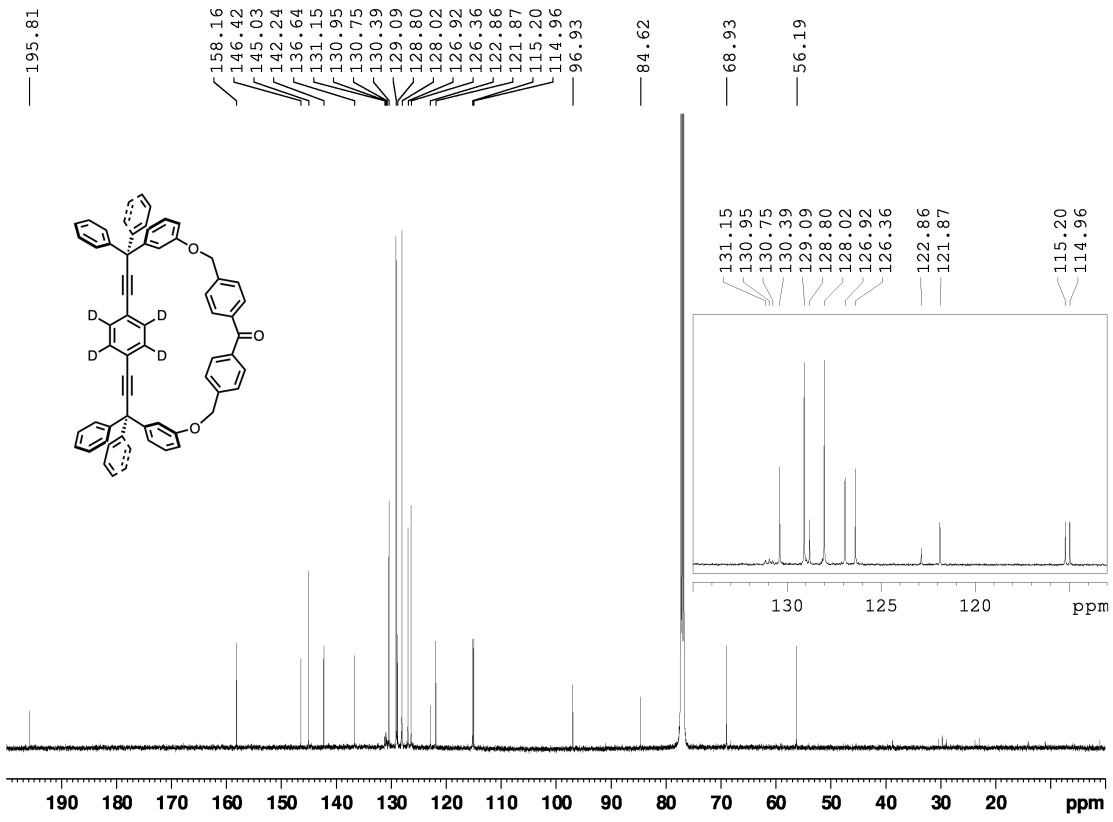

Figure 2.5.2.3. FTIR spectrum of deuterated benzophenone-bridged rotor **4-d$_4$**.

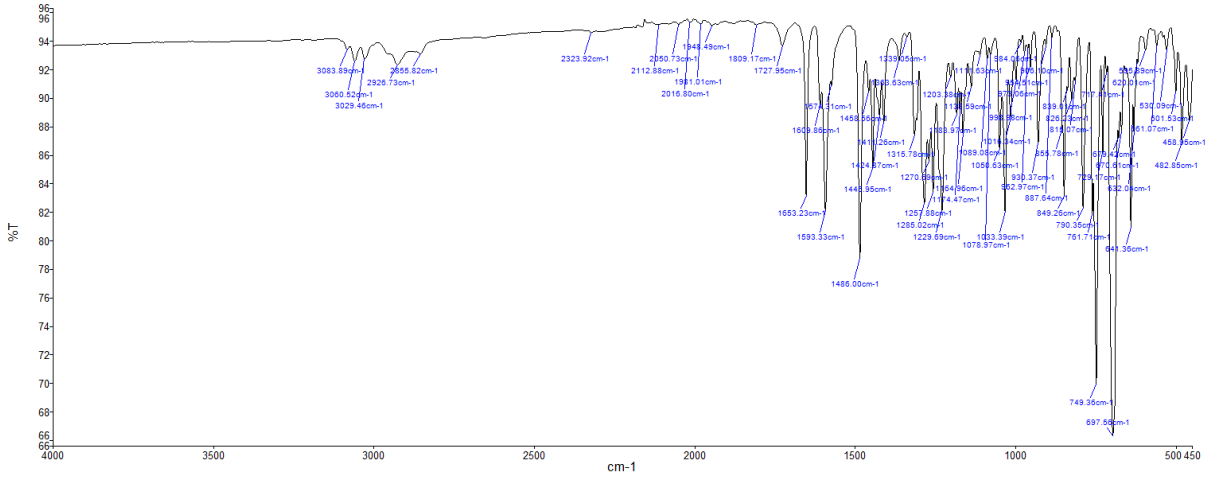

Figure 2.5.2.4. ^{1}H NMR ($CDCl_3$, 500MHz) spectrum of pinacol-bridged rotor **5**.

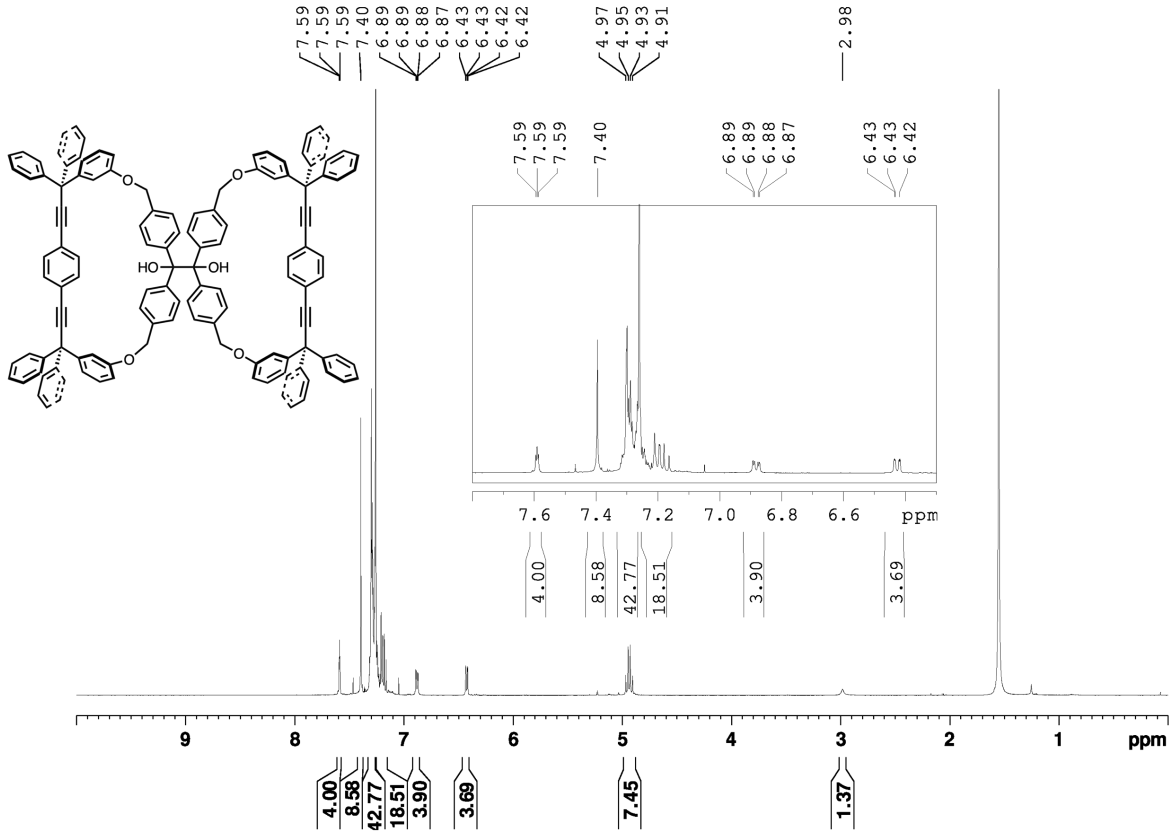

Figure 2.5.2.5. $^{13}C\{^{1}H\}$ NMR ($CDCl_3$, 500MHz) spectrum of pinacol-bridged rotor **5**.

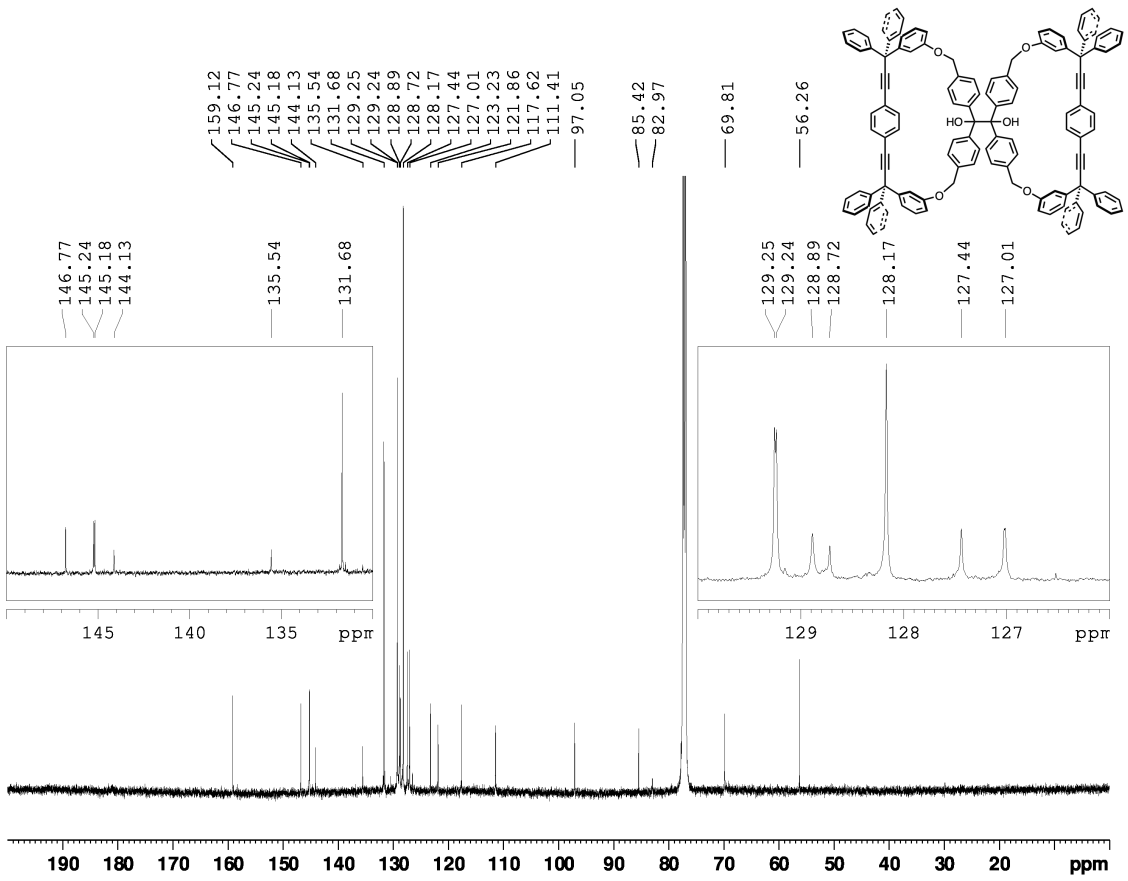

Figure 2.5.2.6. FTIR spectrum of pinacol-bridged rotor **5**.

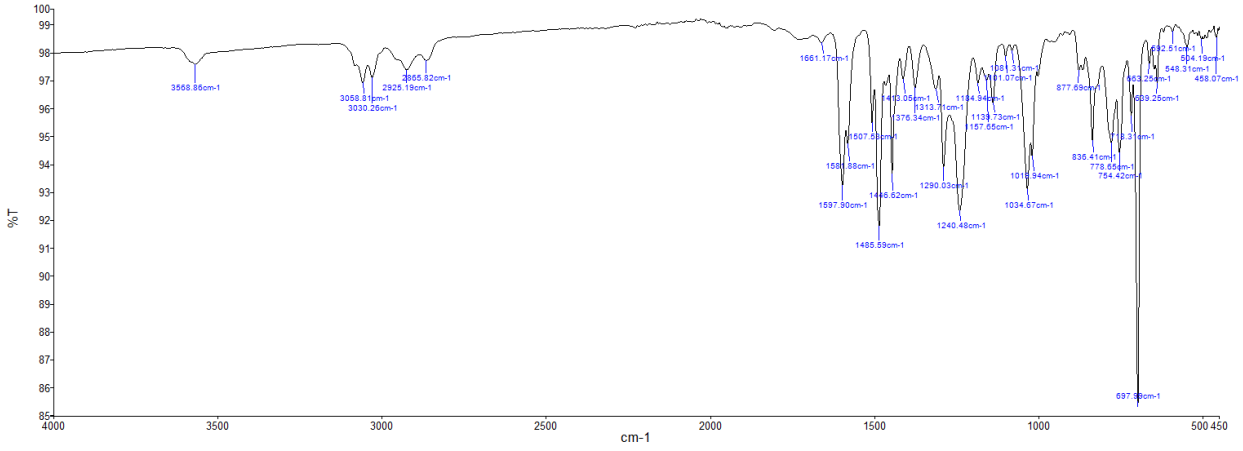

Figure 2.5.2.7. ^{1}H NMR ($CDCl_3$, 500MHz) spectrum of deuterated pinacol-bridged rotor **5-d$_8$**.

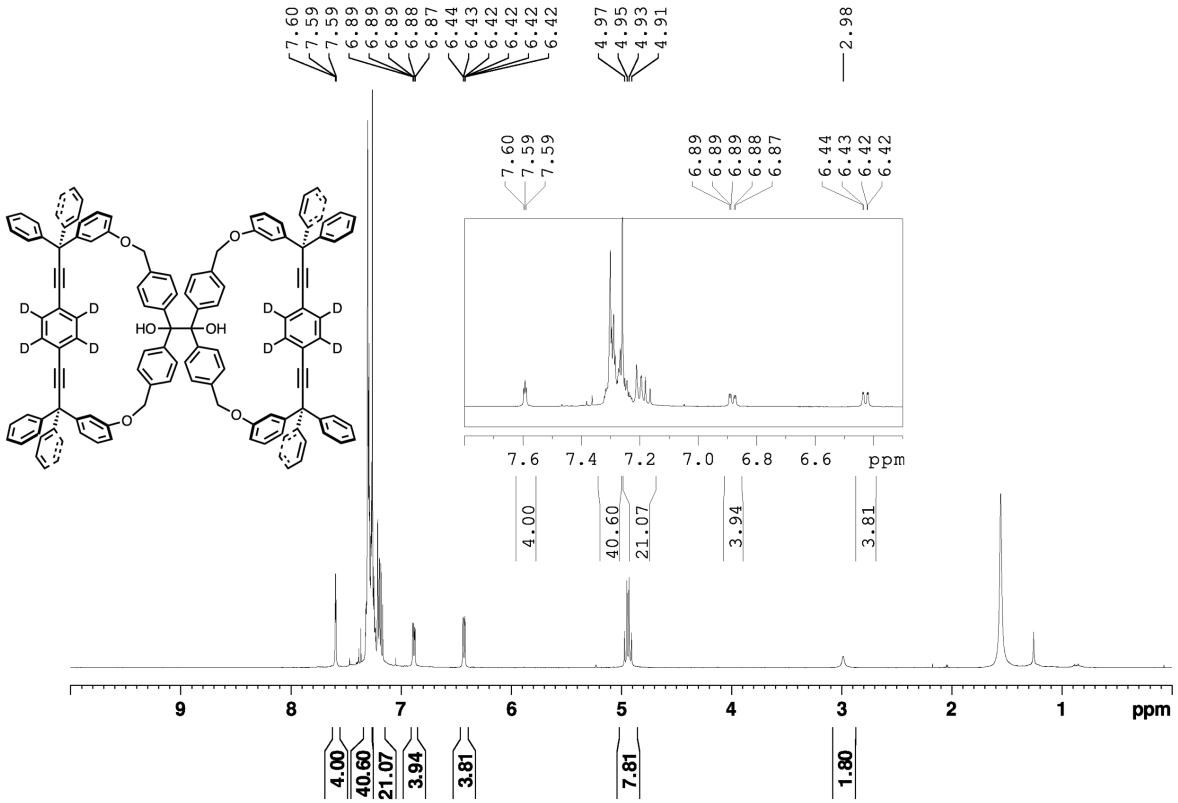

Figure 2.5.2.8. $^{13}C\{^{1}H\}$ NMR ($CDCl_3$, 500MHz) spectrum of deuterated pinacol-bridged rotor **5-d_8**.

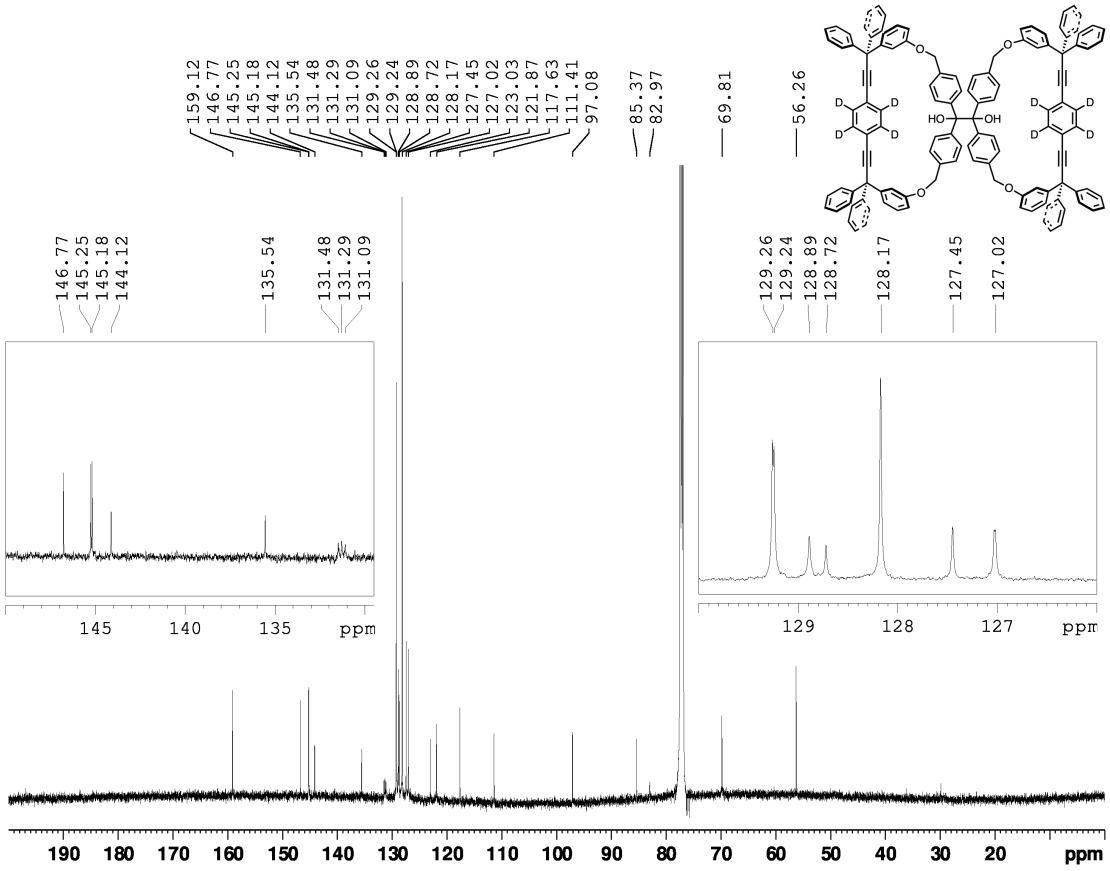

Figure 2.5.2.9. $^{13}C\{^{1}H\}$ NMR (1,1,2,2,-tetrachloroethane, 500MHz) spectrum of deuterated pinacol-bridged rotor **5-d$_8$** at 300K and 348 K.

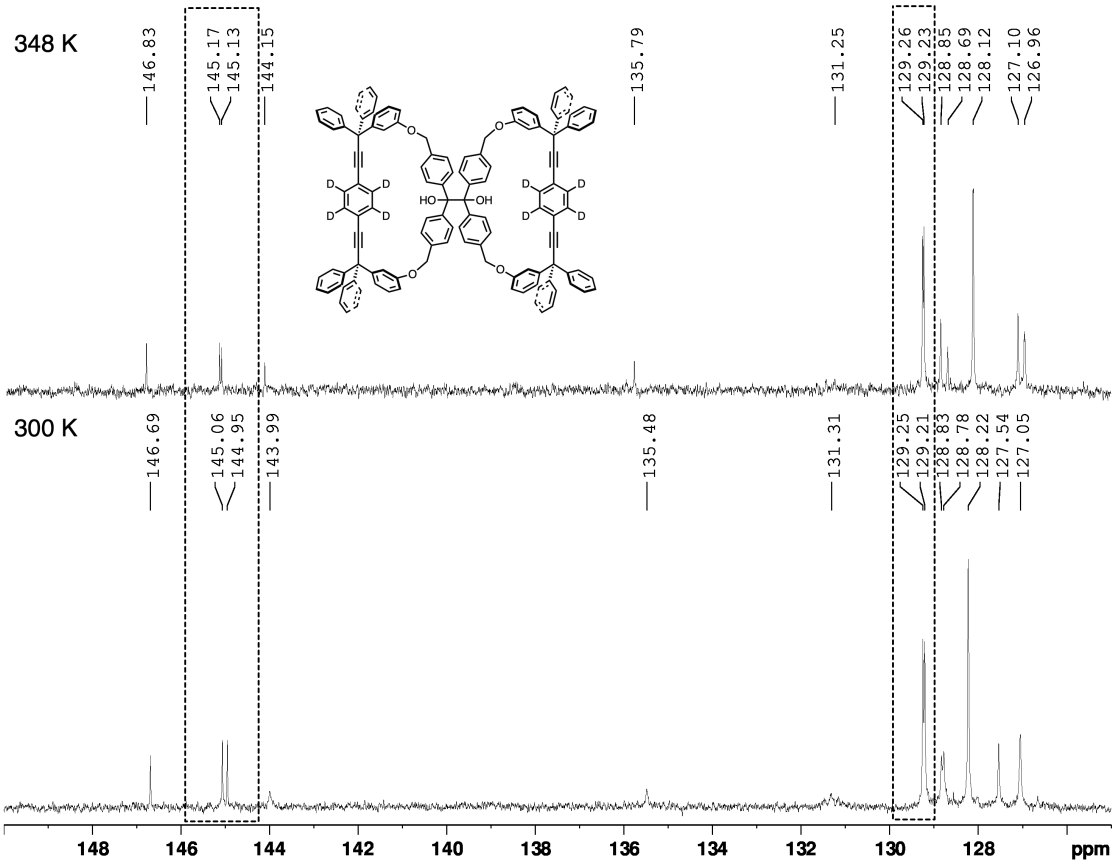

Figure 2.5.2.10. FTIR spectrum of deuterated pinacol-bridged rotor **5-d$_8$**.

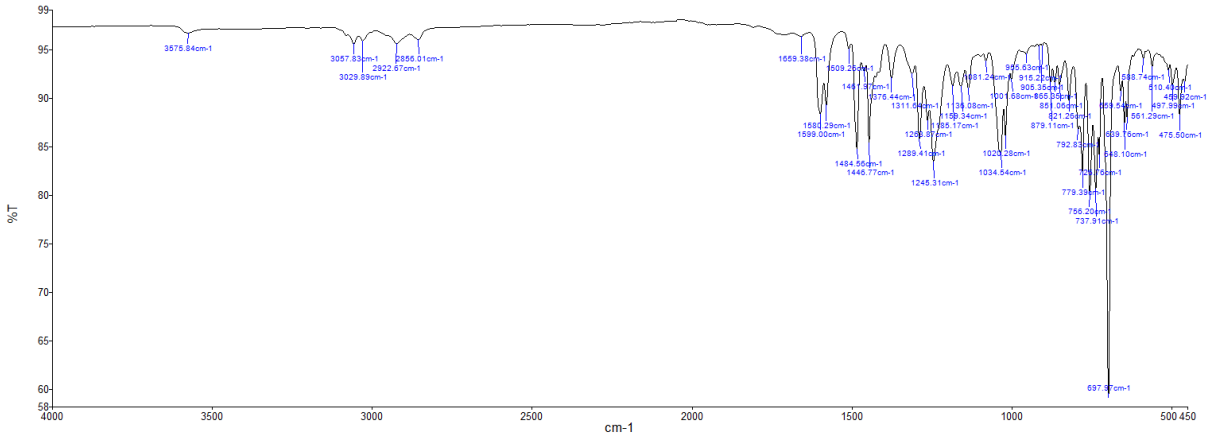

Figure 2.5.2.11. ^{1}H NMR ($CDCl_3$, 500MHz) spectrum of tetraphenylethylene-bridged rotor **2**.

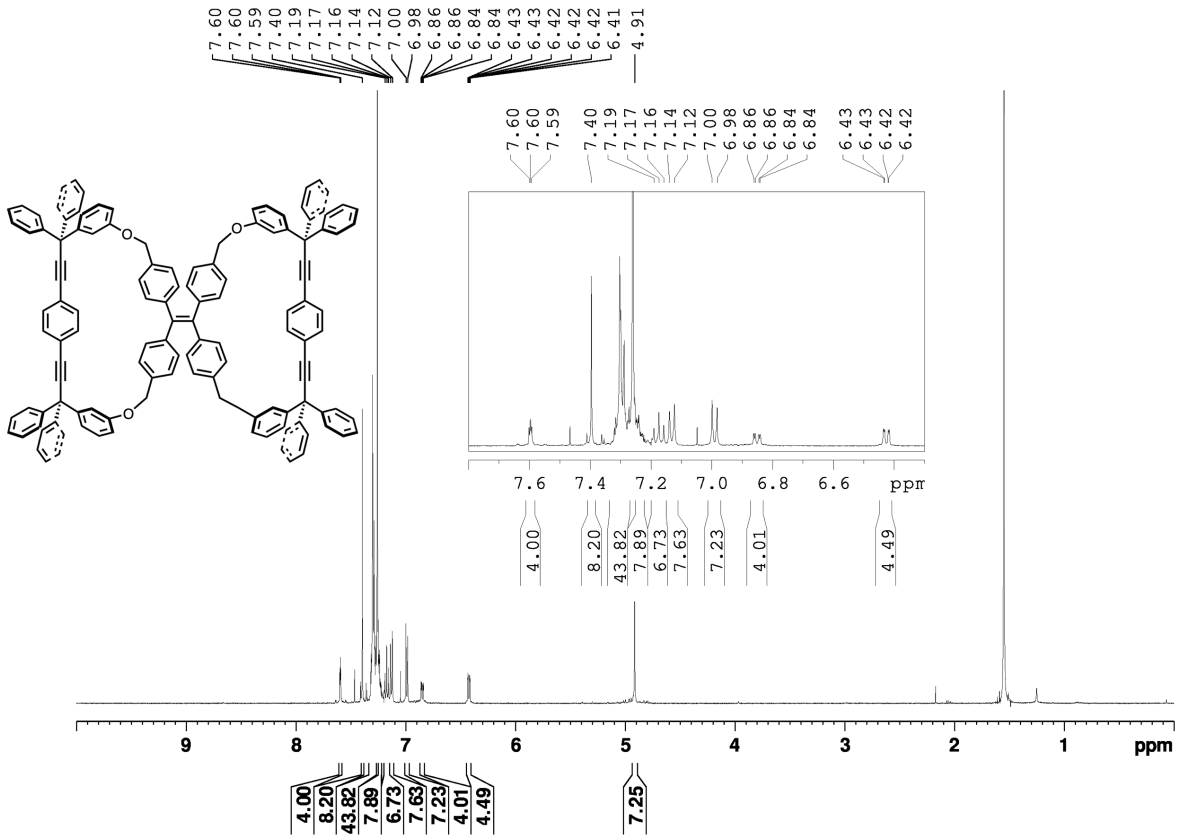

Figure 2.5.2.12. $^{13}C\{^{1}H\}$ NMR ($CDCl_3$, 500MHz) spectrum of tetraphenylethylene-bridged rotor **2**.

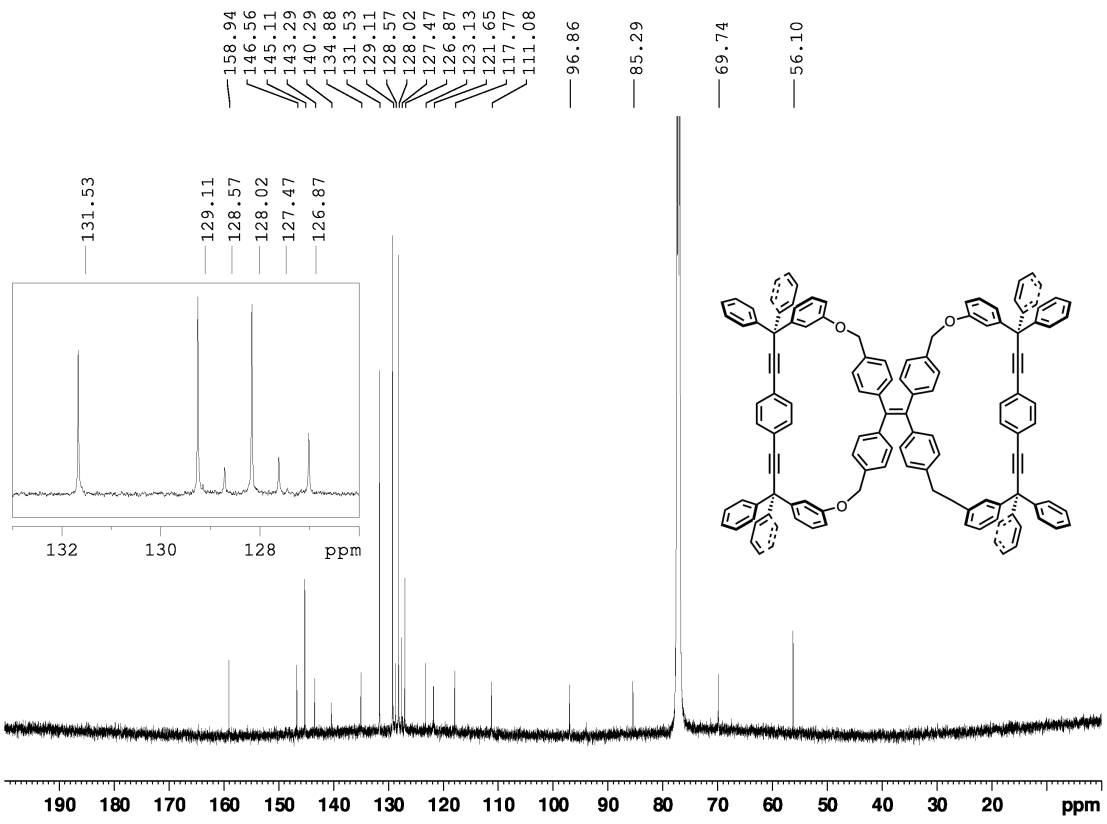

Figure 2.5.2.13. HSQC spectrum of tetraphenylethylene-bridged rotor **2**.

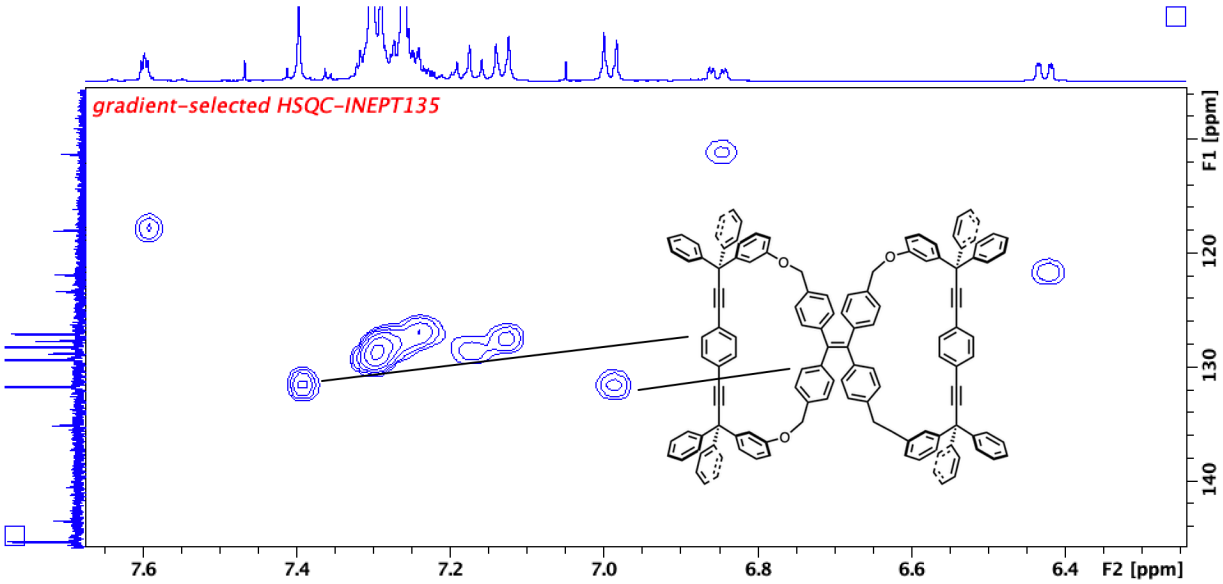

Figure 2.5.2.14. FTIR spectrum of tetraphenylethylene-bridged rotor **2**.

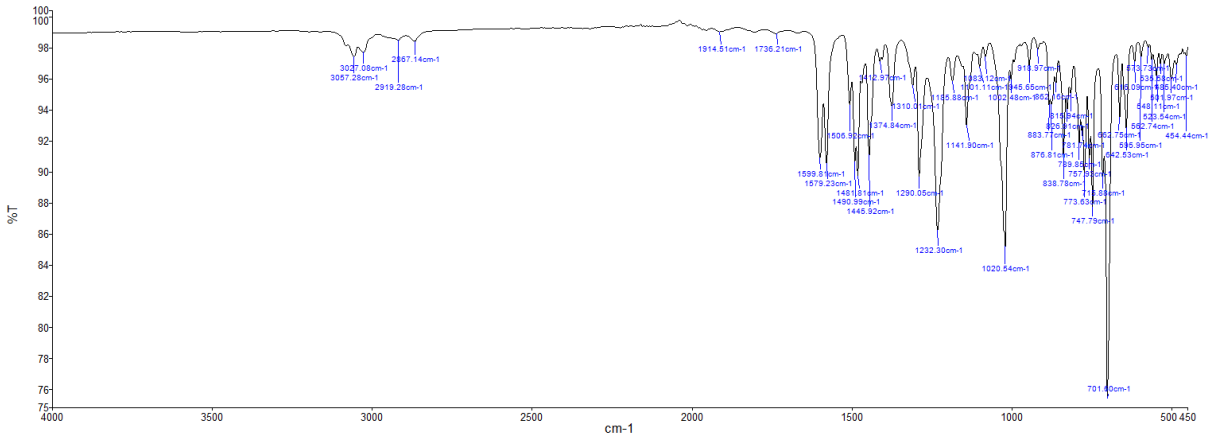

Figure 2.5.2.15. ^{1}H NMR ($CDCl_3$, 500MHz) spectrum of deuterated tetraphenylethylene-bridged rotor **2-d$_8$**.

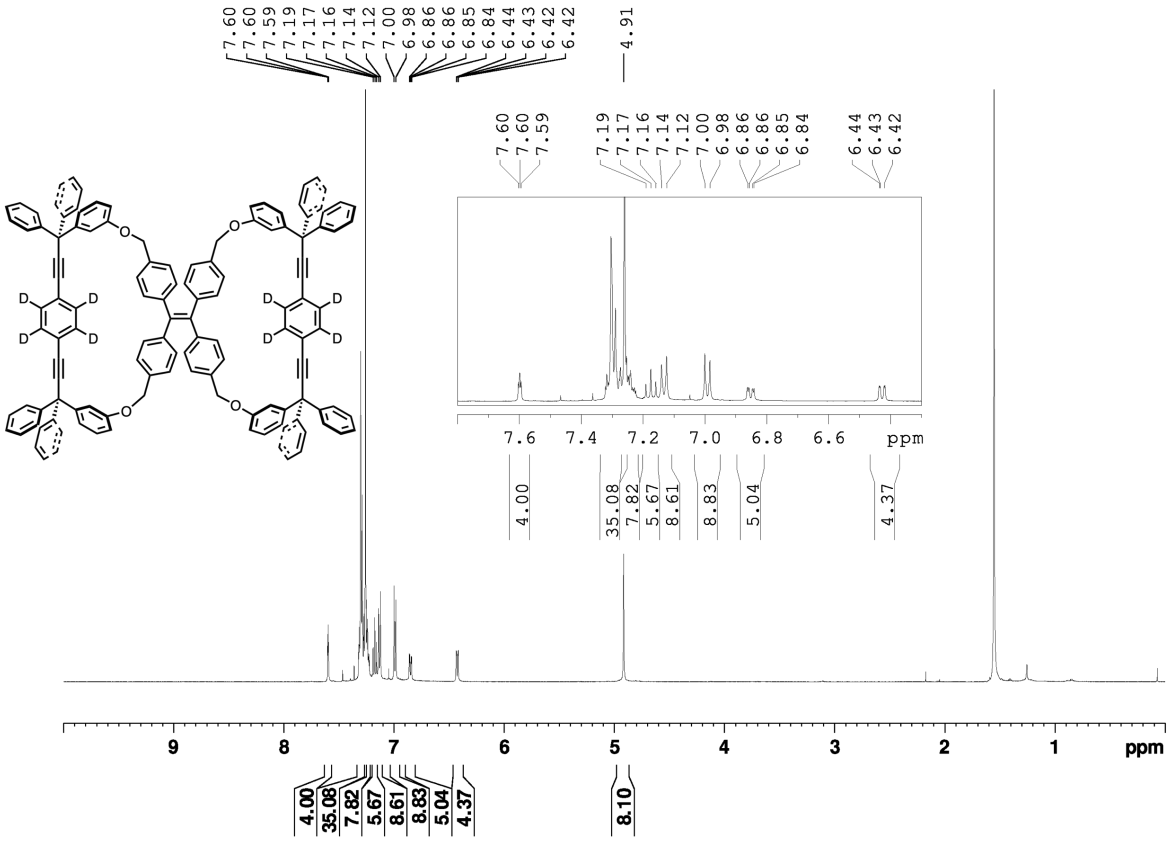

Figure 2.5.2.16. $^{13}C\{^{1}H\}$ NMR ($CDCl_3$, 500MHz) spectrum of deuterated tetraphenylethylene-bridged rotor **2-d$_8$**.

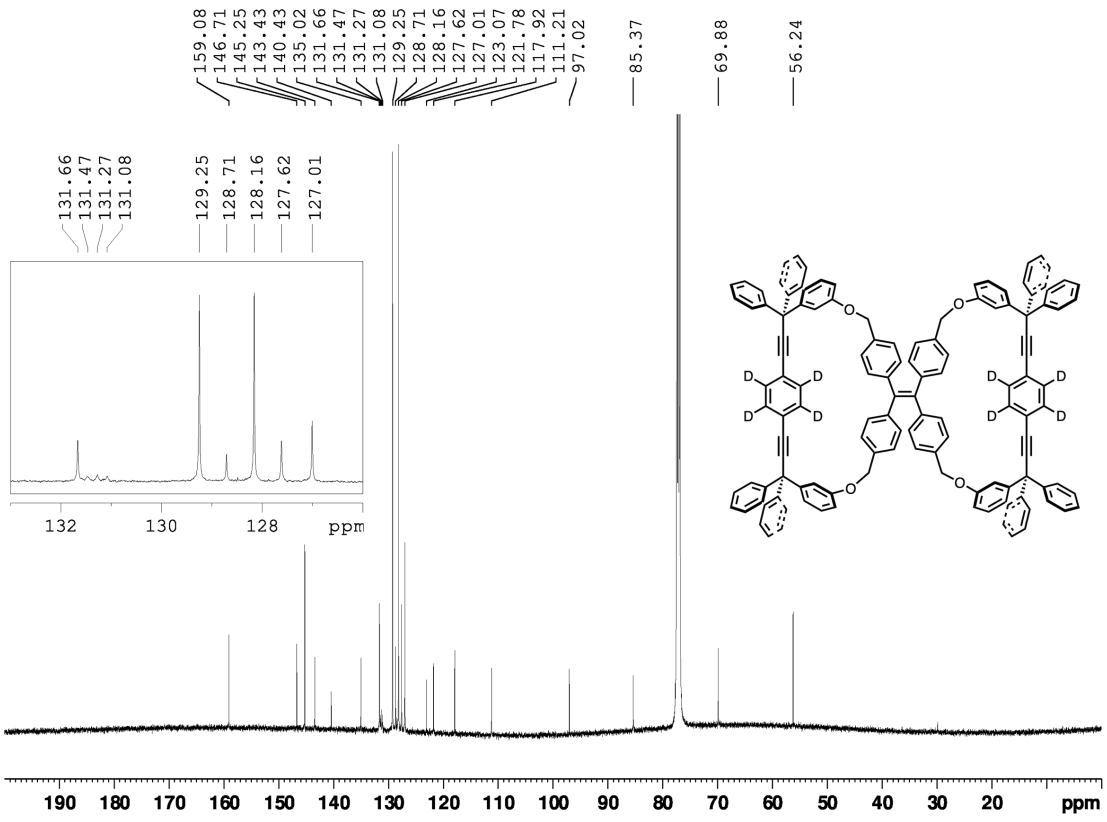

Figure 2.5.2.17. FTIR spectrum of deuterated tetraphenylethylene-bridged rotor **2-d$_8$**.

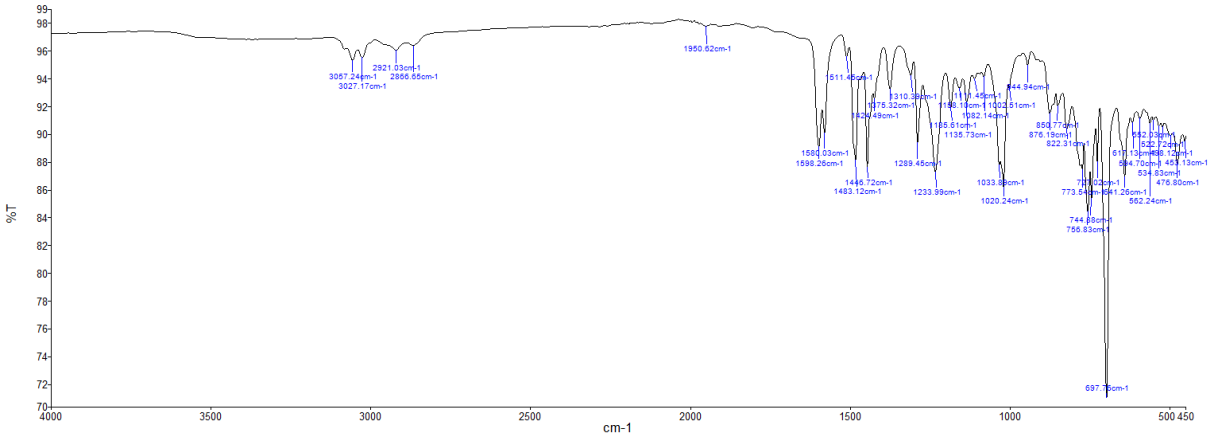

*2.5.3. Solution-state lifetime measurements of aggregation of **2***

Figure 2.5.3.1. Fluorescence lifetime at 467 nm of 4.4 μM **2** in THF over 10 days when excited at 300 nm.

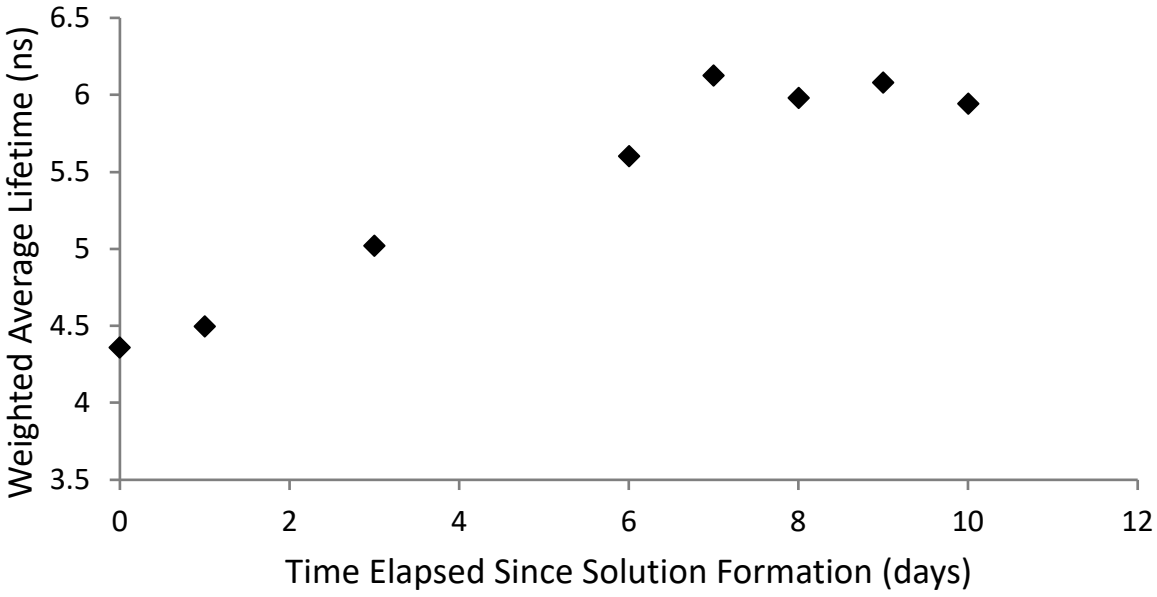

*2.5.4. Fluorescence emission spectrum of **2** irradiated as a powder*

Figure 2.5.4.1. Fluorescence emission of **2** that was first irradiated as a powder, and then dissolved in THF for fluorescence analysis.

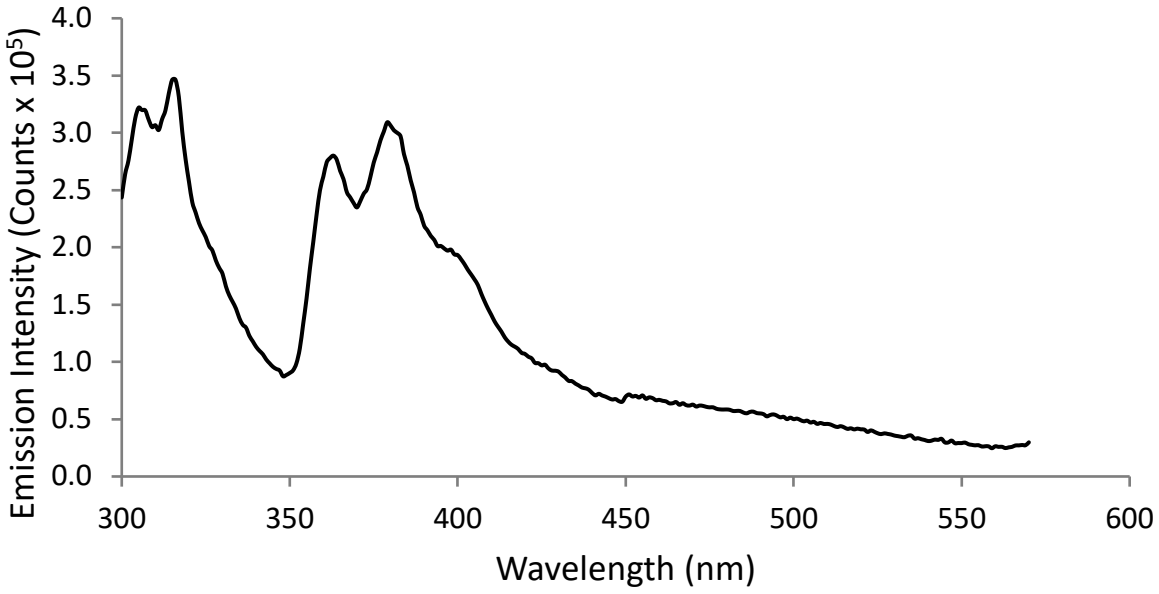

2.6. References

[1] (a) Erbas-Cakmak, S.; Leigh, D. A.; Mcternan, C. T.; Nussbaumer, A. L. Artificial Molecular Machines. *Chem. Rev.* **2015**, *115*, 10081−10205. (b) *Molecular Machines and Motors*; Credi, A., Silvi, S., Venturi, M., Eds.; Springer, **2014**. (c) Kassem, S.; van Leeuwen, T.; Lubbe, A. S.; Wilson, M. R.; Feringa, B. L.; Leigh, D. A. Artificial Molecular Motors. *Chem. Soc. Rev.* **2017**, *46*, 2592−2621.

[2] (a) Khuong, T. A. V.; Nuñez, J. E.; Godinez, C. E.; Garcia- Garibay, M. A. Crystalline Molecular Machines: A Quest Toward Solid-State Dynamics and Function. *Acc. Chem. Res.* **2006**, *39*, 413− 422. (b) Catalano, L.; Naumov, P. Exploiting Rotational Motion in Molecular Crystals. *CrystEngComm* **2018**, *20*, 5872−5883.

[3] (a) Dominguez, Z.; Dang, H.; Strouse, M. J.; Garcia-Garibay, M. A. "Molecular Compasses and Gyroscopes I. Expedient Synthesis and Solid State Dynamics of an Open Rotor with a Bis(triarylmethyl) Frame. *J. Am. Chem. Soc.* **2002**, *124*, 2398−2399. (b) Dominguez, Z.; Dang, H.; Strouse, J. M.; Garcia-Garibay, M. A. Molecular "Compasses" and "Gyroscopes." III. Two-Fold Flipping of a Phenylene Rotor and Six-Fold Rotation of Clathrated Benzene in a Slipping-Gear Crystal Lattice. *J. Am. Chem. Soc.* **2002**, *124*, 7719− 7727. (c) Khuong, T. A. V.; Zepeda, G.; Ruiz, R.; Kahn, S. I.; Garcia- Garibay, M. A. Molecular Compasses and Gyroscopes. Engineering Molecular Crystals with Internal Rotation in the Gigaherz Regime. *Cryst. Growth Des.* **2004**, *4*, 15−18.

[4] Kottas, G. S.; Clarke, L. I.; Horinek, D.; Michl, J. Artificial Molecular Rotors. *Chem. Rev.* **2005**, *105*, 1281−1376.

[5] Jarowski, P. D.; Houk, K. N.; Garcia-Garibay, M. A. Importance of Correlated Motions on the Low Barrier Rotational Potentials of Crystalline Molecular Gyroscopes. *J. Am. Chem. Soc.* **2007**, *129*, 3110−3117.

[6] Jiang, X.; O'Brien, Z. J.; Yang, S.; Buenaflor, J.; Khan, S. I.; Houk, K. N.; Garcia-Garibay, M. A.; et al. Crystal Fluidity Reflected by Fast Rotational Motion at the Core, Branches and Surface Aromatic Groups of a Dendrimeric Molecular Rotor. *J. Am. Chem. Soc.* **2016**, *138*, 4650−4656.

[7] Gould, S. L.; Rodriguez, R. B.; Garcia-Garibay, M. A. Synthesis and Solid State Dynamics of Molecular Dirotors. *Tetrahedron* **2008**, *64*, 8336−8345.

[8] (a) La, D. D.; Bhosale, S. V.; Jones, L. A.; Bhosale, S. V. Tetraphenylethylene-Based AIE-Active Probes for Sensing Applica- tions. *ACS Appl. Mater. Interfaces* **2018**, *10*, 12189−12216. (b) Mei, J.; Leung, N. L. C.; Kwok, R. T. K.; Lam, J. W. Y.; Tang, B. Z. Aggregation-Induced Emission: Together We Shine, United We Soar! *Chem. Rev.* **2015**, *115*, 11718−11940.

[9] (a) Shustova, N. B.; Mccarthy, B. D.; Dinca, M. Turn-On Fluorescence in Tetraphenylethylene-Based Metal- Organic Frame- works: An Alternative to Aggregation-Induced Emission. *J. Am. Chem. Soc.* **2011**, *2*, 20126−20129. (b) Shustova, N. B.; Ong, T.-C.; Cozzolino, A. F.; Michaelis, V. K.; Griffin, R. G.; Dinca, M. Phenyl Ring Dynamics in a Tetraphenylethylene-Bridged

Metal−Organic Framework: Implications for the Mechanism of Aggregation- Induced Emission. *J. Am. Chem. Soc.* **2012**, *134*, 15061−15070.

[10] (a) Jia, X.; Shao, C.; Bai, X.; Zhou, Q.; Wu, B.; Wang, L.; Yue, B.; Zhu, H.; Zhu, L. Photoexcitation-controlled self-recoverable molecular aggregation for flicker phosphorescence. *Proc. Natl. Acad. Sci. U.S.A.* **2019**, *116*, 4186−4821. (b) Zhao, Z.; Chen, C.; Wu, W.; Wang, F.; Du, L.; Zhang, X.; Xiong, Y.; He, X.; Cai, Y.; Kwok, R. T. K.; Lam, J. W. Y.; Gao, X.; Sun, P.; Phillips, D. L.; Ding, D.; Tang, B. Z. Highly efficient photothermal nanoagent achieved by harvesting energy via excited-state intramolecular motion within nanoparticles. *Nat. Commun*. **2019**, *10*, No. 768.

[11] Commins, P.; Nuñez, J. E.; Garcia-Garibay, M. A. Synthesis of Bridged Molecular Gyroscopes with Closed Topologies: Triple One- Pot Macrocyclization. *J. Org. Chem.* **2011**, *76*, 8355−8363.

[12] Commins, P.; Garcia-Garibay, M. A. Photochromic Molecular Gyroscope with Solid State Rotational States Determined by an Azobenzene Bridge. *J. Org. Chem.* **2014**, *79*, 1611−1619.

[13] Turro, N. J.; Ramamurthy, V.; Scaiano, J. C. *Modern Molecular Photochemistry of Organic Molecules*; U Science: Sausalito, CA, **2010**.

[14] (a) Aldred, M. P.; Li, C.; Zhu, M. Q. Optical Properties and Photo-Oxidation of Tetraphenylethene-Based Fluorophores. *Chem. Eur. J.* **2012**, *18*, 16037−16045. (b) Prlj, A.; Dosl̆ić, N.; Corminboeuf, C. How Does Tetraphenylethylene Relax from Its Excited States? *Phys. Chem. Chem. Phys.* **2016**, *18*, 11606−11609. (c) Cai, Y.; Du, L.; Samedov, K.; Gu, X.; Qi, F.; Sung, H. H. Y.; Patrick, B. O.; Yan, Z.; Jiang, X.; Zhang, H.; et al. Deciphering the Working Mechanism of Aggregation-Induced Emission of Tetraphenylethylene Derivatives by Ultrafast Spectroscopy. *Chem. Sci.* **2018**, *9*, 4662−4670.

[15] Macho, V.; Brombacher, L.; Spiess, H. W. The NMR- WEBLAB: An Internet Approach to NMR Lineshape Analysis. *Appl. Magn. Reson.* **2001**, *20*, 405−432.

[16] O'Brien, Z. J.; Karlen, S. D.; Khan, S.; Garcia-Garibay, M. A. Solid State Molecular Rotors with Perdeuterated Stators: Mechanistic Insights from Biphenylene Rotational Dynamics in Ordered and Disordered Crystal Forms. *J. Org. Chem.* **2010**, *75*, 2482−2491.

[17] (a) Lemouchi, C.; Vogelsberg, C. S.; Zorina, L.; Simonov, S.; Batail, P.; Brown, S.; Garcia-Garibay, M. A. Ultra-fast Rotors for Molecular Machines and Functional Materials via Halogen Bonding: Crystals of 1,4-Bis(iodoethynyl)bicyclo[2.2.2]octane with Distinct Gigahertz Rotation at Two Sites. *J. Am. Chem. Soc.* **2011**, *133*, 6371− 6379. (b) Rodríguez-Molina, B.; Perez-Estrada, S.; Garcia-Garibay, M. A. Amphidynamic Crystals of a Steroidal Bicyclo[2.2.2]octane Rotor: A High Symmetry Group that Rotates Faster than Smaller Methyl and Methoxy Groups. *J. Am. Chem. Soc.* **2013**, *135*, 10388−10395. (c)Catalano,L.;Peŕez-Estrada, S.; Terraneo, G.; Pilati, P.; Resnati, G.; Metrangolo, P.; Garcia-Garibay, M. A. Dynamic Characterization of Crystalline Supramolecular Rotors Assembled through Halogen Bonding. *J. Am. Chem. Soc.* **2015**, *137*, 15386−15389. (d) Catalano, L.; Perez-Estrada, S.; Metrangolo, P.; Wang, S. H.;

Ayitou, A. J.-L.; Brown, S.; Garcia-Garibay, M. A.; et al. Rotational Dynamic of a Diazabicyclo[2.2.2]octane in Isomorphous Halogen-Bonded Co- Crystals: Entropic and Enthalpic Effects. *J. Am. Chem. Soc.* **2017**, *139*, 843−848.

[18] Jin, M.; Chung, T. S.; Seki, T.; Ito, H.; Garcia-Garibay, M. A. Phosphorescence Control Meditated by Molecular Rotation and Aurophilic Interactions in Amphidynamic Crystals of 1,4-Bis[tri-(p- fluorophenyl)phosphane-gold(I)-ethynyl]benzene. *J. Am. Chem. Soc.* **2017**, *39*, 18115−18121.

[19] Grützmacher, H.-F.; Husemann, W. Syntheses and Reactions of Some New Dithia[3.1.3.1] Paracyclophanes and [2.1.2.1] Para- cyclophanes. *Tetrahedron* **1987**, *43*, 3205−3211.

CHAPTER 3

Fluorescence Anisotropy Decay of Molecular Rotors with Acene Rotators in Viscous Solution

3.1. Introduction

Over the last few years, we[1] and others[2] have made substantial progress in the design and characterization of molecular rotors in the solid state. We have shown that dumbbell-shaped molecules with small rotating groups linked by triple bonds to bulky substituents constitute a robust design.[1] For example, variable temperature ^{2}H NMR studies show that crystals of 1,4-bis(2-triphenylsilylethynyl)benzene **1** (Scheme 3.1.1) display phenylene rotation in the form of 180^o flips with correlation times of only ca. 166 ns at 298 K.[3] Considering that many other analogs have been documented, we became interested in the potential installation of these and other molecular rotors in confined viscous media, such as monolayers and membranes where internal and whole body rotation may occur within similar time scales. With that in mind, we decided to explore a set of molecular rotors designed to determine their whole body dynamics in a viscous medium by taking advantage of time-resolved fluorescence anisotropy decay.[4] This method has been used extensively to observe the rotation of biomacromolecules[5] and relies on the rapid generation of polarized emission from a suitable fluorophore followed by its loss as a result of molecular rotation. The first step relies on the use of a short pulse of linearly polarized light that selectively excites molecules that happen to have a component of their transition dipole moment for absorption aligned with the direction of polarization. The intensity of polarized emission measured immediately after pulsed excitation reflects the highest anisotropy, which may be positive or negative depending on the relative orientations of the transition dipole moments associated with excitation and emission, and evolves as a function of time as the emitting molecules reach a randomly oriented (isotropic) state.

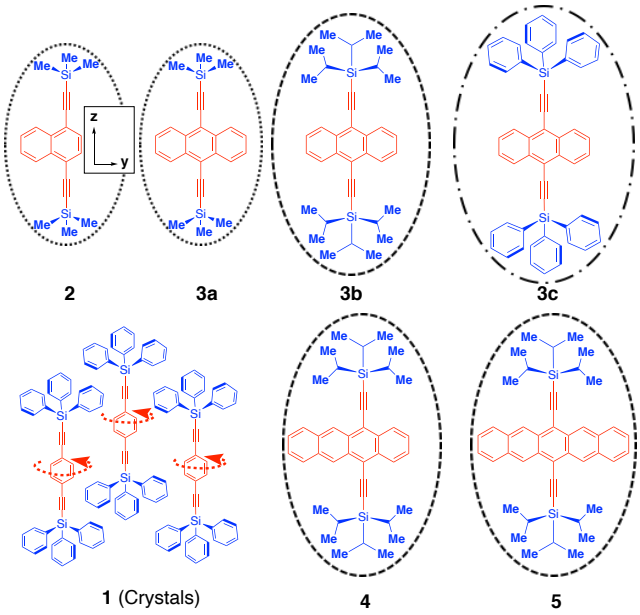

Scheme 3.1.1. Systems of interest and reference coordinate system.

We selected the six molecular rotors shown in Scheme 3.1.1 built with shape-persistent stators of different bulk, including trimethylsilyl (TMS, **2**[6] and **3a**[7]), triisopropylsilyl (TIPS, **3b**,[6] **4**[8] and **5**[5]), and triphenylsilyl (TPS, **3c**[6]). As in the case of **1**, these were linked by triple bonds to substituted acene rotators that include naphthalene (**2**), anthracene (**3a**, **3b** and **3c**), tetracene (**4**) and pentacence (**5**). Knowing that all these acenes have their lowest energy transition dipole moments aligned with the axis of the triple bonds[9] (as indicated with **2**), we expected that the decay of their fluorescence anisotropy would occur as a function of rotation about the x/y axes. We assumed that molecular rotors **2-5** can be viewed as a set of prolate-shaped molecules with sizes determined primarily the by the bulk of the silyl substituents, with Ph > iPr > Me. After determining the absorption and emission characteristics of **2-5** in dilute pentane solutions we carried out analogous measurements in mineral oil along with steady state and time-resolved polarization measurements. Our results are consistent with the emission of these molecules being

polarized along the dialkyne acene z-axis, and we were able to determine that the polarization decay of molecular rotors **2-5** in viscous mineral oil can be fit to single exponential functions in the nanosecond regime, consistent with molecular tumbling along the dialkyne axis. We confirmed that rotational correlation times are determined by the size of the stator, rather than by the nature of the acene rotators.

3.2. Results and Discussion

Molecular rotors with naphthalene (**2**)[6] and anthracene (**3**)[7] rotators were synthesized *via* Sonogashira coupling between the appropriate TMS-, TIPS-, or TPS- silylacetylene and the corresponding dibromoacene according to literature precedent. Compounds **4**[8] and **5**[6] were also synthesized by previously established methods by a double nucleophilic attack of TIPS acetylide on the corresponding quinone followed by re-aromatization. It should be pointed out that compounds **4** and **5** had to be covered in tinfoil to avoid degradation by reaction with singlet oxygen when exposed to light. The photophysics of all molecular rotors were analyzed in pentane and in mineral oil. Solutions in mineral oil were prepared by dissolving the compound of interest in spectrophotometric grade hexane followed by the addition of mineral oil and removal of hexane by rotary evaporation before attaining the desired concentration by diluting with additional oil. This procedure assisted in dissolving the compounds, which would otherwise take days to fully dissolve. However, it must be pointed out that there is some uncertainty in the composition of the oil solutions.

Figure 3.2.1 shows the UV-Vis absorption (purple, Figure 3.2.1a), fluorescence excitation (solid dark blue, Figure 3.2.1b), and fluorescence emission (dashed light blue, Figure 3.2.1b) spectra of **3a** in mineral oil as a representative example of the behavior observed for compounds

2-5 (Figures 3.5.2.1-3.5.2.6). The UV-Vis (purple) and fluorescence excitation (solid blue) spectra

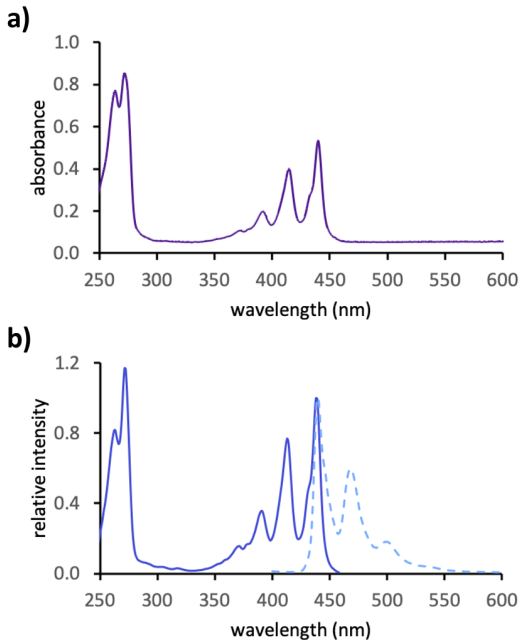

Figure 3.2.1. a) UV-Vis absorption spectrum and b) fluorescence excitation (solid dark blue) and fluorescence emission (dashed light blue) spectra of **3a** in mineral oil. Fluorescence excitation and emission spectra were normalized at the 0-0 transition. UV-Vis was obtained in a 7.1 μM pentane solution, 9.4 μM in mineral oil. Fluorescence in pentane: 1.8 μM, excitation scan collected for emission at 463 nm, emission scan collected for excitation at 272 nm with a 350 nm longpass emission filter. Fluorescence in mineral oil: 0.9 μM, excitation scan collected for emission at 468 nm, emission scan collected for excitation at 272 nm with a 350 nm longpass emission filter.

have an excellent agreement with the lowest energy transition displaying a mirror image relation with a strong 0-0 overlap for all compounds. As shown in Figures 3.5.2.1-3.5.2.6, no significant differences were observed between the spectra obtained in pentane and those measured in mineral oil.

As previously reported and illustrated for TMS-anthracene rotor **3a** in Figure 3.2.1, two main spectral bands were observed for all compounds in the series. A high-energy transition (HE) with relatively narrow overlapping peaks with maxima that ranged from 249 nm for **2** to 309 nm for **5**, as summarized in Table 3.2.1 (Figures 3.5.2.1-3.5.2.6). A lower energy transition (LE) displayed the characteristic vibrational structure of the rigid acene chromophores. The wavelength of maximum intensity in mineral oil ranged 349 nm for **2** to 642 nm for **5** (Table 3.2.1). The absorption and emission maxima of **2**-**5** in mineral oil are summarized in Table 3.2.1. As expected, the absorption and emission maxima red-shift as the number of rings in the acene increases from two to five (Table 3.2.1).

Molecular Rotor	UV HE λ_{max} (nm)	UV LE λ_{max} (nm)	Fluor em λ_{max} (nm)	Lifetime (ns)	Rotational correlation time (ns)
2	249	349	350	1.9	3.27
3a	271	440	440	5.4	3.92
3b	273	441	441	4.9	5.08
3c	269	446	446	4.4	8.19
4	292	535	534	10.3	5.66
5	309	642	643	19.1	5.15

Table 3.2.1. Summary of fluorescence and UV-Vis data for molecular rotors **2**-**5** in mineral oil.

The fluorescence lifetimes of molecular rotors **2**-**5** were obtained in mineral oil using a time correlated single photon counting spectrometer. The results summarized in Table 3.2.1 indicate that the lifetimes of the acenes vary by a factor of 10, from 1.90 ns in the case of naphthalene rotator **2** up to 19.1 ns for pentacene rotator **5**. Changing the stator in the case of anthracenes **3a**, **3b** and **3c** resulted in relatively small lifetime variations where the lifetimes shorten as the stator size increases, from 5.4 ns in the case of the smaller TMS-anthracene **3a**

down to 4.4 ns in the case of the larger TPS-Anthracene **3c**. Not surprisingly, with a lifetime of 10.3 ns, the TIPS-tetracene rotator falls in between the two neighboring compounds in the acene series.

Following the photophysical characterization of molecular rotors **2-5** we set out to measure their steady-state anisotropy to determine whether mineral oil is viscous enough to slow down their whole-body rotational dynamics to the time scale of their lifetimes in the ca. 2-20 ns range. Anisotropy "*r*" is defined by the Equations 3.2.1 and 3.2.2,

$$r = \frac{I_{VV} - G I_{VH}}{I_{VV} + 2G I_{VH}} \qquad \textit{Eq 3.2.1}$$

$$G = \frac{I_{HV}}{I_{HH}} \qquad \textit{Eq. 3.2.2}$$

where I_{XY} represents the fluorescence intensity of the sample when the excitation polarizer is set to *X* and the emission polarizer is set to *Y*. The subscripts H and V indicate the orientations of the polarizers: H for horizontal (90°) and V for vertical (0°). The value G is a correction factor that accounts for the difference in the instrument's sensitivity to horizontally and vertically polarized light. The anisotropy *r* in isotropic solution can range from a maximum positive value of 0.4 to a maximum negative value of -0.2. Positive values indicate a preference for emission to occur parallel to the excitation polarization and are expected to occur when absorption and emission occur from the same excited state. By contrast, negative values indicate a preference for emission to occur perpendicular to excitation as is expected when the states involved absorption and emission are different and have orthogonal transition dipole moments.

Figure 3.2.2 shows the steady-state anisotropy of **3a** overlaid with its steady-state isotropic fluorescence excitation and emission spectra in mineral oil. The solid dark orange line reveals a complex anisotropy pattern when emission is detected at 468 nm (marked with a * in Figure 3.2.2). We interpret changes in anisotropy as a function of excitation wavelength as an

indication of multiple overlapping transitions to higher excited states with dipole moment directions that are aligned either parallel or perpendicular to the lowest energy transition responsible for the emission at 468 nm. The anisotropy of the emission is more straightforward: the solid light orange line shows a small negative emission anisotropy when excited at 272 nm (•, in Figure 3.2.2), while the solid medium orange line reflects a much larger positive anisotropy when excited at 413 nm (°, Figure 3.2.2). These constant values for emission anisotropy suggest that emission at all wavelengths occurs in the same orientation. By analogy to **1** shown in Figure 3.2.1, we expect that this emission is occurring on the z-axis, parallel to the alkyne (Figure 3.2.1). The steady-state anisotropy profiles of each compound allowed us to determine emission and excitation wavelengths at which the anisotropy signal would be strongest and therefore at which it would be easiest to observe the time-resolved fluorescence anisotropy decay of **2**-**5**.

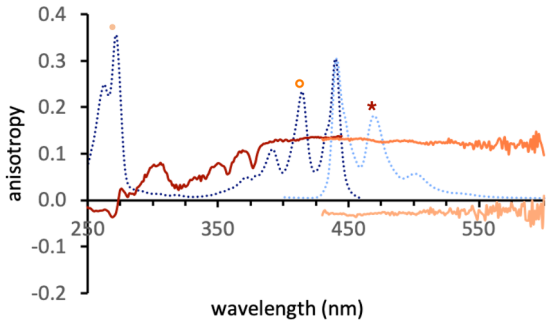

Figure 3.2.2. Steady state anisotropy (solid lines) overlaid with the isotropic fluorescence excitation (dark blue dotted line) and emission (light blue dotted line) spectra of compound **3a** (0.9 μM in mineral oil). The solid dark orange line is the anisotropy of **3a** when emission is detected at 468 nm (*). The medium orange line is the anisotropy for excitation at 413 nm (°), and the light orange line is the anisotropy for excitation at 272 nm (•).

The time-resolved anisotropies were then measured for each compound, and were compared with their lifetime decay traces, as shown in Figure 3.2.3a and 3.2.3b. All compounds had a fundamental anisotropy at t=0 that is less than 0.4, suggesting rapid depolarization

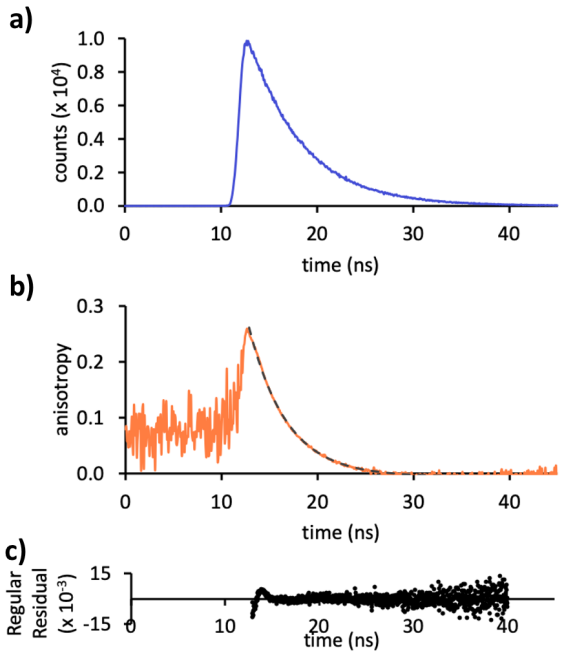

Figure 3.2.3. a) fluorescence lifetime decay curve of **3a** (0.9 μM in mineral oil) for excitation at 375 nm and emission at 440 nm. b) time-resolved anisotropy decay (orange, solid) with the fitted decay curve overlaid (black, dashed). Anisotropy measurements were taken with the same conditions as the lifetime measurement. c) residuals for the fitted decay curve.

mechanisms. Compounds **2**, **3b**, **4**, and **5** displayed behavior similar to that of **3a** shown in Figure 3a where the anisotropy decayed to zero before the fluorescence signal did. Molecular rotor **3c** with a triphenylsilyl stator had a slower anisotropy decay, but most of it occurred well before the fluorescence signal disappeared.

In order to quantify the rate of anisotropy decay, we fitted the curves to exponential decay functions (Figure 3.2.3b, dashed), and found that all of the anisotropy decays were

monoexponential, as summarized in Table 3.2.1. While the residuals of these fits (Figure 3.2.3c) are not as randomly distributed at early time points as would be ideal, adding a second exponential term yielded two functionally identical lifetimes and the residuals did not improve. Since there is no way to incorporate an instrumental response measurement into the anisotropy scans, it is possible that the fluctuations in the first few nanoseconds of the anisotropy decay are due to the reflected incident beam. Regardless of fast electronic processes, the fitted curves match well with the behavior on longer time scales, and therefore can still give an idea of the slower rotational behavior of the molecules in viscous solution. The decay values are roughly clustered by the size of the stator group: **2** and **3a** with TMS stators have decay constants in the range of 3-4 ns, **3b**, **4**,

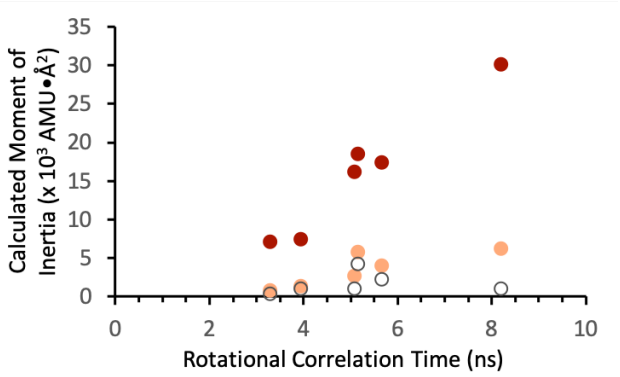

Figure 3.2.4. Rotational correlation times of compounds 2-5 as compared to their own calculated moments of inertia (dark orange, rotation around y-axis; light orange, rotation around z-axis) and the moment of inertia of the isolated associated acene that would correspond to rotation about the z-axis (open circle).

and **5** with TIPS stators have decay constants in the range of 5-6 ns, and **3c** with the TPS stator has the longest decay with a time constant of 8.19 ns. Calculated correlation times predicted using established methods[10] also fell into the same groupings, although the calculated values displayed an expected amount of discrepancy with experimental values.[11] This suggests that the motion we

are observing with the anisotropy decay is rotation around the y-axis axis: molecular tumbling, rather than the rotation of the acene around the z-axis (Figure 3.2.1).

The conclusion that the observed rotation occurs around the y-axis is strengthened by plotting the time constants for fluorescence anisotropy decay against several relevant moments of inertia calculated with the Spartan modeling software. Figure 3.2.4 shows the rotational correlation times plotted versus two principal moments of inertia of **2**-**5** (orange filled circles, light for rotation around z-axis and dark for rotation around y-axis) as well as the moment of inertia of the associated acene that would correspond to its rotation about an alkyne axis (open circles). If the anisotropy decay were reflecting the rotation of the acene about the z-axis, we would expect to see a correlation between the anisotropy decay constants and the lowest moment of inertia (light orange). However, a correlation is more clearly observed between the anisotropy decay constant and the highest moment of inertia (dark orange). The highest moment of inertia is associated with rotation about the y-axis, so we conclude that the motion observed by anisotropy decay is molecular tumbling rather than acene rotation about the alkyne. This aligns with previous work that suggests that the transition dipole moment associated with the emission of **1** is aligned with the z-axis and would therefore indicate motion about the y-axis.[9]

3.3. Conclusions

Compounds **2**-**5** featuring silyl-protected alkyne stators attached to acene rotators were selected as test systems to evaluate the viability of this type of molecule as a tool for measuring rotation in confined viscous media. These compounds were observed in pentane solutions to evaluate their isotropic behavior, and were studied in mineral oil solutions to simulate their behavior in a more restricted environment. UV-Vis and steady-state fluorescence measurements yielded the expected behavior, with a good match between absorption and excitation spectra and

low Stokes shifts. The fluorescence lifetimes of **2-5** increased with increasing acene size and decreasing stator size.

Steady state anisotropy measurements in mineral oil revealed a complex series of overlapping transitions in the excitation spectrum that all emit in the same orientation regardless of the wavelength of emission detection. From comparison to previous work, we conclude that this emission is in the z-axis. This is corroborated by the time-resolved anisotropy decay measurements, which give time constants that cluster by stator size rather than by rotator size when fitted to monoexponential decays. The anisotropy decay constants were plotted against the moments of inertia that correspond to rotation about both the y- and z- axes of compounds **2-5**, and a correlation emerged with the moment of inertia associated with rotation about the y-axis. This further strengthens the conclusion that the polarization of the emission is in the z-axis and the rotation observed by fluorescence anisotropy decay is molecular tumbling rather than acene rotation about the alkyne.

The evidence presented herein suggests that fluorescence anisotropy decay is a suitable method for observing rotation of bis(silylethynyl)acenes in restricted media provided that the anisotropy decay occurs on a shorter timescale or a comparable timescale to fluorescence emission so that there is still a fluorescence signal by which to measure anisotropy. Additionally, the transition dipole moment of the fluorescence emission must be oriented perpendicular to the axis of rotation of the molecule in question. In the case of compounds **2-5**, the emission is polarized in the z-axis, so the axis of rotation would need to be established along the y-axis, or the long axis of the acene, as shown in Figure 3.2.1. Alternatively, a rotator that rotates about the z-axis could be observed if a donor-acceptor type system were synthesized in order to force the fluorescence emission to occur in along the y-axis of the acene. Such a system could be

incorporated into a MOF or a molecular crystal in a similar fashion to other bulky rotors in order to accommodate its rotation.

3.4. Experimental Section

General Experimental Details

IR Spectra were acquired on a PerkinElmer Spectrum Two spectrometer equipped with a universal ATR sampling accessory. Compounds **2**,[6] **3a**,[7a] **3b**,[7b] **3c**,[7c] **4**,[8] and **5**[6] were synthesized by previously established methods. The compounds and solvents used in these procedures were commercially available and used without further purification. THF used for synthesis was freshly distilled from sodium. Solutions of **4** and **5** were kept wrapped in tinfoil to prevent photodegradation.

Spectrophotometric grade pentane and mineral oil for fluorescence and UV-Vis studies were commercially available from Fisher Scientific and Alfa Aesar, respectively, and used without further purification. Solutions in mineral oil were prepared as discussed in the text by dissolving the compound of interest in hexanes, mixing that solution with mineral oil, removing the hexanes by rotary evaporation, and then diluting the resulting mineral oil solution to the desired concentration. All isotropic lifetime measurements in mineral oil were taken with an emission polarizer set to 55° in order to account for any anisotropy caused by the polarization of the excitation laser.

UV-Vis spectra were obtained using an Ocean Optics Flame Spectrometer with DH-MINI UV-Vis-NIR light source and Oceanview software package. Fluorescence spectra were obtained using an Edinburgh Instruments FLS 920 spectrometer equipped with a 450 W ozone-free xenon arc lamp for steady state measurements, as well as EPLED-300, EPL-375, and EPL-510

picosecond pulsed laser diodes for lifetime measurements. Fluorescence data were collected using the F900 software package.

3.5. Appendix

Supplementary Information For Chapter 3

*3.5.1. General Comments About Spectroscopic Characterization of **2-5***

UV-vis spectra in mineral oil are cut off at 250 nm due to strong absorption of the that did not allow for accurate determination of compound absorption below that wavelength. UV-vis spectra were obtained at a concentration such that the acene vibrational transitions are visible, so more intense features may not be scaled appropriately.

*3.5.2. Isotropic Spectroscopic Characterization of Compounds **2-5***

Figure 3.5.2.1. UV-Vis (purple, solid), fluorescence excitation (dark blue, dashed), and fluorescence emission (light blue, dotted) spectra of **2** in a) pentane and b) mineral oil. UV-vis: 17.4 μM in pentane, 22.5 μM in mineral oil. Fluorescence in pentane: 3.2 μM, excitation scan collected for emission at 365 nm, emission scan collected for excitation at 246 nm. Fluorescence in mineral oil: 3.4 μM, excitation scan collected for emission at 387 nm, emission scan collected for excitation at 253 nm. Fluorescent background of oil was subtracted to obtain excitation and emission spectra in b).

a) pentane

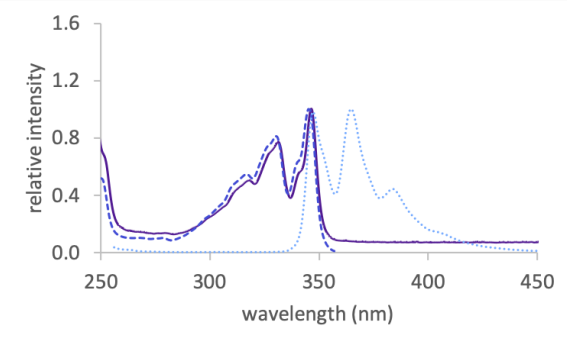

b) mineral oil

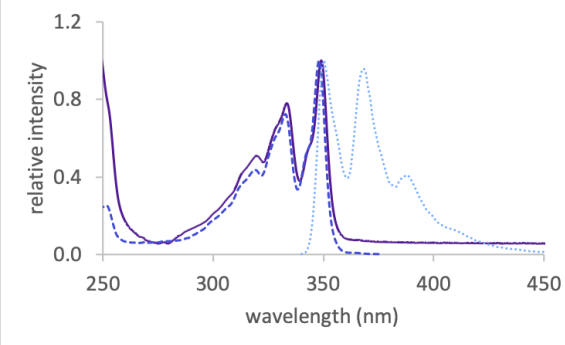

Figure 3.5.2.2. UV-Vis (purple, solid), fluorescence excitation (dark blue, dashed), and fluorescence emission (light blue, dotted) spectra of **3a** in a) pentane and b) mineral oil. UV-vis: 7.1 μM in pentane, 9.4 μM in mineral oil. Fluorescence in pentane: 1.8 μM, excitation scan collected for emission at 463 nm, emission scan collected for excitation at 272 nm with a 350 nm longpass emission filter. Fluorescence in mineral oil: 0.9 μM, excitation scan collected for emission at 468 nm, emission scan collected for excitation at 272 nm with a 350 nm longpass emission filter.

a) pentane

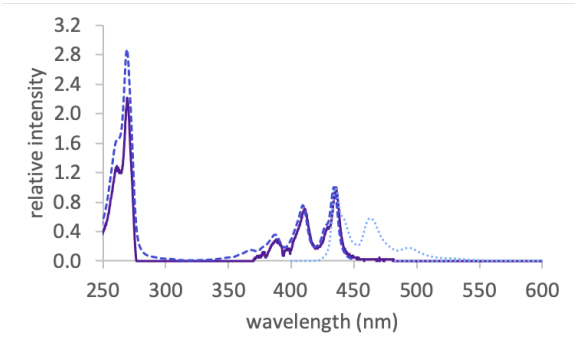

b) mineral oil

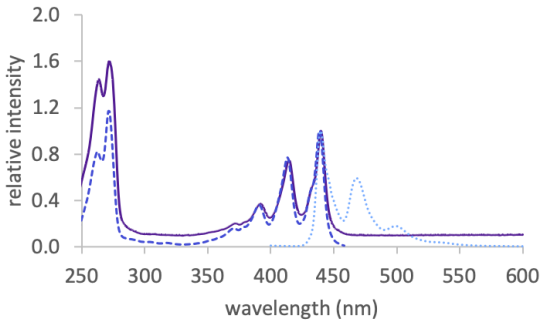

Figure 3.5.2.3. UV-Vis (purple, solid), fluorescence excitation (dark blue, dashed), and fluorescence emission (light blue, dotted) spectra of **3b** in a) pentane and b) mineral oil. UV-vis: 6.7 μM in pentane, 7.0 μM in mineral oil. Fluorescence in pentane: 1.3 μM, excitation scan collected for emission at 465 nm, emission scan collected for excitation at 270 nm with a 350 nm longpass emission filter. Fluorescence in mineral oil: 0.7 μM, excitation scan collected for emission at 470 nm, emission scan collected for excitation at 272 nm with a 350 nm longpass emission filter.

a) pentane

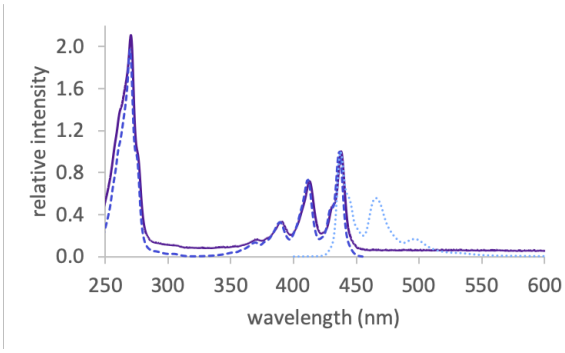

b) mineral oil

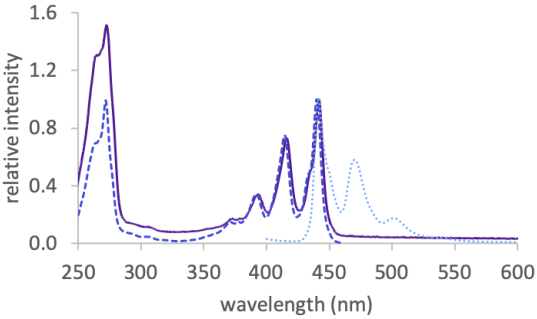

Figure 3.5.2.4. UV-Vis (purple, solid), fluorescence excitation (dark blue, dashed), and fluorescence emission (light blue, dotted) spectra of **3c** in a) pentane and b) mineral oil. UV-vis: 6.1 μM in pentane, 5.7 μM in mineral oil. Fluorescence in pentane: 0.4 μM, excitation scan collected for emission at 470 nm with a 455 nm longpass emission filter, emission scan collected for excitation at 268 nm with a 350 nm longpass emission filter. Fluorescence in mineral oil: 0.5 μM, excitation scan collected for emission at 465 nm with a 455 nm longpass emission filter, emission scan collected for excitation at 267 nm with a 350 nm longpass emission filter.

a) pentane

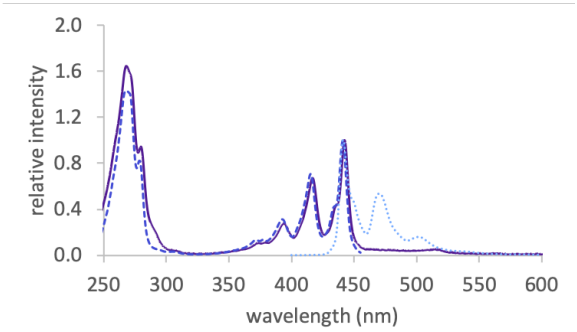

b) mineral oil

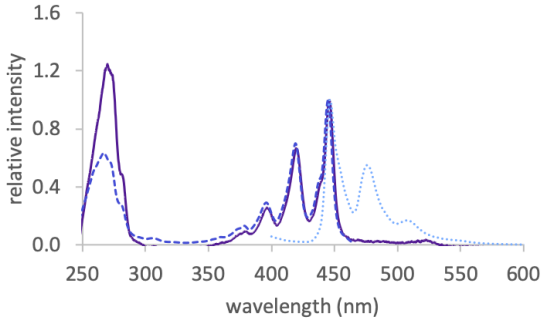

Figure 3.5.2.5. UV-Vis (purple, solid), fluorescence excitation (dark blue, dashed), and fluorescence emission (light blue, dotted) spectra of **4** in a) pentane and b) mineral oil. UV-vis spectra were obtained at a concentration such that the acene vibrational transitions are visible, so more intense features are not scaled appropriately. UV-vis: 20.4 μM in pentane, 10.9 μM in mineral oil. Fluorescence in pentane: 0.7 μM, excitation scan collected for emission at 570 nm with a 500 nm longpass emission filter, emission scan collected for excitation at 283 nm with a 350 nm longpass emission filter. Fluorescence in mineral oil: 0.5 μM, excitation scan collected for emission at 576 nm with a 350 nm longpass emission filter, emission scan collected for excitation at 290 nm with a 350 nm longpass emission filter.

a) pentane

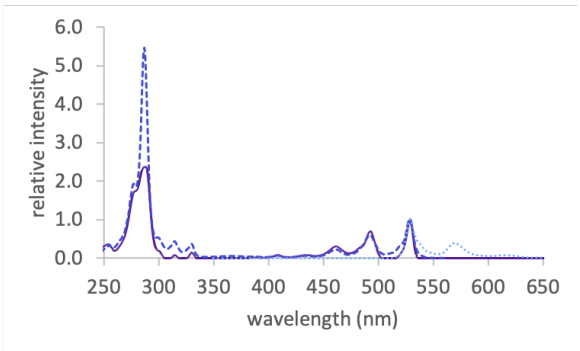

b) mineral oil

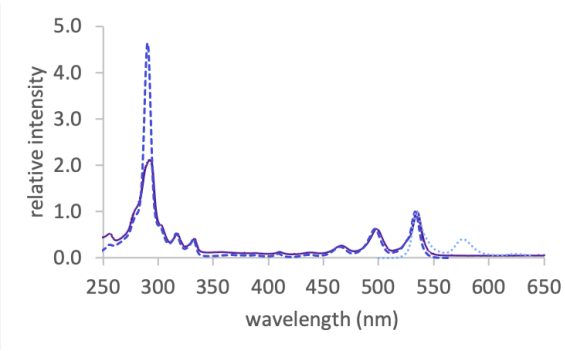

Figure 3.5.2.6. UV-Vis (purple, solid), fluorescence excitation (dark blue, dashed), and fluorescence emission (light blue, dotted) spectra of **5** in a) pentane and b) mineral oil. UV-vis spectra were obtained at a concentration such that the acene vibrational transitions are visible, so more intense features are not scaled appropriately. UV-vis: 133.9 μM in pentane, 19.2 μM in mineral oil. Fluorescence in pentane: 1.5 μM, excitation scan collected for emission at 692 nm with a 655 nm longpass emission filter, emission scan collected for excitation at 304 nm with a 590 nm longpass emission filter. Fluorescence in mineral oil: 1.4 μM, excitation scan collected for emission at 704 nm with a 650 nm longpass emission filter, emission scan collected for excitation at 308 nm with a 610 nm longpass emission filter.

a) pentane

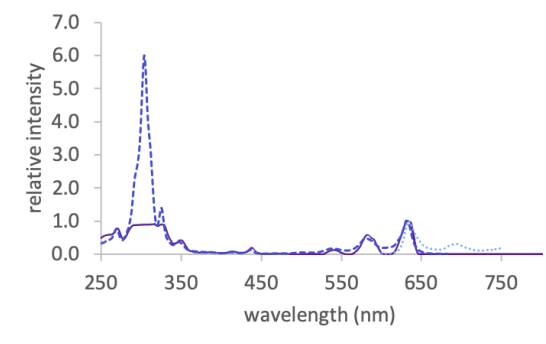

b) mineral oil

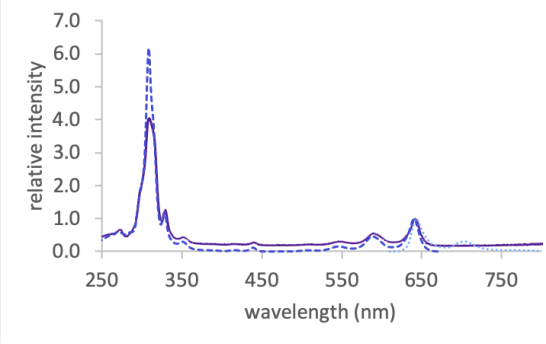

*3.5.3. Anisotropic Spectroscopic Characterization of Compounds **2-5***

Figure 3.5.3.1. a) Steady state anisotropy (solid lines) overlaid with the isotropic fluorescence excitation (dark blue dotted line) and emission (light blue dotted line) spectra of compound **2** (3.4 μM in mineral oil, see Figure 3.5.2.1 for instrument parameters). The solid dark orange line is the anisotropy of **2** when emission is detected at 387 nm (*). The solid medium orange line is the anisotropy for excitation at 333 nm (°), and the solid light orange line is the anisotropy for excitation at 247 nm (•). b) time-resolved anisotropy decay (yellow), fitted decay curve (black, dashed), and scaled fluorescence decay (blue) of **2** (3.4 μM in mineral oil) for excitation at 300 nm and detection at 368 nm. The fluorescence decay is displayed with a linear y-axis. c) residuals for the fitted decay curve.

a)

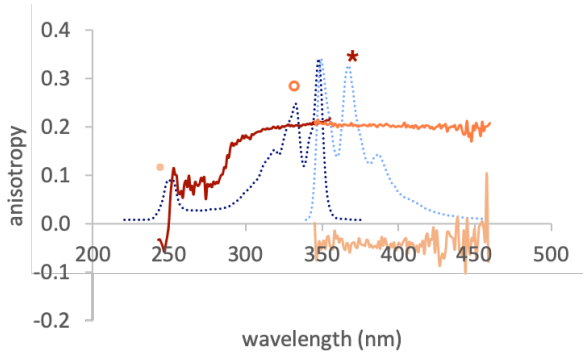

b)

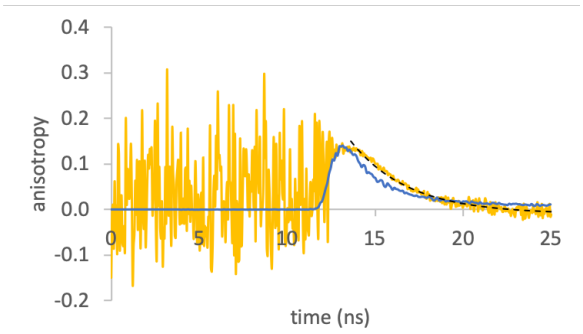

c)

Figure 3.5.3.2. a) Steady state anisotropy (solid lines) overlaid with the isotropic fluorescence excitation (dark blue dotted line) and emission (light blue dotted line) spectra of compound **3a** (0.9 μM in mineral oil, see Figure 3.5.2.2 for instrument parameters). The solid dark orange line is the anisotropy of **3a** when emission is detected at 468 nm (*). The solid medium orange line is the anisotropy for excitation at 413 nm (°), and the solid light orange line is the anisotropy for excitation at 272 nm (•). b) time-resolved anisotropy decay (yellow), fitted decay curve (black, dashed), and scaled fluorescence decay (blue) of **3a** (0.9 μM in mineral oil) for excitation at 375 nm and detection at 440 nm. The fluorescence decay is displayed with a linear y-axis. c) residuals for the fitted decay curve.

a)

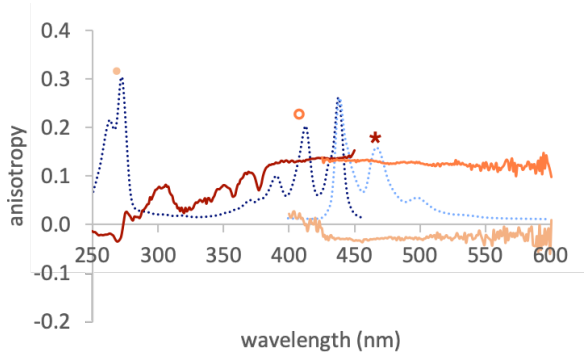

b)

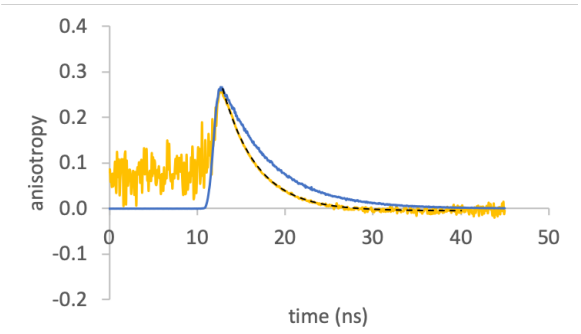

c)

Figure 3.5.3.3. a) Steady state anisotropy (solid lines) overlaid with the isotropic fluorescence excitation (dark blue dotted line) and emission (light blue dotted line) spectra of compound **3b** (0.7 μM in mineral oil, see Figure 3.5.2.3 for instrument parameters). The solid dark orange line is the anisotropy of **3b** when emission is detected at 470 nm (*). The solid medium orange line is the anisotropy for excitation at 415 nm (°), and the solid light orange line is the anisotropy for excitation at 272 nm (•). b) time-resolved anisotropy decay (yellow), fitted decay curve (black, dashed), and scaled fluorescence decay (blue) of **3b** (0.9 μM in mineral oil) for excitation at 375 nm and detection at 441 nm. The fluorescence decay is displayed with a linear y-axis. c) residuals for the fitted decay curve.

a)

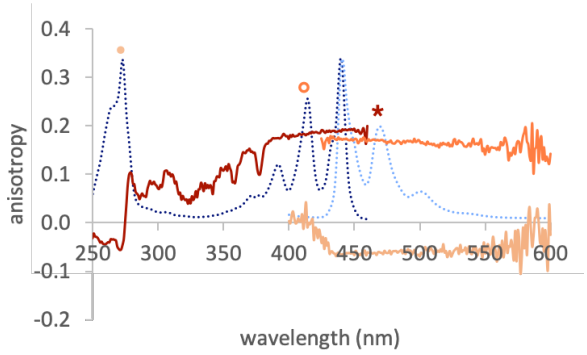

b)

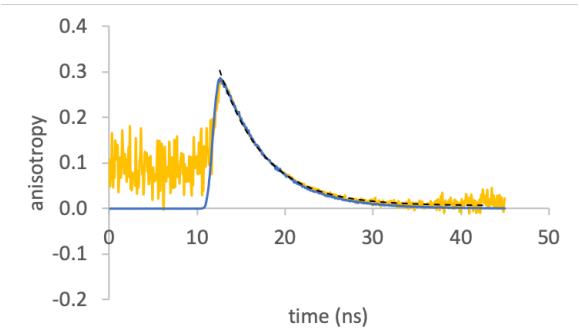

c)

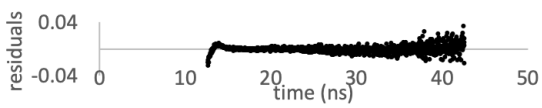

Figure 3.5.3.4. a) Steady state anisotropy (solid lines) overlaid with the isotropic fluorescence excitation (dark blue dotted line) and emission (light blue dotted line) spectra of compound **3c** (0.5 μM in mineral oil, see Figure 3.5.2.4 for instrument parameters). The solid dark orange line is the anisotropy of **3c** when emission is detected at 475 nm (*). The solid medium orange line is the anisotropy for excitation at 418 nm (°), and the solid light orange line is the anisotropy for excitation at 270 nm (•). b) time-resolved anisotropy decay (yellow), fitted decay curve (black, dashed), and scaled fluorescence decay (blue) of **3c** (0.5 μM in mineral oil) for excitation at 375 nm and detection at 440 nm. The fluorescence decay is displayed with a linear y-axis. c) residuals for the fitted decay curve.

a)

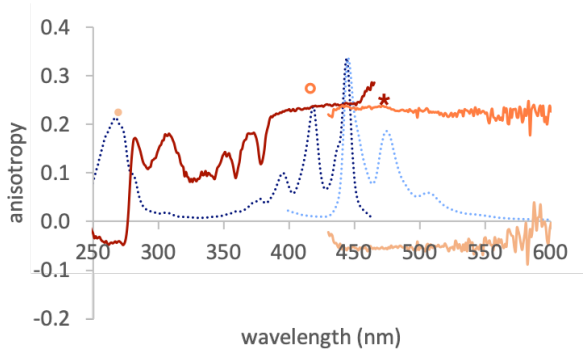

b)

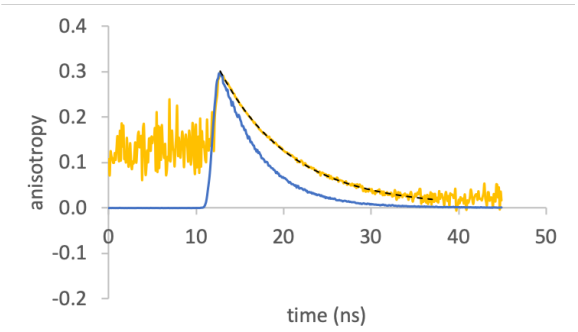

c)

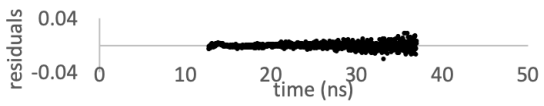

Figure 3.5.3.5. a) Steady state anisotropy (solid lines) overlaid with the isotropic fluorescence excitation (dark blue dotted line) and emission (light blue dotted line) spectra of compound **4** (0.5 μM in mineral oil, see Figure 3.5.2.5 for instrument parameters). The solid dark orange line is the anisotropy of **4** when emission is detected at 576 nm (*). The solid medium orange line is the anisotropy for excitation at 497 nm (°), and the solid light orange line is the anisotropy for excitation at 290 nm (•). b) time-resolved anisotropy decay (yellow), fitted decay curve (black, dashed), and scaled fluorescence decay (blue) of **4** (0.5 μM in mineral oil) for excitation at 510 nm and detection at 535 nm. The fluorescence decay is displayed with a linear y-axis. c) residuals for the fitted decay curve.

a)

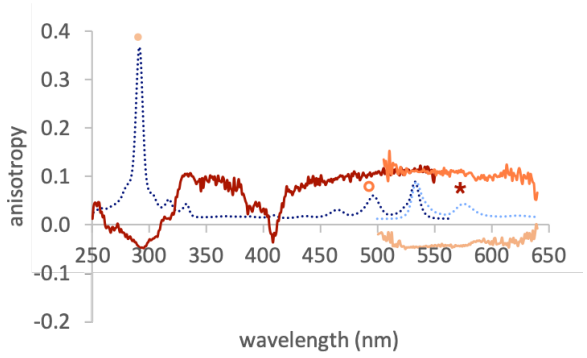

b)

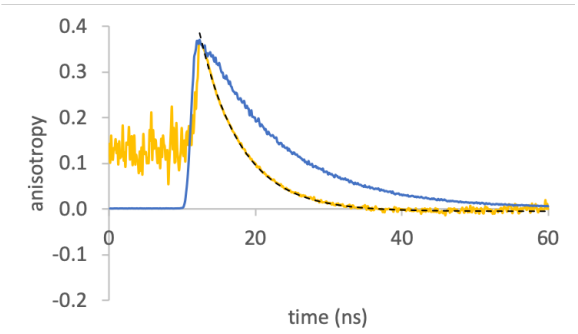

c)

Figure 3.5.3.6. a) Steady state anisotropy (solid lines) overlaid with the isotropic fluorescence excitation (dark blue dotted line) and emission (light blue dotted line) spectra of compound **5** (1.4 μM in mineral oil, see Figure 3.5.2.6 for instrument parameters). The solid dark orange line is the anisotropy of **5** when emission is detected at 655 nm (*). The solid medium orange line is the anisotropy for excitation at 583 nm (°), and the solid light orange line is the anisotropy for excitation at 352 nm (•). b) time-resolved anisotropy decay (yellow), fitted decay curve (black, dashed), and scaled fluorescence decay (blue) of **5** (1.4 μM in mineral oil) for excitation at 510 nm and detection at 643 nm. The fluorescence decay is displayed with a linear y-axis. c) residuals for the fitted decay curve.

a)

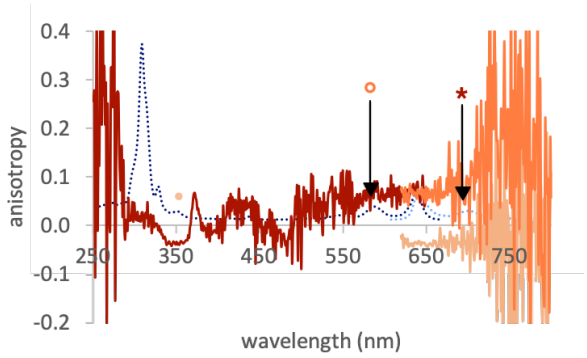

b)

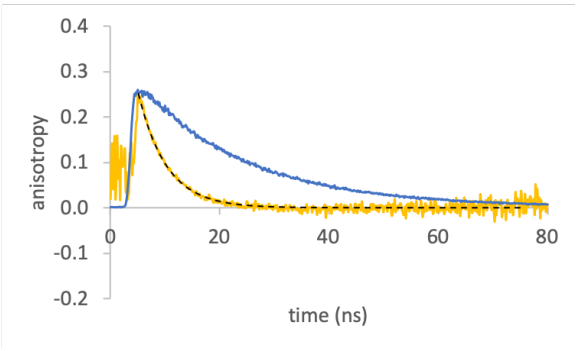

c)

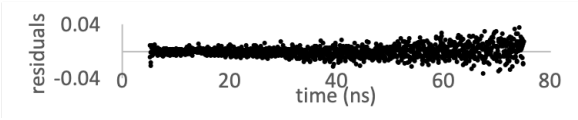

*3.5.4. Moments of Inertia and Molecular Volumes of **2-5** and Their Associated Acenes*

Table 3.5.4.1. Columns 1–3: The moments of inertia of **2-5** and their associated unsubstituted acenes from smallest (1) to largest (3) as calculated by Spartan using Molecular Mechanics. Column 4: The average of the two largest moments as a representation of the moment of inertia for molecular tumbling in solution for **2-5**. Columns 5–7: Calculated inertial rotation times based on the moments of inertia 1–3.[10,12] Column 8: Molecular volumes calculated by Spartan.

	Moments of Inertia (AMU•Å^2)				Calculated Inertial Rotational Correlation Times (ps)			Molecular Volume (Å^3)
	1	2	3	Average 2/3	1	2	3	
naphthalene	160	409	569	--	0.56	0.90	1.06	150
2	901	6851	7434	7142	1.33	3.67	3.82	384
anthracene	230	1114	1345	--	0.67	1.48	1.63	201
3a	1467	6950	8099	7525	1.70	3.70	3.99	434
3b	2765	15653	16752	16203	2.33	5.55	5.74	657
3c	6324	29596	30718	30157	3.53	7.63	7.78	829
tetracene	301	2355	2656	--	0.77	2.15	2.29	252
4	4095	16013	18828	17420	2.84	5.61	6.09	707
pentacene	372	4282	4654	--	0.86	2.90	3.03	303
5	5906	16417	20795	18606	3.41	5.68	6.40	759

*3.5.5. Fluorescence Lifetimes of **2-5***

Table 3.5.5.1. The lifetimes of **2-5** in pentane, the type of IRF that was incorporated into their measurements, the wavelengths at which they were excited, and the wavelengths at which emission was detected. "Sample" means the fluorescence sample was used to collect an IRF measurement.

	Lifetime in Pentane (ns)	Pentane IRF	Concentration in Pentane (μM)	Excitation Wavelength (nm)	Detection Wavelength (nm)
2	1.44	sample	3.56	300	347
3a	5.63	sample	1.78	375	435
3b	4.96	sample	1.28	375	437
3c	4.65	sample	0.91	375	441
4	8.41	pentane blank	1.54	510	529
5	17.76	sample	15.33	510	635

Table 3.5.5.2. The lifetimes of **2**-**5** in mineral oil, the type of IRF that was incorporated into their measurements, the wavelengths at which they were excited, and the wavelengths at which emission was detected. “Sample” means the fluorescence sample was used to collect an IRF measurement. “Scattering suspension” indicates that a particulate suspension was used to collect an IRF measurement. *The mineral oil used as a solvent was emissive at 368 nm when excited at 300 nm. The lifetime measurements of solutions of **2** in mineral oil displayed biexponential decays with a 1.90 ns lifetime that was attributed to **2** and a second lifetime of 18.04 ns that matched with the decay of an oil blank and was attributed to the oil itself.

	Lifetime in mineral oil (ns)	Mineral oil IRF	Concentration in Mineral Oil (μM)	Excitation Wavelength (nm)	Detection Wavelength (nm)
2*	1.90	scattering suspension	3.37	300	368
3a	5.39	sample	0.94	375	440
3b	4.91	sample	0.70	375	441
3c	4.42	sample	0.48	375	440
4	10.30	mineral oil blank	0.54	510	535
5	19.12	mineral oil blank	1.35	510	643

3.6. References

[1] a) Howe, M. E.; Garcia-Garibay, M. A. The Roles of Intrinsic Barriers and Crystal Fluidity in Determining the Dynamics of Crystalline Molecular Rotors and Molecular Machines. *J. Org. Chem.*, **2019**, *84*, 9835-9849. b) Vogelsberg, C. S.; Garcia-Garibay, M. A. Crystalline molecular machines: function, phase order, dimensionality, and composition. *Chem. Soc. Rev.*, **2012**, *41*, 1892-1910. c) Karlen, S. D.; Garcia-Garibay, M. A. Amphidynamic crystals: Structural blueprints for molecular machines. *Top. Curr. Chem.*, **2005**, *262*, 179−227.

[2] a) Kottas, G. S.; Clarke, L. I.; Horinek, D.; Michl, J. Artificial Molecular Rotors. *Chem. Rev.*, **2005**, *105*, 1281−1376. b) Kushida, S.; Smarsly, E.; Bojanowski, N. M.; Wacker, I.; Schröder, R. R.; Oki, O.; Yamamoto, Y.; Melzer, C.; Bunz, U. H. F. Dipole-Switchable Poly(para-phenyleneethynylene)s: Ferroelectric Conjugated Polymers. *Angew. Chem., Int. Ed.*, **2018**, *57*, 17019− 17022. c) Kaleta, J.; Wen, J.; Magnera, T. F.; Dron, P. I.; Zhu, C.; Michl, J. Structure of a monolayer of molecular rotors on aqueous subphase from grazing-incidence X-ray diffraction. *Proc. Natl. Acad. Sci. U. S. A.*, **2018**, *115*, 9373−9378. d) Dron, P. I.; Zhao, K.; Kaleta, J.; Shen, Y.; Wen, J.; Shoemaker, R. K.; Rogers, C. T.; Michl, J. Bulk Inclusions of Pyridazine-Based Molecular Rotors in Tris(o- phenylenedioxy)cyclotriphosphazene (TPP). *Adv. Funct. Mater.*, **2016**, *26*, 5718−5732. e) Yoshida, Y.; Shimizu, Y.; Yajima, T.; Maruta, G.; Takeda, S.; Nakano, Y.; Hiramatsu, T.; Kageyama, H.; Yamochi, H.; Saito, G. Molecular Rotors of Coronene in Charge-Transfer Solids. *Chem. Eur. J.*, **2013**, *19*, 12313-12324. f) Horinek, D.; Michl, J. Molecular dynamics of a grid-mounted molecular dipolar rotor in a rotating electric field. *Proc. Natl. Acad. Sci. U. S. A.*, **2005**, *102*, 14175−14180. g) Vacek, J.; Michl, J. Artificial Surface-Mounted Molecular Rotors: Molecular Dynamics Simulations. *Adv. Funct. Mater.*, **2007**, *17*, 730−739. h) Thomas, J. C.; Schwartz, J. J.; Hohman, J. N.; Claridge, S. A.; Auluck, H. S.; Serino, A. C.; Spokoyny, A. M.; Tran, G.; Kelly, F.; Mirkin, C. A.; Gilles, J.; Osher, S. J.; Weiss, P. S. Defect tolerant aligned dipoles within two-dimensional lattices. *ACS Nano*, **2015**, *9*, 4734−4742.

[3] Karlen, S.D.: Reyes, H.; Taylor, R. E.; Khan, S.I.; Hawthorne, M.F.; Garcia-Garibay, M.A. Symmetry and Dynamics of Molecular Rotors in Amphidynamic Molecular Crystals. *Proc. Nat. Acad. Sci. USA*, **2010**, 107, 14973-14978.

[4] a) Lackowicz, J. R. Principles of Fluorescence Spectroscopy, 3rd ed.; Springer: Boston, **2006**. b) Michl, J.; Thulstrup, E. W. Spectroscopy with Polarized Light: Solute Alignment by Photoselection, Liquid Crystal, Polymers, and Membranes, 1st ed.; Wiley: Hoboken, **1995**.

[5] a) Tramier, M.; Coppey-Moisan, M. Fluorescence Anisotropy Imaging Microscopy for Homo-FRET in Living Cells. *Method Cell Biol.*, **2008**, *85*, 395-414. b) Lakowicz, J. R.; Cherek, H.; Kuśba, J.; Gryczynski, I.; Johnson, M. L. Review of fluorescence anisotropy decay analysis by frequency-domain fluorescence spectroscopy. *J. Fluoresc.*, **1993**, *3*, 103-116. c) Bucci, E.; Steiner, R. F. Anisotropy decay of fluorescence as an experimental approach to protein dynamics. *Biophysical Chemistry*, **1988**, *30*, 199-224.

[6] Fudickar, W.; Linker, T. Why Triple Bonds Protect Acenes from Oxidation and Decomposition. *J. Am. Chem. Soc.*, **2012**, *134*, 15071-15082.

[7] a) Li, Y.; Köse, M. E.; Schanze, K. S. Intramolecular Triplet Energy Transfer in Anthracene-Based Platinum Acetylide Oligomers. *J. Phys. Chem. B*, **2013**, *117*, 9025-9033. b) Goldsmith, R. H.; Vura-Weis, J.; Scott, A. M.; Borkar, S.; Sen, A.; Ratner, M. A.; Wasielewski, M. R. Unexpectedly Similar Charge Transfer Rates through Benzo-Annulated Bicyclo[2.2.2]octanes. *J. Am. Chem. Soc.*, **2008**, *130*, 7659-7669. c) Takahashi, K.; Reiko, H.; Daisuke, N.; Shiki, N.; Norihisa, K.; Akihide, K. Photoluminescence and Electroluminescence of 9,10-Bis(silylethynyl)anthracene. *J. Photopolym. Sci. Technol.*, **2005**, *18*, 65-68.

[8] Odom, S. A.; Parkin, S. R.; Anthony, J. E. Tetracene Derivatives as Potential Red Emitters for Organic LEDs. *Org. Lett.*, **2003**, *5*, 4245-4248.

[9] Levitus, M.; Garcia-Garibay, M. A. Polarized Electronic Spectroscopy and Photophysical Properties of 9,10-Bis(phenylethynyl)anthracene. *J. Phys. Chem.*, **2000**, *104*, 8632-8637.

[10] Kawski, A. Fluorescence Anisotropy: Theory and Applications of Rotational Depolarization. *Crit. Rev. Anal. Chem.*, **1993**, *23*, 459-529.

[11] Correlation times of 23, 26, 49, 71, 49, and 53 ns were calculated for **2**, **3a**, **3b**, **3c**, **4**, and **5**, respectively, using equations 165 and 166 from reference 10. These times are noticeably longer than those recorded experimentally in Table 3, but the discrepancy is not unexpected given the authors note that "For small molecules in liquid solutions, the experimentally determined rotational-correlation times are often 5 or 10 times shorter than those calculated on the stick-boundary condition." The viscosity for these calculations was based on the Certificate of Analysis provided by Alfa Aesar for the batch used in these experiments. The certificate reported a kinematic viscosity of 25.32 cSt at 40 °C and a specific gravity of 0.8535, which correspond to an absolute viscosity of 21.61 cP.

[12] The inertial correlation times were calculated using equation 166 from Reference 10 based on the moments of inertia obtained from Spartan (shown in the first three columns of Table 3.5.4.1).

CHAPTER 4

Encapsulating a Glucose Sensing Assay in a Hydrogel to Investigate Sensing Pathways in a High School Laboratory

4.1. Introduction

Nanoscience, or the study of objects on the nanometer (10^{-9} m) scale, has given rise to many advances in the field of materials science in the past forty years due to the unique properties possessed by objects of this size. One of the important features of nanoscale architectures is that they match the size of biological molecules such as nucleic acids (*e.g.* DNA and RNA), proteins, and many enzymes (biological catalysts), which makes them uniquely capable of interacting with biological systems. This has led to advances in bionanotechnology such as imaging and diagnostic tools, as well as regenerative medicine.[1] Nanomaterials have been used to improve everything from consumer electronics, automobiles, and sports equipment to spacecraft, and their responsiveness to many different stimuli also makes them excellent sensors.

Many sensors require specialized equipment or knowledge to read information from them, but colorimetric sensors circumvent that by giving a readout either as a scale of different colors or the intensity of a single color that can be easily interpreted by a non-expert. This particular experiment uses a colorimetric scale to sense the presence of glucose. However, glucose itself does not change color, so it needs to be coupled with something that does. In this case, it is coupled with an assay (adapted from previous conditions[2]) that consists of glucose oxidase, horseradish peroxidase, and a two-component dye (**3** and **4**) shown in Figure 4.1.1. Glucose oxidase and horseradish peroxidase are both enzymes, so they do not permanently change their structures during the reactions shown: they simply make it easier for the reactions in Figure 4.1.1 to occur. Glucose oxidase (GOx) is normally found in different types of insects and fungi, and shows antibacterial properties due its ability to produce hydrogen peroxide: in the presence of oxygen, glucose oxidase will facilitate the oxidation of β-D-glucose **1** to D-glucono-δ-lactone **2** while producing hydrogen peroxide (H_2O_2) as a byproduct. This hydrogen peroxide then allows the

horseradish peroxidase to assist in combining the two colorless dye molecules **3** and **4** to form the single pink dye molecule **5**. Horseradish peroxidase (HRP) is typically found in the roots of horseradish plants, and can pair with hydrogen peroxide to oxidize many different molecules. The glucose oxidase/horseradish peroxidase combination has been used in classrooms as a color-changing sensor for glucose by coupling it with different dyes in several different contexts.[3]

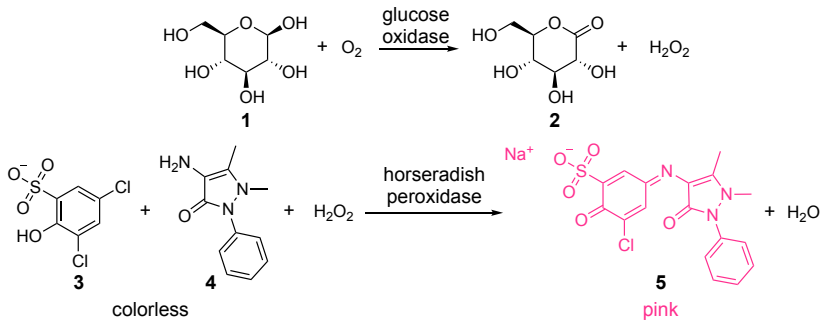

Figure 4.1.1. Glucose sensing pathway of glucose oxidase coupled with horseradish peroxidase and a dye composed of sodium 3,5-dichloro-2-hydroxybenzenesulfonate **3** and 4-aminoantipyrine **4**.

While enzymes can help accomplish many chemical tasks that would otherwise be unfeasible, they can also be very unstable, requiring specific temperature and pH ranges in order to maintain their structures and catalytic abilities. This is where nanoscale architectures become important: the enzymatic assay can be incorporated into a hydrogel in order to provide added stability.[4] Hydrogels are nanostructured networks of water and polymers, which form an aqueous-like environment that is solid-like and maintains its shape. There are two main advantages to using hydrogels to encapsulate the assay: portability and stability. The hydrogel makes it easier to carry the assay in single-use portions that can easily be placed in a small amount of liquid to test. It also prevents the enzymes from degrading while still providing a microenvironment in which a

necessary series of reactions can take place. In this experiment, the color change within the hydrogel bead acts as a sensor system for the amount of glucose present in a liquid sample.

The following experiment is designed to explore the sensing pathway used in the glucose oxidase / horseradish peroxidase assay, demonstrate the pH resistance provided by the hydrogel bead, and use the assay to sense the amount of glucose in a series of unknown drinks.

4.2. Experimental

The experiment consists of four main parts: the assembly of the beads containing the assay, the analysis of the sensing pathway, the analysis of bead functionality, and the quantification of sugar in unknowns using a calibration curve. In order to make the sensing beads, each of the components of the assay must be added to a working solution, starting with the dye and followed by each enzyme separately. After each component is added, several beads are allowed to swell in the solution to create beads that contain each of the following combinations: dye only, dye and one enzyme, and the full assay (dye plus both enzymes).

The remainder of the experiment takes place in different columns of a 48-well plate, as summarized in Figure 4.2.1. The well plate allows students to visually display a wide range of results in order to draw conclusions. Column 1 uses beads containing different components to identify which components respond to hydrogen peroxide and which respond to sugar. Columns 2 and 3 run in parallel, where the assay is in a bead in Column 2 and is added as a free solution in Column 3 to elucidate the role of the hydrogel network in protecting functionality of the assay in different pH environments. Column 4 contains a series of sugar solutions that act as a calibration curve for students to determine the amount of sugar in the unknowns they place in column 6. Sucrose is substituted for glucose since it is easily purchased from a grocery store rather than a chemical company.

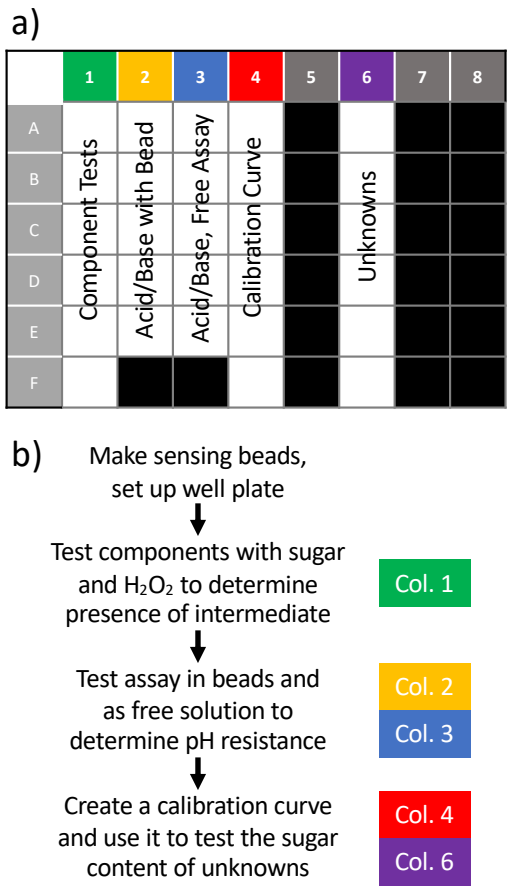

Figure 4.2.1. a) The experiment is conducted in a 48-well plate, with each section of the experiment in a different column. b) The experiment contains four main conceptual steps. Students will first make the beads, and will then use the beads to test the capabilities and limitations of the assay.

This procedure is best carried out in groups of at least four students. Our recommended assignments for performing this experiment in a single class period is as follows:

- All: Label and distribute supplies
- Student 1: Make assay solution and beads
- Student 2: Make sugar solutions and calibration curve (Column 4)
- Student 3: Obtain acids and bases to fill Columns 2 and 3
- Student 4: Obtain hydrogen peroxide and unknowns to fill Columns 1 and 6
- All: Add beads and observe results

The beads and assay solution can also be kept for up to a week if covered in tinfoil (keeping it in the dark will slow the gradual color change that occurs), so the experiment can be broken into two periods if necessary. If this is done, the assay solution will turn slightly pink, but a distinct color change is still visible when exposed to sugar.

4.3. Hazards

This experiment was designed to be suitable for high school students, so the hazards are minimal. All of the dried powders (both dye components and both enzymes) are inhalation hazards, so the instructor should dilute these in a buffer solution before giving to students. For best safety practices, students should wear gloves and eye protection while working with all solutions, and none of the materials should be ingested.

4.4. Results and Discussion

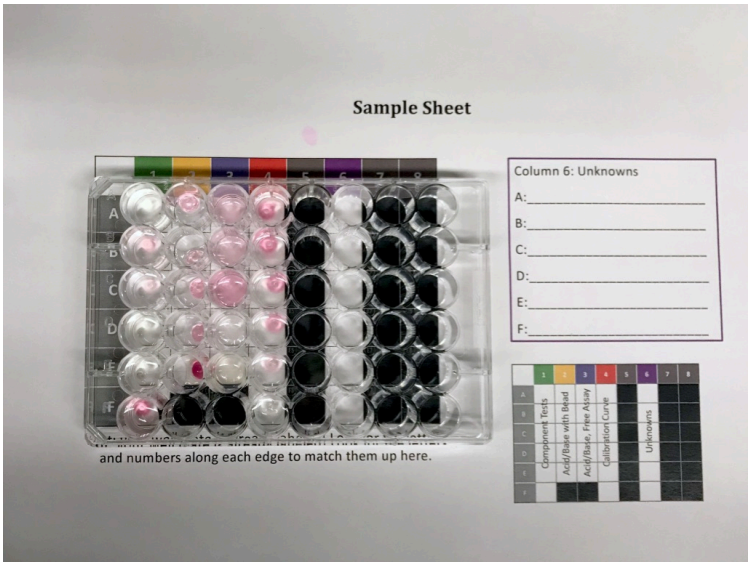

Figure 4.4.1. An example of a completed well plate. The hydrogen peroxide results (Wells 1A, 1B, and 1C) are weak because their color fades quickly, while the sugar solutions take 15-20 minutes to develop fully.

By the end of the experiment, students will have a well plate that looks similar to Figure 4.4.1. The color develops over time, but the results are generally visible by 20 minutes after adding assay to sugar solutions and 5 minutes after adding assay to hydrogen peroxide solutions.

4.4.1. Analysis of Sensing Pathway: Column 1

The goal of this section is for students to use each of the component beads to determine which component reacts to sugar, and which reacts to hydrogen peroxide. The first column of the well plate contains three wells with dilute hydrogen peroxide (1A, 1B, and 1C) and three with sugar (1D, 1E, and 1F), and each well has a bead with a different combination of sensing components, as summarized in Table 4.4.1.1. The beads with only dye in them (1A and 1D) react to neither since the dye changes color when both pieces of the two-component dye (**3** and **4**) are combined to form **5**, which only occurs with HRP in the presence of hydrogen peroxide. Similarly, the beads with dye and GOx cannot respond to either hydrogen peroxide (1B') or sugar (1E') because while the sugar and GOx produce hydrogen peroxide, there is no HRP to use that hydrogen peroxide to combine the dye. The beads with dye and HRP can respond to hydrogen peroxide (1B) since it bypasses the need for sugar and GOx. Providing the hydrogen peroxide intermediate allows the HRP to combine the dye, causing a color change. However, the dye and HRP will not respond to sugar (1E) since there is now no source of hydrogen peroxide. In order to respond to sugar, all three components are necessary: the GOx to oxidize sugar and produce hydrogen peroxide, which couples with HRP to combine the dye and change the color (1F). The full assay will also respond to hydrogen peroxide: it will simply bypass the need for the GOx as the HRP did (1C). In summary, this section shows that the dye alone will not respond to anything, that hydrogen peroxide can cause a color change when HRP is present with the dye, and that sugar will only produce a color change when all components are present.

Well[a]	*Analyte*	*Sensing Components*	*Color Change?*	*Reason*
1A	H_2O_2	Dye	No	No HRP to combine dye
1B'	H_2O_2	Dye, GOx	No	No HRP to combine dye
1B	H_2O_2	Dye, HRP	**Yes**	H_2O_2 and HRP can combine dye without GOx
1C	H_2O_2	Dye, GOx, HRP	**Yes**	H_2O_2 and HRP can combine dye (GOx is not doing anything)
1D	Sugar	Dye	No	No HRP to combine dye
1E'	Sugar	Dye, GOx	No	No HRP to combine dye
1E	Sugar	Dye, HRP	No	No source of H_2O_2 to let HRP combine dye
1F	Sugar	Dye, GOx, HRP	**Yes**	Sugar and GOx produce H_2O_2 that allows HRP to combine dye

[a]*One group of four students has beads with only GOx and dye, while the other has beads with only HRP and dye. The two groups compare their results from wells 1B and 1E to get a complete set of results.*

Table 4.4.1.1. Summary of Column 1 Results

4.4.2. Analysis of Bead Functionality: Columns 2 and 3

This section highlights the utility of the nanoenvironment in making a convenient sensor that is functional in a wide range of conditions. Columns 2 and 3 have a range of household chemicals with different pH values: windex and a solution of baking soda (bases), water (neutral), and vinegar and lemon juice (acids). All of the wells in both columns also have sugar solution in them. When beads are added to Column 2, they all change color, but when the free assay solution is added to Column 3, only the neutral and basic wells (3 A-C) change color. Since sugar is present in all wells, they should all change color, but the enzymes denature and lose their shape in acidic environments. However, the nanostructured hydrogel beads are able to protect the enzymes in an environment that is resistant to changes in pH while still allowing all of the reactions to occur that make up the sensing pathway (2D, 2E). If desired, this section can also provide a lead-in for a discussion of buffers, pH, and enzyme activity.

4.4.3. Quantification of Sugar in Unknowns Using a Calibration Curve: Columns 4 and 6

Columns 4 and 6 are used to determine the amount of sugar in unknown solutions. This has two main goals: first, students learn how to use a calibration curve to determine the concentration of an unknown, and second, students explore enzyme specificity. The calibration curve features a concentrated stock sugar solution (4A), four diluted sugar solutions (4B-E), and a water blank (4F), and results in a gradation of colors that range from deep pink to colorless. This calibration curve can be pedagogically incorporated with discussions of color, absorption spectroscopy, and Beer's Law (as the gradation of colors is essentially a qualitative Beer's Law plot). When sugary drinks are tested as the unknowns, students can come to a variety of conclusions. We suggest that the instructor provide a drink sweetened with high-fructose corn syrup or a synthetic sweetener, which will give a very weak signal due to the specificity of the GOx, which only responds to glucose or sucrose (which has a glucose unit). Students sometimes also note that colored drinks make it difficult to judge the final color, and that a blank bead swollen in the drink alone may be a good control with which to compare the final color. If students bring in cloudy drinks, they may also note that the response is difficult to judge, and that the bead may need to be removed and rinsed to judge the color, but that this may interfere with the development of the color over time.

4.5. Use and Assessment

This experiment was developed as part of the California NanoSystems Institute Education Program. As part of this program, the experiment has been carried out by almost 100 high school students during summer camp programs at UCLA. The students performed the experiment over the course of 2 hours in groups of 4 with roughly one graduate student per 10 students. It has also been presented to 40 high school teachers as part of professional development workshops over the past two years. The version thus far presented at the workshops used a different dye, Amplex Red, instead of the combination presented here. However, the Amplex Red tended to change color in

response to light exposure,[5] so the dye was switched to the current combination. Both student and teacher feedback suggest that the level of organization necessary to follow the complex procedure makes the experiment best suited for more advanced high school students or potentially even introductory undergraduate students. Teachers indicate that the procedure can be completed in an hour if students are sufficiently prepared, but that two periods are likely to be necessary. The version with the new dye that can be kept for up to a week is more accommodating of this option.

Several of the teachers who attended the workshops have performed the experiment with classrooms of up to 30 students, and some elected to have students work in larger groups where they felt it would be easier to have students work together on each task instead of complete each one alone. The teachers report that they intend to run the experiment again with future classes and that the experiment, while on the challenging side for high school students, is suitable for their classrooms. In surveys administered following the experiment, 68 out of the 70 surveyed 9th, 10th, and 11th grade students indicated that they found the material interesting, and 67 out of 70 indicated that they wanted to learn more about sensing and nanoscale interactions.

4.6. Appendix

Supplementary Information For Chapter 4

Biosensors

The California NanoSystems Institute
University of California, Los Angeles
High School Nanoscience Institute

Teacher's Manual – Fall 2019

Table of Contents

Purpose: Biosensors are a specific class of sensor that targets a biological molecule such as an enzyme, carbohydrate, toxin, or bacterium. They are used for a wide variety of research, industrial, and biomedical applications, and many take advantage of nanomaterials or biomolecules as part of the sensor itself. Portable, robust sensors are desirable for sensing toxins, contaminants, and pathogens that might spread, as well as biologically important molecules like glucose whose presence or absence can be important for normal biological function.

In this experiment, you will make a glucose-sensing assay encapsulated in a nanoporous gel bead and see what different components of the assay respond to in order to figure out its mechanism. Then you will test the assay under a variety of conditions to measure its limitations. Lastly, you will use the assay and a series of sugar solutions with known concentrations to figure out how much sugar is in different sugary drinks.

Overview: In groups of four, students will make a glucose-sensing assay in a gel bead, determine its mechanism, observe its limitations, and use it to quantify how much sugar is in different drinks.

Next Generation Science Standards

To be Next Generation Science Standards (NGSS) compliant we have highlighted ways in which this experiment addresses key aspects of NGSS. Specifically, this experiment addresses engineering design, biology, chemistry, and physics.

High School Disciplinary Core Concepts

1. Engineering Design:
   a. HS-ETS1-2. Design a solution to a complex real-world problem by breaking it down into smaller, more manageable problems that can be solved through engineering.
   b. HS-ETS1-3. Evaluate a solution to a complex real-world problem based on prioritized criteria and trade-offs that account for a range of constraints, including cost, safety, reliability, and aesthetics, as well as possible social, cultural, and environmental impacts.
2. Biology:
   a. HS-LS1-2. Develop and use a model to illustrate hierarchical organization of interacting systems that provide specific functions within multicellular organisms.
   b. HS-LS1-3. Plan and conduct an investigation to provide evidence that feedback mechanisms maintain homeostasis.
   c. HS-LS1-6. Construct and revise an explanation based on evidence for how carbon, hydrogen, and oxygen from sugar molecules may combine with other elements to form amino acids and/or other large carbon-based molecules.
3. Chemistry:
   a. HS-PS1-2. Construct and revise an explanation for the outcome of a simple chemical reaction based on the outermost electron states of atoms, trends in the periodic table, and knowledge of the patterns of chemical properties.
   b. HS-PS1-3. Plan and conduct an investigation to gather evidence to compare the structure of substances at the bulk scale to infer the strength of electrical forces between particles.
   c. HS-PS1-5. Apply scientific principles and evidence to provide an explanation about the effects of changing the temperature or concentration of the reacting particles on the rate at which a reaction occurs.
   d. HS-PS1-6. Refine the design of a chemical system by specifying a change in conditions that would produce increased amounts of products at equilibrium.
   e. HS-PS3-2. Develop and use models to illustrate that energy at the macroscopic scale can be accounted for as a combination of energy associated with the motions of particles (objects) and energy associated with the relative position of particles (objects).
4. Physics:
   a. HS-PS2-6. Communicate scientific and technical information about why the molecular-level structure is important in the functioning of designed materials.
   b. HS-PS3-2. Develop and use models to illustrate that energy at the macroscopic scale can be accounted for as a combination of energy associated with the motions of particles (objects) and energy associated with the relative position of particles (objects).
   c. HS-PS4-5. Communicate technical information about how some technological devices use the principles of wave behavior and wave interactions with matter to transmit and capture information and energy.
   d. HS-PS4-3. Evaluate the claims, evidence, and reasoning behind the idea that electromagnetic radiation can be described either by a wave model or a particle model, and that for some situations, one model is more useful than the other.

Background on sensors

Sensors allow us to obtain information about the world around us that is too subtle or of the wrong type to be able to interpret with our own senses. At its core, any sensor takes one type of signal, brings it through a **transduction** pathway that effectively translates the signal, and then produces a response. For example, in a photoelectric smoke detector, the smoke particles (signal) in the air disrupt a beam of light and deflect it towards a sensor (transduction), which sets off the alarm (Fig 1a). Sometimes, this transduction/response process is repeated multiple times before the final response is produced, such as in a CD player. In a CD, the reflective bumpy pattern on the disk (the signal) has a reflective beam passed over it (transduction). The reflected beam hits a light detector called a photocell, which produces an electric current (response). This current is a second signal, which is then passed through a series of circuits (transduction) to produce a different electrical signal (response, third signal) that a loudspeaker (transduction) turns into sound that you can hear (final response) (Fig 1b).

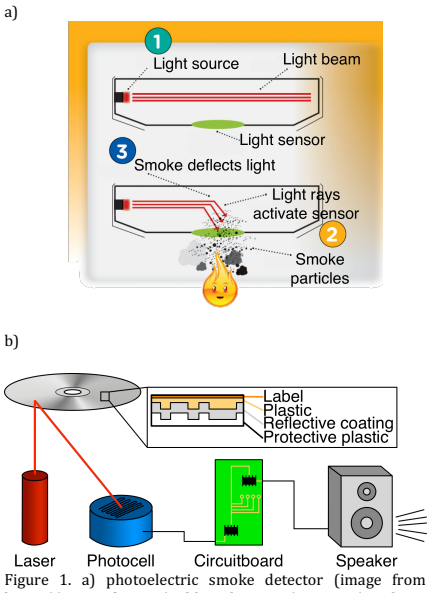

Figure 1. a) photoelectric smoke detector (image from https://www.nfpa.org/Public-Education/By-topic/Smoke-alarms/Ionization-vs-photoelectric) b) CD player schematic (image from www.explainthatstuff.com)

A sensor's specificity and limits of detection both play a large role in determining what it can be used for. **Specificity** refers to how many things will cause the sensor to produce a response. For instance, a very specific chemical sensor that is used for detecting explosives might respond only to TNT, while a very general one might also respond to other explosives as well. Sensors based on microorganisms have been developed that feature both specific sensing of TNT and a wider variety of explosive compounds.[1] The sensor in this experiment only senses glucose, which means it will respond to glucose and fructose (which contains a glucose unit), but not to synthetic sweeteners like aspartame. A sensor's desired **limits of detection** are also specific to its application. A laboratory balance needs to be able to weigh out grams or milligrams precisely, but a scale used to weigh trucks doesn't need that level of precision.

Biosensors are a specific class of sensors that detect the presence of a biological molecule. Oftentimes, the sensors themselves also feature biological molecules, including

enzymes (discussed in the next section), DNA, and bacteria. This type of sensor takes advantage of the highly specific molecular recognition that has developed in biological systems. Many biosensors also feature nanostructured materials such as carbon nanotubes, nanoparticles, and monolayers. Nanomaterials are uniquely suited for biosensing because their high surface area allows for increased sensitivity, and the size of their features is matched to the molecules they are trying to sense. The biosensor in this experiment is referred to as an **assay**, which is simply another way to refer to a system that measures the amount, presence, or activity of an analyte. Aside from the assay used in this experiment, there are many other glucose sensing systems that produce fluorescent, colorimetric, or electrical responses. Other biosensors are used to test for food toxins, and a biological system has even been developed to test for UV irradiation.[2]

Background on enzymes

Enzymes are important biological macromolecules that catalyze chemical reactions. They are essential in living creatures, because they allow reactions to occur at a higher rate by lowering the required activation energy (Fig 2). Enzymes recognize their substrates very specifically, because an enzyme's substrate binding pocket is uniquely shaped and charged for that specific substrate. Due to an enzyme's unique ability to carry out reactions selectively and efficiently, they are extremely useful in biotechnological applications.

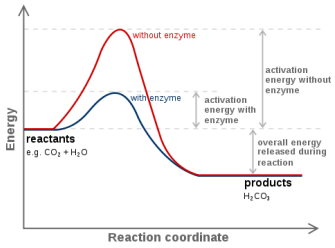

Figure 2. Enzymes lower the activation energy required for a certain chemical reaction to take place. Figure from https://en.wikibooks.org/wiki/Structural_Biochemistry/Enzyme/Activation_energy

In biotechnological applications, enzymes are usually in pure form. This means that they are not in their natural biological environment within an organism. To keep an enzyme catalytically active, scientists must make sure to place the isolated protein in a compatible buffer maintained at the correct temperature, pH, and salt concentration. If an enzyme is placed in an incompatible buffer, it may **denature**, or unfold, and an unfolded enzyme cannot carry out its function (Fig 3). However, industrial processes are often very different from biological ones.

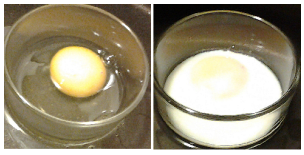

Figure 3. The proteins present within an egg are denatured when it is heated. Figure by RMADLA - Own work, CC BY-SA 3.0, https://commons.wikimedia.org/w/index.php?curid=24606372

Enzyme immobilization is a developing method that is used to stabilize enzymes. Immobilization may have many other benefits, such as improving activity and allowing enzymes to be reused in multiple rounds of reactions.[3-5] In this experiment, we encapsulate two

enzymes (glucose oxidase, GOx, and horseradish peroxidase, HRP) in a **gel,** which we define in a later section. This stabilizes the enzymes in our experiment by slowing the diffusion of acid/base into the bead despite a pH change in the surrounding solution.

*Note: For those who are unfamiliar with biological naming conventions, the suffix *–ase* indicates that something is an enzyme.

Glucose oxidase (GOx) is an enzyme that oxidizes glucose to hydrogen peroxide (Fig 4). It is produced by several species of fungi and insects, and its role is to oxidize glucose to D-glucono-δ-lactone, producing hydrogen peroxide as a byproduct. In some cases, the hydrogen peroxide is produced as an antibacterial agent. In this experiment, the hydrogen peroxide has another role.

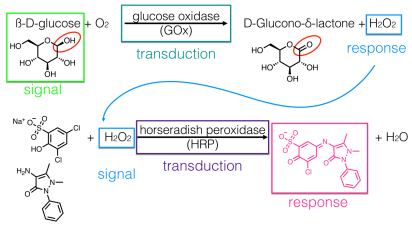

Figure 4. Reaction schemes of the enzymes used in this experiment. Top: Glucose oxidase (GOx). Bottom: Horseradish peroxidase (HRP).

Horseradish peroxidase (HRP) can utilize the hydrogen peroxide to oxidize another substrate: the two colorless dye molecules (Fig 4). This chemical reaction causes colorless precursors to become combined into a red molecule shown on the right. Together, these two enzymes work in concert to create our biosensor!

Background on color (and absorption spectroscopy)

What we perceive as color is actually electromagnetic waves with different energies, wavelengths, and frequencies. Each wavelength of light corresponds with a different color (Fig 5). When we perceive an object as colored, it means that the material making up that object is absorbing some portion of the visible spectrum of light, and what we see is the portion of the visible spectrum left over after that light is absorbed. Therefore if something absorbs red light, it will appear green, because red and green are complementary colors.

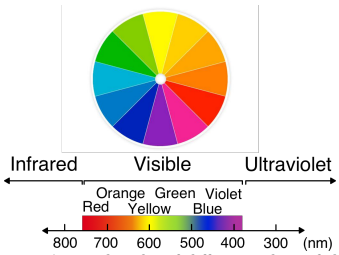

Figure 5. Wavelengths of different colors of the visible light spectrum.

Compounds that absorb in the UV-visible range are easy to detect using a technique called **absorption spectroscopy**. A beam of light is passed through a solution, and a detector on the other side of the solution registers the intensity of the light after it goes through, reported as absorbance (Fig 6a). If a solution is strongly colored, it absorbs a lot of light, and the absorbance will be high. Conversely, solutions that don't absorb light will have high low absorbance because more light is transmitted through the solution. UV-visible absorption spectroscopy

can be carried out at a single wavelength (in which case the absorbance will be reported as a single number, Fig 6c), or over the full spectrum of UV-visible wavelengths (which will give a full spectrum of absorbance values: one for each wavelength, Fig 6b).

Absorption spectroscopy is very useful for quantitatively analyzing solutions that absorb light because the absorption of a molecule in solution is directly proportional to its concentration. This relationship, known as **Beer's Law**, states that A = εcl, where c is the concentration of the solution being tested in mol/L, l is the distance that the light has to travel through solution before it hits the detector (also known as the path length, and typically 1cm), and ε is the molar absorptivity of the compound in question. Since ε and l are constant, a plot of concentration vs. absorbance gives a straight line (Fig 7). In this experiment, students will employ a qualitative version of Beer's Law by visually comparing the color response of the assay when exposed to sugary drinks to the response in various solutions of known concentration.

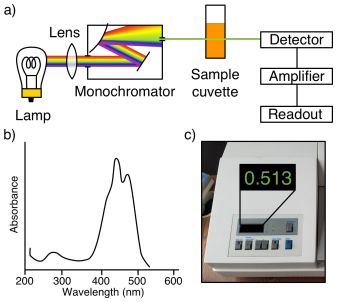

Figure 6. a) UV-vis spectrometer setup (image adapted from http://elchem.kaist.ac.kr/vt/chem-ed/spec/uv-vis/uv-vis.htm) b) an example UV-vis spectrum c) the readout of a monochromatic UV-vis detector

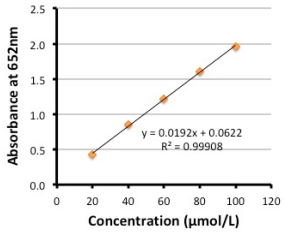

Figure 7. An example of a calibration curve obtained by UV-vis spectroscopy, showing the linear correlation between concentration of iron in solution and absorbance at 652 nm.

Background on gels

As mentioned above, we encapsulate two enzymes in a small gel bead during the course of this experiment. A **hydrogel** is a jelly-like substance, composed of a large amount of liquid held within a scaffold of cross-linked polymer chains (Fig 8a). A **polymer** chain is composed of repeating **monomers**, or single units, held together by covalent bonds (Fig 8b). Depending on the amount of cross-linking between individual polymer chains, the scaffold can have smaller or larger pore sizes. In this experiment, the pores are the right size to hold the enzymes involved in the assay.

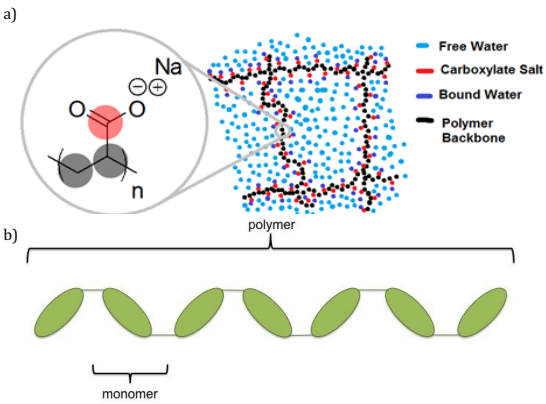

Figure 8. a) Polymer chains form the scaffold of a hydrogel. The monomer unit of sodium polyacrylate is shown at the left, and a schematic of the hydrogel is shown at the right (image from CNSI biopolymers manual) b) A polymer is composed of repeating monomers (green ovals) linked by covalent bonds (green lines). Figure adapted from General Chemistry: Principles, Patterns, and Applications, v. 1.0, by Bruce Averill and Patricia Eldredge.

If you are unfamiliar with polymers and gels, CNSI offers an additional workshop on biopolymers that may be of interest to you.

Summary of Experiment

Students will combine two enzymes and a two-component dye to create an assay solution to sense sugar. Along the way, they will allow the different components to be absorbed by polymer beads. They will then take the beads containing the individual components and test their responses to two different signal molecules: sugar (in the form of sucrose) and a hydrogen peroxide solution. Only the beads containing all components of the assay will give a colorimetric response to the sugar. However, since hydrogen peroxide is an intermediate signal in the process, if it is unintentionally introduced into the sample, it will cause a color change to occur when only horseradish peroxidase (HRP) and the dye are present.

Next, the students will examine the stability gained by encapsulating the assay into a gel bead. The beads containing the assay will be submerged in sugar solutions containing various acids and bases, and the responses will be compared to those of the free assay solution in the same acid/base/sugar combinations. The assay is stable both in the free and

encapsulated form at high pH values (basic conditions), but will only produce a color change at low pH values (acidic conditions) when encapsulated in the bead.

Lastly, students will make a series of sugar solutions of varying concentration in order to create a calibration curve. They will compare the response (or color intensity) of the assay in sugary drinks of unknown concentration to the response in the known solutions to determine the sugar content of their drinks. Drinks sweetened with high-fructose corn syrup or artificial sweeteners such as aspartame, saccharin, and sucralose will not produce a response, but naturally sweetened drinks will because the assay is specific to glucose. (Fig. 9)

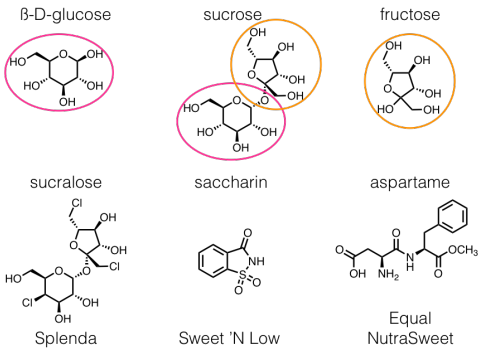

Figure 9. Naturally occurring sugars and synthetic sweeteners used in drinks. The assay is specific to glucose, so it will respond to both pure glucose and sucrose (which contains a glucose unit, circled in pink), but not to fructose, sucralose, saccharin, or aspartame.

Bibliography

1. Shelmer, B.; Palevsky, N.; Yagur-Kroll, S.; Belkin, S. Genetically engineered microorganisms for the detection of explosives' residues. *Front Microbiol.* **2015**, *6*, 1175.
2. Karentz, D.; Lutze, L.H. Evaluation of biologically harmful ultraviolet radiation in Antarctica with a biological dosimeter designed for aquatic environments. *Limnol. Oceanogr.* **1990**, *35*, 549.
3. Garcia-Galan, C.; Berenguer-Murcia, Á.; Fernandez-Lafuente, R.; Rodrigues, R.C. Potential of Different Enzyme Immobilization Strategies to Improve Enzyme Performance. *Adv. Synth. Catal.* **2011**, *353*, 2885.
4. Rodrigues, R.C.; Ortiz, C.; Berenguer-Murcia, Á.; Torres, R.; Gernández-Lafuente, R. Modifying enzyme activity and selectivity by immobilization. *Chem. Soc. Rev.* **2013**, *42*, 6290.
5. Mohamad, N.R.; Marzuki, N.H.C.; Buang, N.A.; Huyop, F.; Wahab, R.A. An overview of technologies for immobilization of enzymes and surface analysis techniques for immobilized enzymes. *Biotechnology & Biotechnological Equipment* **2015**, *29*, 205.

Biosensors Supplies List

The following is a list of all of the supplies contained in your kit. Students will work in groups of four. This kit consists of ***consumable*** *and* ***reusable*** *items. There are enough consumable items for a total of 23 groups (with 4-5 students per group) to perform the experiment. There are enough reusable items for 8 groups to work simultaneously.*

Supplies Provided by Teacher:

- 1 L water
- ASK STUDENTS to bring in sugary drinks they want to test. You may also want to bring in a couple drinks with high fructose corn syrup (they will taste sweet but will not trigger a color change in the assay)
- Balance that can weigh 15 g of material (can be substituted by ½ tbsp measuring spoon, included: 15g sucrose = 2.5 x ½ tbsp)
- Optional: it is ideal for students to have access to one camera/smartphone per group, but the experiment can be conducted without it

Reusable Supplies Included in the Kit:

- 24 well plates
- 115 transfer pipets
- 69 plastic spatulas
- 46 white plastic cups
- 69 petri dishes
- 2 clear cups to hold 15mL tubes (class stock)
- 1 15mL graduated cylinder
- 2 ½ tsp measuring spoons
- 4 Sharpies for labeling

Consumable Supplies Included in the Kit:

- 3 x 8 = 24 mg Glucose oxidase (Store in fridge until use)
- 3 x 2.5 = 7.5 mg Horseradish peroxidase (Store in fridge until use)
- 3 x 10 = 30 mg 4-aminoantipyrine
- 3 x 62 = 186 mg sodium 3,5-dichloro-2-hydroxybenzenesulfonate
- 500 mL PBS buffer
- 1 pint hydrogen peroxide solution
- 400 g Sucrose
- ~625 growing spheres
- Lemon juice
- Vinegar
- Windex
- 10 mg/mL baking soda solution in water

*******SAFETY INFORMATION*******

Please check with your school or school district's safety officer to address any concerns regarding chemicals or lab safety procedures. Please also dispose of all hazardous chemicals in a manner compliant with your school district's procedures.

Possible hazardous materials and proper procedure:

1. Glucose oxidase is an irritant when inhaled as a solid. Only the teacher should handle the solid powder, and should be cautious not to breathe it in while dissolving it in buffer.

Teacher Pre-Lab

The following contains instruction for preparing the supplies needed for this lab.

During the previous class:

- Ask students to each bring a sugary drink they want to test. They only need ~1 mL of it.

Group supply preparation:

Note on enzymes: Powdered forms of enzymes are stable in the freezer until the expiration date indicated by the manufacturer. If dissolved into solution, enzymes are stable in solution in the refrigerator for a week. Once an enzyme has been placed into solution, it should not be subjected to freeze/thaw cycles, so DO NOT put these solutions into the freezer. Freeze/thaw cycles contribute to protein degradation.

- Add PBS buffer to the 8 mL mark on each vial of glucose oxidase to be used and label a transfer pipet "GOx" for distribution of solution (enzyme lasts ~1 week after adding buffer if kept in a fridge). Each vial is good for up to 8 groups.
- Add PBS buffer to the 8 mL mark on each vial of horseradish peroxidase to be used and label a transfer pipet "HRP" for distribution of solution (enzyme lasts ~1 week after adding buffer if kept in a fridge). Each vial is good for up to 8 groups.
- Add PBS buffer to the 8 mL mark on each vial of the 4-aminoantipyrine to be used and label a transfer pipet "AAP" for distribution of the solution. Each vial is good for up to 8 groups)
- Add PBS buffer to the 8 mL mark on each vial of the sodium 3,5-dichloro-2-hydroxybenzenesulfonate to be used and label a transfer pipet "HBS" for distribution of the solution. Each vial is good for up to 8 groups.
- Label a transfer pipet "PBS Buffer" and place next to the remaining buffer.
- Make a diluted solution of hydrogen peroxide by mixing 3 mL of the provided hydrogen peroxide with 27 mL of DI water. This amount is good for up to 10 groups.
- Label a transfer pipet "H_2O_2" and place next to hydrogen peroxide solution.
- Place the sucrose near either the ½ tsp measuring spoon or the balance (you may want to put something down to catch whatever sugar spills here).

Distribute the supplies:

In each group of 4 students, 1 student will make the beads, 1 will make sugar solutions, 1 will prepare acids and bases, and 1 will prepare the unknowns and H_2O_2. For ideas for assigning duties for smaller or larger groups, see the troubleshooting section. Each group of 4 students will need:

Communal supplies at the front of the class (listed per group, do not need to distribute):

- 1 mL glucose oxidase solution
- 1 mL horseradish peroxidase solution
- 1 mL 4-aminoantipyrine solution
- 1 mL sodium 3,5-dichloro-2-hydroxybenzenesulfonate solution
- 8 mL PBS buffer
- 40 mL water
- 3 mL dilute hydrogen peroxide solution
- 15 g (3.5tsp) sucrose
- 2 drops lemon juice
- 2 drops vinegar
- 2 drops 10 mg/mL solution of baking soda
- 2 drops windex

Pre-distributed:

- 3 petri dishes
- 27 growing spheres
- 3-4 transfer pipets
- 3 disposable spatulas
- 2 white plastic cups

Troubleshooting

1. Problem: Students need to have groups with more or less than 4 people.

Solution (small groups): For groups containing 3 students, the Acid/Base (**Section 4**) and H_2O_2/Unknowns (**Section 5**) tasks can be combined most easily. If students work in pairs, one can make solutions (**Sections 3-5**) while the other starts the beads (**Section 2**). The person making the beads can assist with setting up the well plate while beads are swelling.

Solution (large groups): For groups containing 5 students, the fifth student can help with making the beads (**Section 2**) or the sugar solutions (**Section 3**). It is not recommended for six students to be in a single group.

2. Problem: I need to break this experiment into two pieces because of shorter class periods.

Solution: The beads can be stored in petri dishes for up to a week and will still give the provided results. If the students are using old beads, make sure they do not record the

slightly yellow color of some beads as a color change: they should record only the presence of the pink dye. The working solution can be stored in a sealed dark container for up to a week as well (the container needs to prevent evaporation and also keep out light, which will cause the solution to slowly change color). After a week, the working solution is likely to look pink, but when a single drop of the solution is added to the well plate, it is dilute enough that a color change is still visible. Make sure students do not record the slight pink tinge of the initial working solution as a color change for Column 3.

3. Problem: Assay changes color before added to a solution containing sugar or hydrogen peroxide.

Solution: This is likely due to contamination. Check that the students have labeled their pipets and spatulas and are using the correct ones.

4. Problem: The hydrogen peroxide plus "B" bead (Group R only) is not changing color.

Solution: Sometimes this combination only produces a very subtle color change, which is only visible if you look at the sides of the bead or the sides of the well. This is especially true if assay beads are left for several days before being used. Sometimes it just needs to be re-run to produce the color change. Keep an eye on the people performing this test and suggest to them that they re-run it if it doesn't change color since this result is very important in determining the mechanism.

Student Pre-lab

1. Fill in the following color wheel using the colors listed, and then write the three matching pairs of complementary colors in the blanks to the right.

Colors: Red, Orange, Yellow, Green, Blue, Violet

Color Wheel:

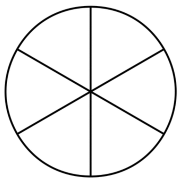

Complementary Colors:

Pair 1:_____, _____

Pair 2:_____, _____

Pair 3:_____, _____

Answer: Red/Green, Orange/Blue, Yellow/Violet.

2. Blue light has a wavelength of 450-490nm. If a molecule absorbs 460nm light, what color will it appear?

Answer: It will appear orange, since orange and blue are complementary colors.

3. The colored indicator used in this experiment turns bright pink. What color light does it absorb?

Answer: It absorbs blue/green light (the absorption maximum of the dye is at about 510nm).

4. If you wanted to analyze this compound using UV-vis spectroscopy, what wavelength or color would you measure for absorption at?

Answer: 450-600nm (blue to green), which is where the dye absorbs the most light.

5. What is the concentration (in g/mL) of a salt solution created by adding 27 grams of salt to 60mL of water if the final total volume of the solution is 70mL?

Answer: 27/70 = 0.39g/mL (make sure to use final total volume, not volume of water added!)

6. If you have a 3mg/mL solution of theobromine (a component of chocolate) in water, how would you go about making 6mL of a 1mg/mL solution? Hint: use the equation $C_iV_i=C_fV_f$, where C is concentration and V is volume, for initial solution *i* and final solution *f*.

Answer: 1*6/3 = 2mL of the original solution plus 4mL of water.

7. The sugar used in this experiment is sucrose, which is made up of one glucose unit bonded to one fructose unit. Therefore, glucose only makes up 52.6% of the mass of the sugar you will weigh out. What is the **glucose** concentration (in g/mL) of a sugar solution created by adding 15 grams of **sucrose** to 30mL of water if the final total volume of the solution is 40mL? This solution will be your sugar stock solution during the experiment.

Answer: (15 x 0.526)/40 = 0.20g/mL (make sure to use the mass of glucose, not sucrose, and the final total volume, not volume of water added!)

8. In order to make a calibration curve during the experiment, you will make a series of diluted sugar solutions from the sugar stock solution in question 3. Let the concentration of your stock solution be "x." If you're going to have the stock solution, a blank solution of just water, and four evenly spaced points between those two concentrations, what are the concentrations of the solutions be **in terms of x**?

Solution 1: _____ (stock solution)

Solution 2: _____ (dilution 1)

Solution 3: _____ (dilution 2)

Solution 4: _____ (dilution 3)

Solution 5: _____ (dilution 4)

Solution 6: _____ (plain water)

Answer: 1) x 2) 0.8x 3) 0.6x 4) 0.4x 5) 0.2x 6) 0x, or just 0.

9. Using your answers to questions 3 and 4, what are the concentrations of the six solutions in g/mL? Solution 1 should be your answer to question 3.

Solution 1: _____ (stock solution)

Solution 2: _____ (dilution 1)

Solution 3: _____ (dilution 2)

Solution 4: _____ (dilution 3)

Solution 5: _____ (dilution 4)

Solution 6: _____ (plain water)

Answer: 1) 0.20g/mL 2) 0.16g/mL 3) 0.12g/mL 4) 0.08g/mL 5) 0.04g/mL 6) 0.0g/mL

10. Using the same equation from question 2 ($C_iV_i=C_fV_f$), calculate how many drops of sugar stock solution and how many drops of water you need to combine to create 15 drops of each solution. Hint: use "drops" as your unit of volume instead of mL, and the math may be simpler if you use the concentrations in terms of x that you calculated in question 3.

Solution	# of drops of sugar stock solution	# of drops of water
Stock solution		
Dilution 1		
Dilution 2		
Dilution 3		
Dilution 4		
Plain water		

Answer: 1) 15, 0 2) 12, 3 3) 9, 6 4) 6, 9 5) 3, 12 6) 0, 15

11. Look through the procedure to fill in the following chart with everything that will go in each well on your well plate. Make sure to include sugar stock, hydrogen peroxide, any acids or bases, and the specific assay components that are present (dye, GOx, HRP) in what form (bead or free solution).

	1	2	3	4	5	6
A	H_2O_2, bead with dye	Sugar stock, Windex, bead with dye, GOx, and HRP	Sugar stock, Windex, solution with dye, GOx, and HRP	Solution 1 (sugar stock), bead with dye, GOx, and HRP		Unknown drink, bead with dye, GOx, and HRP
B	H_2O_2, bead with dye and HRP (Group R) or dye and GOx (Group X)	Sugar stock, baking soda, bead with dye, GOx, and HRP	Sugar stock, baking soda, solution with dye, GOx, and HRP	Solution 2, bead with dye, GOx, and HRP		Unknown drink, bead with dye, GOx, and HRP
C	H_2O_2, bead with dye, GOx, and HRP	Sugar stock, water, bead with dye, GOx, and HRP	Sugar stock, water, solution with dye, GOx, and HRP	Solution 3, bead with dye, GOx, and HRP		Unknown drink, bead with dye, GOx, and HRP
D	Sugar stock, bead with dye	Sugar stock, vinegar, bead with dye, GOx, and HRP	Sugar stock, vinegar, solution with dye, GOx, and HRP	Solution 4, bead with dye, GOx, and HRP		Unknown drink, bead with dye, GOx, and HRP
E	Sugar stock, bead with dye and HRP (Group R) or dye and GOx (Group X)	Sugar stock, lemon juice, bead with dye, GOx, and HRP	Sugar stock, lemon juice, solution with dye, GOx, and HRP	Solution 5, bead with dye, GOx, and HRP		Unknown drink, bead with dye, GOx, and HRP
F	Sugar Stock, bead with dye, GOx, and HRP			Solution 6 (water), bead with dye, GOx, and HRP		Unknown drink, bead with dye, GOx, and HRP

12. What will you learn from the results of each column? Summarize the purpose of each column below.

Column 1: Results from Column 1 indicate which assay component responds to H_2O_2 and which responds to sugar.

Columns 2/3: Results from Columns 2 and 3 show which pH environments the assay can function in when encapsulated in a bead versus when it is a free solution.

Columns 4/6: Results from Column 6 can be compared to those from Column 4 to determine the approximate amount of sugar in each drink.

Student Procedure

Section 1. Setup and Organization

Materials:

- 2 white plastic cups
- 3 transfer pipets
- 3 disposable spatulas
- 3 petri dishes

Procedure:

1. Form groups of 4 people.

2. Pair up with another group of four and make one group "Group R" and the other one "Group X." You will share your results later on in the experiment.

Group R Only

3. Label your pipets:
   - -sugar stock solution
   - -water
   - -unknown drinks

   Label your spatulas:
   - -A
   - -B
   - -D

   Label your petri dishes
   - -A
   - -B
   - -D

   Label your white cups:
   - -working solution
   - -sugar stock solution

Group X Only

4. Label your pipets:
   - -sugar stock solution
   - -water
   - -unknown drinks

   Label your spatulas:
   - -A
   - -C
   - -D

   Label your petri dishes
   - -A
   - -C
   - -D

   Label your white cups:
   - -working solution
   - -sugar stock solution

Both Groups

5. Assign one person to each of the following roles, and go to the indicated section to begin individual procedures:
   - -Make beads (Jump to Section 2, step 6 (*Group R*) or step 9 (*Group X*))
   - -Sugar solutions (Jump to Section 3, step 12)
   - -Acids and Bases (Jump to Section 4, step 14)
   - -H_2O_2 and unknowns (Jump to Section 5, step 16)

   You will all complete Section 6 (starting step 18) together once Sections 1-5 are complete.

Section 2. Make beads with different assay components

Materials:

Front of the room:

- 1X PBS buffer
- "GOx" (glucose oxidase) stock solution in PBS buffer
- "HRP" (horseradish peroxidase) stock solution in PBS buffer
- "AAP" (4-aminoantipyrine) stock solution in PBS buffer
- "HBS" (sodium 3,5-dichloro-2-hydroxybenzenesulfonate) stock solution in PBS buffer

Hint Box!

- When you swell the beads, look for them to be 2-3x their original diameter (takes 5-10 minutes).
- The swelling is difficult to see: tilt the cup or use the appropriate spatula to get a better idea of their size.

At your station:

- White plastic cup labeled "working solution"
- 27 beads
- 3 labeled disposable spatulas
- 3 labeled petri dishes

Procedure:

<u>*Group R*</u> Only

Contamination, especially stray sugar, can affect your results! Be very careful to use the correct pipet and spatula at all times. Wash your hands prior to starting the lab!

6. **"A" Bead preparation: Dye Only**
   Prepare a working solution by pipetting 8 mL 1X PBS buffer into your white cup and adding 1 mL of the AAP stock solution and 1 mL of the HBS stock solution. Add 4 beads to the solution and let swell to 2-3 times their original size. Remove these from the solution using your "A" spatula and place them in the "A" petri dish.

7. **"B" Bead preparation: Dye + HRP**
   Add 1 mL HRP stock solution to the remaining working solution from Step 6 using the HRP pipet. Add 4 beads to the solution and let swell to 2-3 times their original size. Remove these from the solution using your "B" spatula and place in the "B" petri dish.

8. **"D" Bead preparation: Dye+ HRP + GOx**
   Add 1 mL GOx stock solution to the remaining working solution from Step 7 using the GOx pipet. Add ALL of the remaining beads to your solution and let swell to 2-3 times their original size. Remove these from the solution using your "D" spatula and place in the "D" petri dish. SAVE THE REST OF THE WORKING SOLUTION for later in the experiment.

Group X Only

Contamination, especially stray sugar, can affect your results! Be very careful to use the correct pipet and spatula at all times.

9. **"A" Bead preparation: Dye Only**
   Prepare a working solution by pipetting 8 mL 1X PBS buffer into your white cup and adding 1 mL of the AAP stock solution and 1 mL of the HBS stock solution. Add 4 beads to the solution and let swell to 2-3 times their original size. Remove these from the solution using your "A" spatula and place them in the "A" petri dish.

10. **"C" Bead preparation: Dye + GOx**
    Add 1 mL GOx stock solution to the remaining working solution from Step 9 using the GOx pipet. Add 4 beads to the solution and let swell to 2-3 times their original size. Remove these from the solution using your "C" spatula and place in the "C" petri dish.

11. **"D" Bead preparation: Dye + GOx + HRP**
    Add 1 mL HRP stock solution to the remaining working solution from Step 10 using the HRP pipet. Add ALL of the remaining beads to your solution and let swell to 2-3 times their original size. Remove these from the solution using your "D" spatula and place in the "D" petri dish. SAVE THE REST OF THE WORKING SOLUTION for later in the experiment.

Section 3. Sugar solutions for all columns

Materials:

- 15 g sugar
- 30 mL water for stock solution + 5 mL to make dilutions
- White plastic cup labeled "sugar stock solution"
- 2 Labeled transfer pipets: "water" and "sugar stock solution"
- 1 well plate (share with Sections 4-5)
- Color-coded sample sheet (share with Sections 4-5)

Hint Box!

- For best results, before placing each bead into a well, first blot the beads gently with Kimwipes or paper towels to remove remaining solution from the surface of the bead!

Procedure:

12. Make a sugar stock solution by adding 15 g sugar to 30 mL water in a white cup labeled "sugar stock solution." This is a fairly saturated solution, and it will take some work to get it to dissolve completely: make sure the sugar is completely dissolved and mixed before you move on. You can stir it using your sugar stock solution pipet.
13. Make the four dilutions of your sugar stock solution that you calculated in your pre-lab by adding the appropriate number of drops of sugar stock solution and water to each well in column 4. Make sure to use the correct pipet ("water" or "sugar stock solution") to avoid contamination!

    4A: saturated sugar solution
    4B: dilution 1
    4C: dilution 2
    4D: dilution 3
    4E: dilution 4
    4F: water

Section 4. Acid/base tests for Columns 2 and 3

Materials:

- 1 well plate (share with Sections 3,5)
- Color-coded sample sheet (share with Sections 3,5)
- Lemon juice, vinegar, water, baking soda solution, Windex
- Sugar stock solution (from Section 3)

Procedure:

14. Add 1 drop of the appropriate acid or base to the wells in columns 2 and 3.
    2A, 3A: Windex
    2B, 3B: baking soda solution
    2C, 3C: water
    2D, 3D: vinegar
    2E, 3E: lemon juice
    2F, 3F: empty

15. Add 2 drops of saturated sugar solution to wells A-E in columns 2 and 3 using your sugar stock solution pipet. You may have to wait for the person completing Section 3 to make the sugar stock solution before you can use it.

Section 5. H_2O_2 for Column 1 and unknowns for Column 6

Materials:

- 1 well plate (share with Sections 4-5)
- Color-coded sample sheet (share with Sections 4-5)
- Transfer pipet labeled "unknown drinks"
- Sugary drinks to test
- 3 mL dilute H_2O_2 (hydrogen peroxide) solution
- Sugar stock solution (from Section 3)

Procedure:

16. Pipet ~1 mL (or enough liquid to cover a bead) of the drinks you brought with you into the wells in column 6, and record what is in each well on your sample sheet. Be sure to rinse out the pipet with water between each sample!

17. Add 1 mL of each of the following solutions to each well in Column 1 using your sugar stock solution and H_2O_2 pipets. You may have to wait for the person completing Section 3 to make the sugar stock solution before you can use it.

    1A, 1B, 1C: dilute H_2O_2 solution
    1D, 1E, 1F: sugar stock solution

Section 6. Adding the sensors (WAIT FOR ALL GROUP MEMBERS BEFORE STARTING)

Materials:

- All beads from Section 2
- Leftover working solution from Section 2
- Complete well plate, set up as shown in the key on your sample sheet

Hint Box!

- You can add the sensor beads/solution to columns 1-3 whenever you like, but Columns 4 and 6 should be added at the same time
- Be ready to take pictures of your assay in step 23.
- Take a picture at ~5 minute increments.

Procedure:

18. Add the following beads to column 1:
    1A, 1D: "A" bead
    1B, 1E: "B" bead (*Group R*) or "C" bead (*Group X*)
    1C, 1F: "D" bead

19. Using the table on the following page, circle "yes" or "no" to indicate whether each combination produces a color change or not. You should assume that all changes will happen within about 20 minutes, but look carefully: some color changes are subtle! *Group R* and *Group X* should exchange results to get the column that each group is missing. Observe, but DO NOT remove the beads from the solutions to check them. Removing them will affect whether they change color.

	Column 1: Component Tests	Other Observations
A: H_2O_2, "A" bead	yes/no	
B: H_2O_2, "B" bead (*Group R*) H_2O_2, "C" bead (*Group X*)	yes/no yes/no	
C: H_2O_2, "D" bead	yes/no	
D: sugar, "A" bead	yes/no	
E: sugar, "B" bead (*Group R*) sugar, "C" bead (*Group X*)	yes/no yes/no	
F: sugar, "D" bead	yes/no	

20. Add a "D" bead to wells A-E in Column 2, and add 2 drops of the leftover working solution to wells A-E in column 3.

21. Using the table below, indicate whether each combination produces a color change or not. You should assume that all changes will happen within about 20 minutes.

	Column 2: Acids/Bases + Beads	Column 3: Acids/Bases + Solution	Other Observations
A: sugar, Windex	yes/no	yes/no	
B: sugar, baking soda	yes/no	yes/no	
C: sugar, water	yes/no	yes/no	
D: sugar, vinegar	yes/no	yes/no	
E: sugar, lemon juice	yes/no	yes/no	
F: empty			

22. Add a "D" bead to each well in column 4 and 6. The assay changes color over time, so add the beads to all of the solutions as close as you can to the same time.

23. Take a picture every 5 minutes and describe what you see below. How is the bead different in each of the solutions? How does it change over time? Is there a time after which it stops changing?

24. Using the standards in Column 4 as a comparison, estimate the sugar concentration of your drinks.

Drink	Estimated concentration of sugar

Section 7. Cleanup Procedure

1. Remove all beads from your solutions.
2. Throw away beads in trash can.
3. Pour all liquid waste down the drain.

Student Post-lab

1. What are the combinations of components from Column 1 that result in a color change? What do you think this implies about the way the assay works? What other tests would you run to confirm your hypothesis? It's okay if you don't know exactly how a test could be run: just think about what else you would want to do.

Answer: The only combinations that change color are sugar + full assay, H_2O_2 + full assay, and H_2O_2 + HRP + AR. This suggests that the hydrogen peroxide is an intermediate in the sugar-sensing pathway: it is produced by the reaction of sugar with glucose oxidase. The hydrogen peroxide then helps oxidize the dye in the presence of HRP to cause the color change. One way to confirm this hypothesis would be to add sugar and glucose oxidase to a solution and test for the evolution of hydrogen peroxide.

2. In Columns 2 and 3, which acids and bases cause a difference in behavior between the encapsulated assay and the free assay? What advantages or disadvantages are associated with having a solution versus having the assay encapsulated in a bead?

Answer: The acids (lemon juice and vinegar) produce a color change in the beads but not in the free assay because the enzymes are denatured under acidic conditions. The beads prevent this denaturation by putting the enzymes in pores that protect them. They also make it easier to test larger volumes of liquid without needing to add a large volume of assay to get a visible color change. Additionally, the beads can be removed after use (although students should still not drink the liquid they tested).

3. What does it mean if the bead turns the same color in an unknown as it did in the stock sugar solution? How could you go about trying to get a better idea of the actual concentration of sugar in these cases?

Answer: It means the concentration of glucose is equal to or greater than that of the sugar stock solution. It is possible that even though the solution is fairly concentrated for sucrose (the sugar used in this experiment), other sugars might be capable of higher concentrations. In this case, a more accurate concentration could be determined by diluting the solution by, say, 50% and seeing what the concentration of that new solution is.

4. Were there any results that surprised you with respect to your sugary drinks? Why or why not?

Answer: This depends on what drinks students bring in, but one of the results they may see is that drinks sweetened with artificial sweeteners do not give as strong of a color change as expected. This is because the assay only responds to glucose (or sucrose, which is made up of glucose and fructose combined), not high fructose corn syrup or artificial sweeteners. Students sometimes also note that colored drinks make it difficult to judge the final color, and that a blank bead swollen in the drink alone may be a good control with which to compare the final color. If students bring in cloudy drinks, they may also note that the response is difficult to judge, and that the bead may need to be removed and rinsed to judge the color, but that this may interfere with the development of the color over time.

5. What were some of the advantages of the assay used in this experiment? What were some of the limitations?

Answer: Some advantages include that this system is easy to use and is both portable and pH-resistant when incorporated into a hydrogel bead. Some limitations may include that a calibration curve is necessary to get a quantitative measurement, and the precision of those measurements is fairly limited.

6. Considering the detection limits of glucose you discovered for this specific assay, what are some possible applications for the assay? What applications would this assay NOT be suitable for?

Answer: Possible applications include sensing for sugar in beverages as done in the experiment, sensing for blood sugar, and sensing for sugar in urine. This assay would not be suitable for sensing sugars other than glucose and sucrose (because the enzymes are specific to glucose), sensing deeply colored or opaque solutions, and sensing applications that require immediate results (rather than waiting 5-15 minutes for the color to develop). Students may come up with additional answers.

7. Glucose oxidase can be used as part of biofuel cells (batteries that use biological fuels to produce electricity). What would the advantage of putting the glucose oxidase in a hydrogel in this context? What about if the whole biofuel cell were inside someone's body for a pacemaker or similar device?

Answer: Outside of the body, the hydrogel can stabilize the enzymes and help them maintain functionality for a longer period of time and over a wider variety of pH and temperature conditions. Inside the body, temperature and pH are already regulated, but the gel can help immobilize the enzymes and keep them in one place rather than diffusing through the body. In both contexts, the gel can also provide better contact between the biological components and electrical components.

Further Exploration

Additional Activities for Advanced Students

1. Use the "Colorimeter" app to do a quantitative analysis of a colored solution and further explore Beer's Law. You can use the color values in lieu of absorbance values.

2. Explore temperature changes to free or encapsulated enzyme to examine protective effects of immobilization.

3. Can you determine the pH of the acids/bases used in Section 3?

4. Find other sensors/biosensor systems that may be present in your everyday life. What is the signal? How is it transduced? What is the output?

5. In this lab, you used a pre-formed gel network that expanded in order to fit the assay components. What are some other ways to make a gel? What are the advantages and disadvantages of the method you used compared to those other methods?

6. Do an online search on glucose oxidase from aspergillus niger.

   To find a summary of protein characteristics, use UniProt: http://www.uniprot.org/
   To find original research on genes or proteins, use NCBI: https://www.ncbi.nlm.nih.gov/
   To look at protein structures + ligands, use the Protein Data Bank: https://www.rcsb.org/

   *Teachers: this may be a difficult question for your students. Not all proteins have complete information. This is an excellent introduction, however, to the abundant biochemical resources that have become available to scientists in recent years. Depending on how advanced your students are, you may want to direct them to the additional resources listed below on this page.

   a. How many nucleotides code for this protein?
   b. How many amino acids make up this protein?
   c. What is the molecular weight of the protein?
   d. What is its native function?
   e. Where is it normally found?
   f. What are the temperature, pH, or solution conditions for the enzymes? You may have to search some of the referenced articles to find this information, or search on other websites.
   g. Can you find a protein structure for glucose oxidase?
   h. Can you find the pocket where the glucose substrate binds?

To view a structure for glucose oxidase: http://pdb101.rcsb.org/motm/77
^They can read through this information. This webpage leads students to the Protein Data Bank (PDB) structure 1GPE. On the left hand side of the web page, click on 3D view: structure. Then, rotate the protein to get a better look at the way the protein interacts with its substrate. For the structure, click through several representations. For your students, they may find that "backbone" works well. Also, change the representation of the ligand to "spacefill." Students may be interested to know that protein structure is necessary to design new drugs that are capable of tightly interacting with proteins!

Student Pre-lab

1. Fill in the following color wheel using the colors listed, and then write the three matching pairs of complementary colors in the blanks to the right.

Colors: Red, Orange, Yellow, Green, Blue, Violet

Color Wheel:

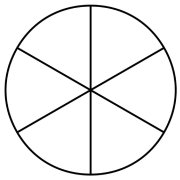

Complementary Colors:

Pair 1:_____, _____

Pair 2:_____, _____

Pair 3:_____, _____

2. Blue light has a wavelength of 450-490nm. If a molecule absorbs 460nm light, what color will it appear?

3. The colored indicator used in this experiment turns bright pink. What color light does it absorb?

4. If you wanted to analyze this compound using UV-vis spectroscopy, what wavelength or color would you measure for absorption at?

5. What is the concentration (in g/mL) of a salt solution created by adding 27 grams of salt to 60mL of water if the final total volume of the solution is 70mL?

6. If you have a 3mg/mL solution of theobromine (a component of chocolate) in water, how would you go about making 6mL of a 1mg/mL solution? Hint: use the equation $C_iV_i=C_fV_f$, where C is concentration and V is volume, for initial solution *i* and final solution *f*.

7. The sugar used in this experiment is sucrose, which is made up of one glucose unit bonded to one fructose unit. Therefore, glucose only makes up 52.6% of the mass of the sugar you will weigh out. What is the **glucose** concentration (in g/mL) of a sugar solution created by adding 15 grams of **sucrose** to 30mL of water if the final total volume of the solution is 40mL? This solution will be your sugar stock solution during the experiment.

8. In order to make a calibration curve during the experiment, you will make a series of diluted sugar solutions from the sugar stock solution in question 3. Let the concentration of your stock solution be "x." If you're going to have the stock solution, a blank solution of just water, and four evenly spaced points between those two concentrations, what are the concentrations of the solutions be **in terms of x**?

Solution 1: _____ (stock solution)

Solution 2: _____ (dilution 1)

Solution 3: _____ (dilution 2)

Solution 4: _____ (dilution 3)

Solution 5: _____ (dilution 4)

Solution 6: _____ (plain water)

9. Using your answers to questions 3 and 4, what are the concentrations of the six solutions in g/mL? Solution 1 should be your answer to question 3.

Solution 1: _____ (stock solution)

Solution 2: _____ (dilution 1)

Solution 3: _____ (dilution 2)

Solution 4: _____ (dilution 3)

Solution 5: _____ (dilution 4)

Solution 6: _____ (plain water)

10. Using the same equation from question 2 ($C_iV_i=C_fV_f$), calculate how many drops of sugar stock solution and how many drops of water you need to combine to create 15 drops of each solution. Hint: use "drops" as your unit of volume instead of mL, and the math may be simpler if you use the concentrations in terms of x that you calculated in question 3.

Solution	**# of drops of sugar stock solution**	**# of drops of water**
Stock solution		
Dilution 1		
Dilution 2		
Dilution 3		
Dilution 4		
Plain water		

11. Look through the procedure to fill in the following chart with everything that will go in each well on your well plate. Make sure to include sugar stock, hydrogen peroxide, any acids or bases, and the specific assay components that are present (dye, GOx, HRP) in what form (bead or free solution).

	1	2	3	4	5	6
A						
B						
C						
D						
E						
F						

12. What will you learn from the results of each column? Summarize the purpose of each column below.

Column 1:

Columns 2/3:

Columns 4/6:

Biosensors

C (N) S I

The California NanoSystems Institute
University of California, Los Angeles
High School Nanoscience Institute

Student Manual – February 2019

Purpose: Biosensors are a specific class of sensor that targets a biological molecule such as an enzyme, carbohydrate, toxin, or bacterium. They are used for a wide variety of research, industrial, and biomedical applications, and many take advantage of nanomaterials or biomolecules as part of the sensor itself. Portable, robust sensors are desirable for sensing toxins, contaminants, and pathogens that might spread, as well as biologically important molecules like glucose whose presence or absence can be important for normal biological function.

In this experiment, you will make a glucose-sensing assay encapsulated in a nanoporous gel bead and see what different components of the assay respond to in order to figure out its mechanism. Then you will test the assay under a variety of conditions to measure its limitations. Lastly, you will use the assay and a series of sugar solutions with known concentrations to figure out how much sugar is in different sugary drinks.

Overview: In groups of four, students will make a glucose-sensing assay in a gel bead, determine its mechanism, observe its limitations, and use it to quantify how much sugar is in different drinks.

Student Procedure

Section 1. Setup and Organization

Materials:

- 2 white plastic cups
- 3 transfer pipets
- 3 disposable spatulas
- 3 petri dishes

Procedure:

1. Form groups of 4 people.

2. Pair up with another group of four and make one group "Group R" and the other one "Group X." You will share your results later on in the experiment.

Group R Only

3. Label your pipets:
   - -sugar stock solution
   - -water
   - -unknown drinks

   Label your spatulas:
   - -A
   - -B
   - -D

   Label your petri dishes
   - -A
   - -B
   - -D

   Label your white cups:
   - -working solution
   - -sugar stock solution

Group X Only

4. Label your pipets:
   - -sugar stock solution
   - -water
   - -unknown drinks

   Label your spatulas:
   - -A
   - -C
   - -D

   Label your petri dishes
   - -A
   - -C
   - -D

   Label your white cups:
   - -working solution
   - -sugar stock solution

Both Groups

5. Assign one person to each of the following roles, and go to the indicated section to begin individual procedures:
   - -Make beads (Jump to Section 2, step 6 (*Group R*) or step 9 (*Group X*))
   - -Sugar solutions (Jump to Section 3, step 12)
   - -Acids and Bases (Jump to Section 4, step 14)
   - -H_2O_2 and unknowns (Jump to Section 5, step 16)

   You will all complete Section 6 (starting step 18) together once Sections 1-5 are complete.

Section 2. Make beads with different assay components

Materials:

Front of the room:

- 1X PBS buffer
- "GOx" (glucose oxidase) stock solution in PBS buffer
- "HRP" (horseradish peroxidase) stock solution in PBS buffer
- "AAP" (4-aminoantipyrine) stock solution in PBS buffer
- "HBS" (sodium 3,5-dichloro-2-hydroxybenzenesulfonate) stock solution in PBS buffer

Hint Box!

- When you swell the beads, look for them to be 2-3x their original diameter (takes 5-10 minutes).
- The swelling is difficult to see: tilt the cup or use the appropriate spatula to get a better idea of their size.

At your station:

- White plastic cup labeled "working solution"
- 27 beads
- 3 labeled disposable spatulas
- 3 labeled petri dishes

Procedure:

<u>*Group R*</u> Only

Contamination, especially stray sugar, can affect your results! Be very careful to use the correct pipet and spatula at all times. Wash your hands prior to starting the lab!

6. **"A" Bead preparation: Dye Only**
   Prepare a working solution by pipetting 8 mL 1X PBS buffer into your white cup and adding 1 mL of the AAP stock solution and 1 mL of the HBS stock solution. Add 4 beads to the solution and let swell to 2-3 times their original size. Remove these from the solution using your "A" spatula and place them in the "A" petri dish.

7. **"B" Bead preparation: Dye + HRP**
   Add 1 mL HRP stock solution to the remaining working solution from Step 6 using the HRP pipet. Add 4 beads to the solution and let swell to 2-3 times their original size. Remove these from the solution using your "B" spatula and place in the "B" petri dish.

8. **"D" Bead preparation: Dye+ HRP + GOx**
   Add 1 mL GOx stock solution to the remaining working solution from Step 7 using the GOx pipet. Add ALL of the remaining beads to your solution and let swell to 2-3 times their original size. Remove these from the solution using your "D" spatula and place in the "D" petri dish. SAVE THE REST OF THE WORKING SOLUTION for later in the experiment.

Group X Only

Contamination, especially stray sugar, can affect your results! Be very careful to use the correct pipet and spatula at all times.

9. **"A" Bead preparation: Dye Only**
   Prepare a working solution by pipetting 8 mL 1X PBS buffer into your white cup and adding 1 mL of the AAP stock solution and 1 mL of the HBS stock solution. Add 4 beads to the solution and let swell to 2-3 times their original size. Remove these from the solution using your "A" spatula and place them in the "A" petri dish.

10. **"C" Bead preparation: Dye + GOx**
    Add 1 mL GOx stock solution to the remaining working solution from Step 9 using the GOx pipet. Add 4 beads to the solution and let swell to 2-3 times their original size. Remove these from the solution using your "C" spatula and place in the "C" petri dish.

11. **"D" Bead preparation: Dye + GOx + HRP**
    Add 1 mL HRP stock solution to the remaining working solution from Step 10 using the HRP pipet. Add ALL of the remaining beads to your solution and let swell to 2-3 times their original size. Remove these from the solution using your "D" spatula and place in the "D" petri dish. SAVE THE REST OF THE WORKING SOLUTION for later in the experiment.

Section 3. Sugar solutions for all columns

Materials:

- 15 g sugar
- 30 mL water for stock solution + 5 mL to make dilutions
- White plastic cup labeled "sugar stock solution"
- 2 Labeled transfer pipets: "water" and "sugar stock solution"
- 1 well plate (share with Sections 4-5)
- Color-coded sample sheet (share with Sections 4-5)

Hint Box!

- For best results, before placing each bead into a well, first blot the beads gently with Kimwipes or paper towels to remove remaining solution from the surface of the bead!

Procedure:

12. Make a sugar stock solution by adding 15 g sugar to 30 mL water in a white cup labeled "sugar stock solution." This is a fairly saturated solution, and it will take some work to get it to dissolve completely: make sure the sugar is completely dissolved and mixed before you move on. You can stir it using your sugar stock solution pipet.
13. Make the four dilutions of your sugar stock solution that you calculated in your pre-lab by adding the appropriate number of drops of sugar stock solution and water to each well in column 4. Make sure to use the correct pipet ("water" or "sugar stock solution") to avoid contamination!

    4A: saturated sugar solution
    4B: dilution 1
    4C: dilution 2
    4D: dilution 3
    4E: dilution 4
    4F: water

Section 4. Acid/base tests for Columns 2 and 3

Materials:

- 1 well plate (share with Sections 3,5)
- Color-coded sample sheet (share with Sections 3,5)
- Lemon juice, vinegar, water, baking soda solution, Windex
- Sugar stock solution (from Section 3)

Procedure:

14. Add 1 drop of the appropriate acid or base to the wells in columns 2 and 3.
    2A, 3A: Windex
    2B, 3B: baking soda solution
    2C, 3C: water
    2D, 3D: vinegar
    2E, 3E: lemon juice
    2F, 3F: empty

15. Add 2 drops of saturated sugar solution to wells A-E in columns 2 and 3 using your sugar stock solution pipet. You may have to wait for the person completing Section 3 to make the sugar stock solution before you can use it.

Section 5. H_2O_2 for Column 1 and unknowns for Column 6

Materials:

- 1 well plate (share with Sections 4-5)
- Color-coded sample sheet (share with Sections 4-5)
- Transfer pipet labeled "unknown drinks"
- Sugary drinks to test
- 3 mL dilute H_2O_2 (hydrogen peroxide) solution
- Sugar stock solution (from Section 3)

Procedure:

16. Pipet ~1 mL (or enough liquid to cover a bead) of the drinks you brought with you into the wells in column 6, and record what is in each well on your sample sheet. Be sure to rinse out the pipet with water between each sample!

17. Add 1 mL of each of the following solutions to each well in Column 1 using your sugar stock solution and H_2O_2 pipets. You may have to wait for the person completing Section 3 to make the sugar stock solution before you can use it.

    1A, 1B, 1C: dilute H_2O_2 solution
    1D, 1E, 1F: sugar stock solution

Section 6. Adding the sensors (WAIT FOR ALL GROUP MEMBERS BEFORE STARTING)

Materials:

- All beads from Section 2
- Leftover working solution from Section 2
- Complete well plate, set up as shown in the key on your sample sheet

Hint Box!

- You can add the sensor beads/solution to columns 1-3 whenever you like, but Columns 4 and 6 should be added at the same time
- Be ready to take pictures of your assay in step 23.
- Take a picture at ~5 minute increments.

Procedure:

18. Add the following beads to column 1:
    1A, 1D: "A" bead
    1B, 1E: "B" bead (*Group R*) or "C" bead (*Group X*)
    1C, 1F: "D" bead

19. Using the table on the following page, circle "yes" or "no" to indicate whether each combination produces a color change or not. You should assume that all changes will happen within about 20 minutes, but look carefully: some color changes are subtle! *Group R* and *Group X* should exchange results to get the column that each group is missing. Observe, but DO NOT remove the beads from the solutions to check them. Removing them will affect whether they change color.

	Column 1: Component Tests	Further Observations
A: H_2O_2, "A" bead	yes/no	
B: H_2O_2, "B" bead (*Group R*) H_2O_2, "C" bead (*Group X*)	yes/no yes/no	
C: H_2O_2, "D" bead	yes/no	
D: sugar, "A" bead	yes/no	
E: sugar, "B" bead (*Group R*) sugar, "C" bead (*Group X*)	yes/no yes/no	
F: sugar, "D" bead	yes/no	

20. Add a "D" bead to wells A-E in Column 2, and add 2 drops of the leftover working solution to wells A-E in column 3.

21. Using the table below, indicate whether each combination produces a color change or not. You should assume that all changes will happen within about 20 minutes.

	Column 2: Acids/Bases + Beads	Column 3: Acids/Bases + Solution	Further Observations
A: sugar, Windex	yes/no	yes/no	
B: sugar, baking soda	yes/no	yes/no	
C: sugar, water	yes/no	yes/no	
D: sugar, vinegar	yes/no	yes/no	
E: sugar, lemon juice	yes/no	yes/no	
F: empty			

22. Add a "D" bead to each well in column 4 and 6. The assay changes color over time, so add the beads to all of the solutions as close as you can to the same time.

23. Take a picture every 5 minutes and describe what you see below. How is the bead different in each of the solutions? How does it change over time? Is there a time after which it stops changing?

24. Using the standards in Column 4 as a comparison, estimate the sugar concentration of your drinks.

Drink	Estimated concentration of sugar

Section 7. Cleanup Procedure

1. Remove all beads from your solutions.
2. Throw away beads in trash can.
3. Pour all liquid waste down the drain.

Student Post-lab

1. What are the combinations of components from Column 1 that result in a color change? What do you think this implies about the way the assay works? What other tests would you run to confirm your hypothesis? It's okay if you don't know exactly how a test could be run: just think about what else you would want to do.

2. In Columns 2 and 3, which acids and bases cause a difference in behavior between the encapsulated assay and the free assay? What advantages or disadvantages are associated with having a solution versus having the assay encapsulated in a bead?

3. What does it mean if the bead turns the same color in an unknown as it did in the stock sugar solution? How could you go about trying to get a better idea of the actual concentration of sugar in these cases?

4. Were there any results that surprised you with respect to your sugary drinks? Why or why not?

5. What were some of the advantages of the assay used in this experiment? What were some of the limitations?

6. Considering the detection limits of glucose you discovered for this specific assay, what are some possible applications for the assay? What applications would this assay NOT be suitable for?

7. Glucose oxidase can be used as part of biofuel cells (batteries that use biological fuels to produce electricity). What would the advantage of putting the glucose oxidase in a hydrogel in this context? What about if the whole biofuel cell were inside someone's body for a pacemaker or similar device?

4.6.4. Recipe List

Recipe Sheet

Column 1 Recipes:

A: 1 mL dilute H_2O_2, 1 "A" bead
B: 1 mL dilute H_2O_2, 1 "B" bead (*Group R*)
1 "C" bead (*Group X*)
C: 1 mL dilute H_2O_2, 1 "D" bead
D: 1 mL sugar, 1 "A" bead
E: 1 mL sugar, 1 "B" bead (*Group R*)
1 "C" bead (*Group X*)
F: 1 mL sugar, 1 "D" bead

Column 2 Recipes:

A: 1 drop Windex, 2 drops sugar, 1 "D" bead
B: 1 drop baking soda, 2 drops sugar, 1 "D" bead
C: 1 drop water, 2 drops sugar, 1 "D" bead
D: 1 drop vinegar, 2 drops sugar, 1 "D" bead
E: 1 drop lemon juice, 2 drops sugar, 1 "D" bead
F: empty

Column 3 Recipes:

A: 1 drop Windex, 2 drops sugar, 2 drops working solution
B: 1 drop baking soda, 2 drops sugar, 2 drops working solution
C: 1 drop water, 2 drops sugar, 2 drops working solution
D: 1 drop vinegar, 2 drops sugar, 2 drops working solution
E: 1 drop lemon juice, 2 drops sugar, 2 drops working solution
F: empty

Column 4 Recipes:

A: Saturated sugar solution, 1 "D" bead
B: Dilution 1, 1 "D" bead
C: Dilution 2, 1 "D" bead
D: Dilution 3, 1 "D" bead
E: Dilution 4, 1 "D" bead
F: Water, 15 drops water, 1 "D" bead

Column 6 Recipes:

A: 1 mL drink 1, 1 "D" bead
B: 1 mL drink 2, 1 "D" bead
C: 1 mL drink 3, 1 "D" bead
D: 1 mL drink 4, 1 "D" bead
E: 1 mL drink 5, 1 "D" bead
F: 1 mL drink 6, 1 "D" bead

4.6.5. Additional Handouts

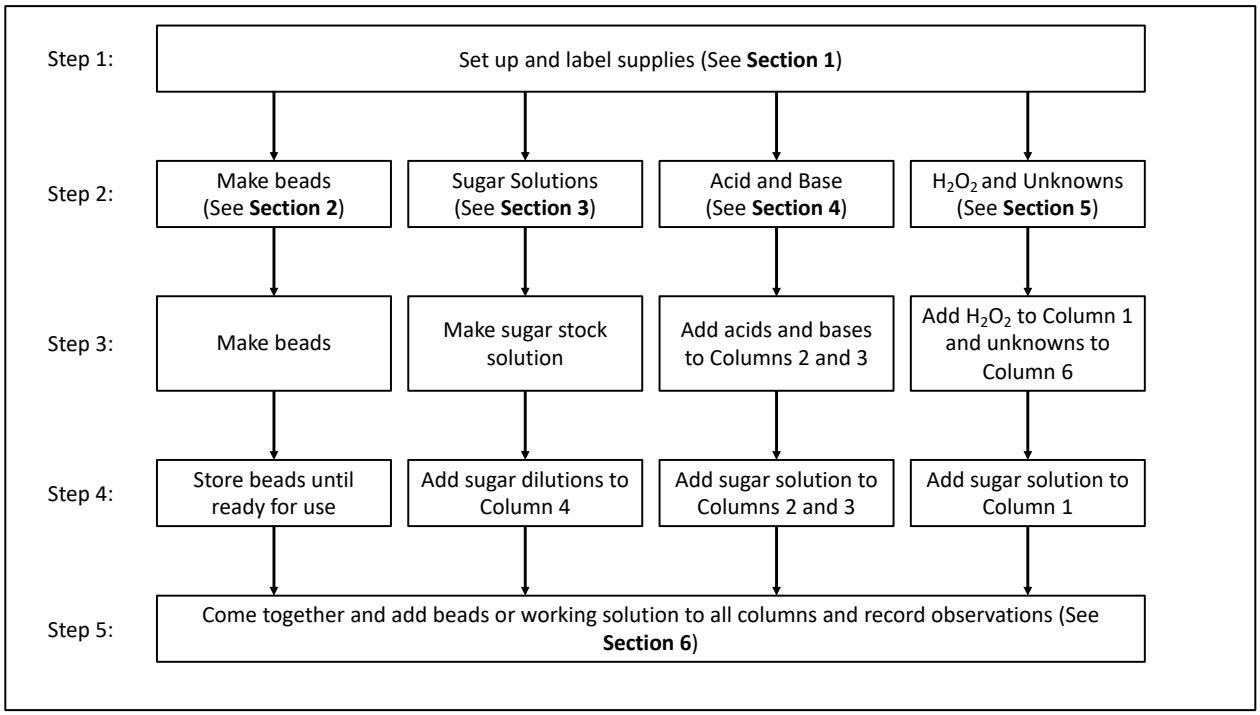

Sample Sheet

	1	2	3	4	5	6	7	8
A								
B								
C								
D								
E								
F								

Hint: your well plate is already labeled! Look for the letters and numbers along each edge to match them up here.

Column 6: Unknowns

A:_____

B:_____

C:_____

D:_____

E:_____

F:_____

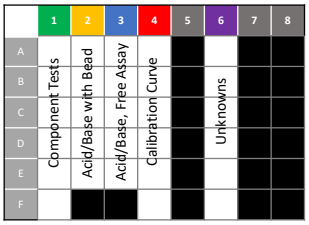

4.6.6. Well Plate Key for Teachers

Key: Group R

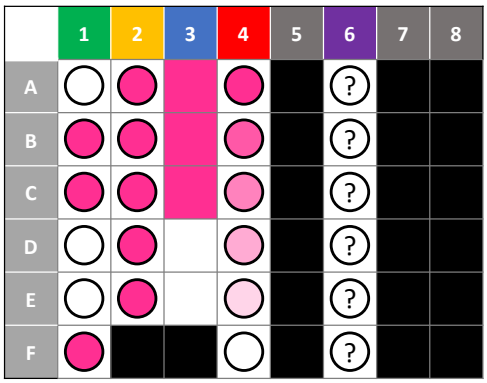

Key: Group X

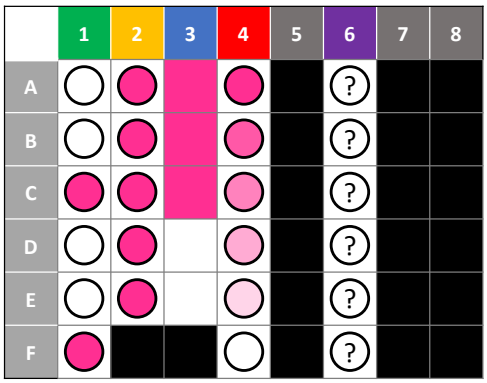

4.7. References

[1] A) Gupta, A. K.; Gupta, M. Synthesis and surface engineering of iron oxide nanoparticles for biomedical applications. *Biomaterials*. **2005**, *26* (18), 3995–4021. B) Jain, P. K.; Huang, X.; El-Sayet, I. H.; El-Sayed, M. A. Noble Metals on the Nanoscale: Optical and Pototherma l Properties and Some Applications in Imaging, Sensing, Biology, and Medicine. *Acc. Chem. Res.*, **2008**, *41* (12), 1578–1586.

[2] Glucose Colorimetric Assay Kit Booklet; Cayman Chemical Company: Ann Arbor, MI, 2017.

[3] A) Frost, L. D. Glucose Assays Revisited: Experimental Determination of the Glucose Concentration in Honey. *Chem. Educator* **2004**, *9* (X), 239–241. B) Amor-Gutiérrez, O.; Rama, E. C.; Fernández-Abedul, M. T.; Costa-García, A. Bioelectroanalysis in a Drop: Construction of a Glucose Biosensor. *J. Chem. Educ.* **2017**, *94* (6), 806–812. C) Toren Jr., E. C. Determination of glucose: A kinetics experiment for the analytical course. *J. Chem. Educ.* **1967**, *44* (3), 172.

[4] A) Jin, W.; Brennan, J. D. Properties and applications of proteins encapsulated within sol–gel derived materials. *Analytica Chimica Acta* **2002**, *461* (1), 1–36. B) Reetz, M. T.; Tielmann, P.; Wiesenhöfer, W.; Könen, W.; Zonta, A. Second Generation Sol-Gel Encapsulated Lipases: Robust Heterogeneous Biocatalysts. *Adv. Synth. Catal.* **2003**, *345* (6-7), 717–728. C) Kulkarn, S; Tran, V.; Ho, M. K.-M.; Phan, C.; Chin, E.; Wemmer, Z.; Sommerhalter, M. Biocatalysis with Sol–Gel Encapsulated Acid Phosphatase. *J. Chem. Educ.* **2010**, *87* (9), 958–960.

[5] Zhao, B.; Summers, F. A.; Mason, R. P. Photooxidation of Amplex red to resorufin: Implications of exposing the Amplex red assay to light. *Free Radical Biology and Medicine* **2012**, *53* (5), 1080–1087.